

T. FIDAN ASLAN

IZMIR KATIP CELEBI UNIVERSITY

2019

**IZMIR KATIP CELEBI UNIVERSITY
GRADUATE SCHOOL OF NATURAL AND APPLIED SCIENCES**

**PREPARATION AND CHARACTERIZATION OF CARBON-BASED
NANOFLUIDS**

M.Sc. THESIS

Tuğçe FİDAN ASLAN

Department of Materials Science and Engineering

AUGUST 2019

İZMİR KATİP ÇELEBİ UNIVERSITY
GRADUATE SCHOOL OF NATURAL AND APPLIED SCIENCES

**PREPARATION AND CHARACTERIZATION OF CARBON-BASED
NANOFLUIDS**

M.Sc. THESIS

Tuğçe FİDAN ASLAN
(Y160219004)

Department of Materials Science and Engineering

Thesis Advisor: Asst. Prof. Dr. Elif ALYAMAÇ SEYDİBEYOĞLU

AUGUST 2019

İZMİR KATİP ÇELEBİ ÜNİVERSİTESİ
FEN BİLİMLERİ ENSTİTÜSÜ

KARBON BAZLI NANOAKIŞKANLARIN HAZIRLANMASI VE
KARAKTERİZASYONU

YÜKSEK LİSANS TEZİ

Tuğçe FİDAN ASLAN
(Y160219004)

Malzeme Bilimi ve Mühendisliği Ana Bilim Dalı

Tez Danışmanı: Dr. Öğr. Üyesi Elif ALYAMAÇ SEYDİBEYOĞLU

AĞUSTOS 2019

Tuğçe FİDAN ASLAN, a **M.Sc.** student of **IKCU Graduate School of Natural and Applied Sciences**, successfully defended the thesis entitled “**PREPARATION AND CHARACTERIZATION OF CARBON-BASED NANOFLUIDS**”, which she prepared after fulfilling the requirements specified in the associated legislations, before the jury whose signatures are below.

Thesis Advisor : **Elif ALYAMAÇ SEYDİBEYOĞLU**

Asst. Prof. Dr.
İzmir Katip Çelebi University

Jury Members : **Mehmet Özgür SEYDİBEYOĞLU**

Prof. Dr.
İzmir Katip Çelebi University

Alpaslan TURGUT

Assoc. Prof. Dr.
Dokuz Eylül University

Date of Submission : 22.07.2019

Date of Defense : 26.08.2019

*To my always supportive husband,
my family with strong ties,
and
my childhood who wanted to be a scientist.*

FOREWORD

The development of nanotechnology and the production of carbon-structured nanoparticles have popularized the production of nanofluidics, one of the most interesting subjects in the scientific world. Carbon-based nanoparticles have been used in heat transfer fluids due to their high thermal conductivity. Although many studies have been conducted in this field over the last fifteen years, some important issues have not yet been clarified. The most important issue is the stability of nanofluids. This thesis has been financially supported as TÜBİTAK 3001 project entitled “Preparation of Stable Nanofluids with Surface Functionalized Nanoparticles and Determination of the Change in Thermal Conductivity of Nanofluids”.

I would like to express my gratitude to my advisor, Asst. Prof. Dr. Elif Alyamaç Seydibeyođlu for her help at all stages of this thesis. Assoc. Prof. Dr. Alpaslan Turgut and Prof. Dr. Mehmet Özgür Seydibeyođlu's valuable contributions are very important for the execution of this study and I would like to thank them for their support. I would like to thank my husband, Gürcan Aslan for his unconditional love and encouragement. I would like to express my special thanks to my parents who made sacrifices for me. I would also like to thank my grandmother, my grandfather, and my brother who were proud of me during this adventure.

August 2019

Tuğçe FİDAN ASLAN

TABLE OF CONTENTS

	<u>Page</u>
FOREWORD	v
ABBREVIATIONS	vii
ABSTRACT	xiv
ÖZET	xv
1. INTRODUCTION	1
1.1 Graphene	3
1.2 Carbon Nanotubes	4
1.3 Polyhedral Oligomeric Silsesquioxane (POSS)	5
1.4 Stability of Nanofluids and Zeta Potential	7
1.5 Determination of Stability by UV-Vis Spectrophotometry.....	10
1.6 Theory of 3ω Method	13
1.7 Rheology Measurements	15
1.8 Contact Angle and Surface Tension	17
2. LITERATURE SURVEY	22
3. EXPERIMENTAL	29
3.1 Preparation of Nanofluids	31
3.1.1 Preparation of aqueous nanofluids	32
3.1.2 Preparation of EG-based nanofluids	35
3.1.3 Preparation of compressor oil-based nanofluids	35
3.2 Characterization of Nanofluids	38
3.2.1 Zeta potential measurement	38
3.2.2 UV-Vis spectrophotometry	39
3.2.3 Rheology measurements	40
3.2.4 3ω thermal conductivity measurement method.....	41
3.2.5 Contact angle and surface tension measurements.....	42
4. RESULTS AND DISCUSSION	43
4.1 Stability Evaluation of Nanofluids	43
4.1.1 Results of zeta potential measurements	43
4.1.2 Determination of relative concentration of nanofluids by UV-Vis spectrophotometry.....	46
4.2 Rheology Measurements	55
4.3 3ω Thermal Conductivity Measurements.....	86
4.4 Contact Angle and Surface Tension Measurements.....	93
5. CONCLUSIONS	104
REFERENCES	107

ABBREVIATIONS

CNT	: Carbon Nanotube
CTAB	: Cetyl Trimethyl Ammonium Bromide
DLVO	: Derjaguin, Landau, Verwey, and Overbeek Theory
DWCNT	: Double-Walled Carbon Nanotube
EDL	: Electrical Double Layer
EG	: Ethylene Glycol
GNP	: Graphene Nanoplatelet
LDV	: Laser Doppler Velocimetry
MWCNT	: Multi-Walled Carbon Nanotube
PEG-POSS	: Polyethylene Glycol-derived Polyhedral Oligomeric Silsesquioxane
rGO	: Reduced Graphene Oxide
SDBS	: Sodium Dodecyl Benzene Sulfonate
SDS	: Sodium Dodecyl Sulphate
SEM	: Scanning Electron Microscopy
STM	: Scanning Tunneling Microscopy
SWCNT	: Single Walled Carbon Nanotube
THW	: Transient Hot Wire

LIST OF TABLES

	<u>Page</u>
Table 3.1 : Material properties of nanoparticles.	29
Table 3.2 : Material properties of base fluids.....	30
Table 3.3 : Material properties of PEG-POSS.	30
Table 3.4 : Aqueous SWCNT nanofluids based on the nanoparticle concentration, stabilizer concentration, and ultrasonication time.....	33
Table 3.5 : Aqueous GNP nanofluids based on the nanoparticle surface area and concentration, stabilizer concentration, and ultrasonication time.....	34
Table 3.6 : EG based nanofluids according to the nanoparticle and stabilizer concentrations.	36
Table 3.7 : Oil-based nanofluids according to the nanoparticle and stabilizer concentrations.	37

LIST OF FIGURES

	<u>Page</u>
Figure 1.1 : Some applications of carbon nanotubes, re-drawn from [32].	5
Figure 1.2 : Silsesquioxanes (a) randomly arranged; (b) ladder; (c), (d), and (e) cage; (f) partially cage.	6
Figure 1.3 : Chemical structure of PEG-POSS.	7
Figure 1.4 : EDL regions and electrical potentials of a particle (adapted from [40]).	9
Figure 1.5 : Zetasizer Nano device cuvette, electrodes, and direction of movement of charged ions.	10
Figure 1.6 : Possible electron transitions (energy increases from left to right).	11
Figure 1.7 : Working principle of UV-Vis Spectrophotometry.	11
Figure 1.8 : Viscosity versus shear rate (a) and shear stress vs shear rate (b) plots of different fluid types.	16
Figure 1.9 : Shaft types (a) concentric cylinder, (b) cone, (c) parallel plate and (d) torsion.	17
Figure 1.10 : Pendant drop and sessile drop methods.	18
Figure 1.11 : Contact angle between droplet and surface.	19
Figure 1.12 : Variables used in surface tension calculation according to the hanging drop method (from Kruss Scientific).	20
Figure 3.1 : Preparation of nanofluids with Hielscher ultrasonication device.	31
Figure 3.2 : Malvern Zetasizer Nano ZS 90 device.	39
Figure 3.3 : Samples with high concentration (a) and adjusted concentration (b) for zeta potential measurement.	39
Figure 3.4 : Perkin Elmer, LAMBDA 950 UV-Vis Spectrophotometer.	40
Figure 3.5 : TA Instruments, HR-2 rheometer.	40
Figure 3.6 : Lab-made 3ω set-up.	41
Figure 3.7 : Thermal probe operating both as heater and thermometer.	41
Figure 3.8 : Surface tension (a) and contact angle (b) measurements performed with a goniometer.	42
Figure 4.1 : Zeta potential as a function of GNP (800 m ² /g) concentration for aqueous nanofluids at different PEG-POSS concentrations.	44
Figure 4.2 : Zeta potential as a function of GNP concentration (320, 530, and 800 m ² /g) for aqueous nanofluids without PEG-POSS.	44
Figure 4.3 : Zeta potential as a function of SWCNT concentration for aqueous nanofluids at different PEG-POSS concentrations.	45
Figure 4.4 : Zeta potential as a function of GNP (800 m ² /g) concentration for EG-based nanofluids at different PEG-POSS concentrations.	46
Figure 4.5 : UV-Vis Spectra of aqueous nanofluids at different GNP (800 m ² /g) concentrations with no PEG-POSS.	47
Figure 4.6 : UV-Vis Spectra of aqueous nanofluids at different GNP (800 m ² /g) concentrations with 0.1 wt% PEG-POSS.	48

Figure 4.7 : UV-Vis Spectra of aqueous nanofluids at different GNP (800 m ² /g) concentrations with 0.2 wt% PEG-POSS.	48
Figure 4.8 : UV-Vis Spectra of aqueous nanofluids at different GNP (800 m ² /g) concentrations with 0.3 wt% PEG-POSS.	49
Figure 4.9 : Calibration graphs of GNP (800 m ² /g) nanofluids with (a) no PEG-POSS, (b) 0.1 wt% PEG-POSS, (c) 0.2 wt% PEG-POSS, and (d) 0.3 wt% PEG-POSS; relative concentration of GNP (800 m ² /g) nanofluids with (e) no PEG-POSS, (f) 0.1 wt% PEG-POSS, (g) 0.2 wt% PEG-POSS, and (h) 0.3 wt% PEG-POSS at the end of the 60 days.	51
Figure 4.10 : UV-Vis Spectra of aqueous nanofluids at different SWCNT concentrations with no PEG-POSS.	51
Figure 4.11 : UV-Vis Spectra of aqueous nanofluids at different SWCNT concentrations with 0.1 wt% PEG-POSS.	52
Figure 4.12 : UV-Vis Spectra of aqueous nanofluids at different SWCNT concentrations with 0.2 wt% PEG-POSS.	52
Figure 4.13 : Calibration graphs of SWCNT nanofluids with (a) no PEG-POSS, (b) 0.1 wt% PEG-POSS, and (c) 0.2 wt% PEG-POSS; relative concentration of SWCNT nanofluids with (d) no PEG-POSS, (e) 0.1 wt% PEG-POSS, and (f) 0.2 wt% PEG-POSS at the end of the 60 days.	53
Figure 4.14 : Stable aqueous SWCNT samples (a), sedimented samples (b), re-dispersible samples.	54
Figure 4.15 : Viscosity as a function of shear rate for aqueous GNP (800 m ² /g) nanofluids with no PEG-POSS.	56
Figure 4.16 : Viscosity as a function of temperature for aqueous GNP (800 m ² /g) nanofluids with no PEG-POSS.	56
Figure 4.17 : Viscosity as a function of shear rate for aqueous GNP (800 m ² /g) nanofluids with 0.1 wt% PEG-POSS.	57
Figure 4.18 : Viscosity as a function of temperature for aqueous GNP (800 m ² /g) nanofluids with 0.1 wt% PEG-POSS.	57
Figure 4.19 : Viscosity as a function of shear rate for aqueous GNP (800 m ² /g) nanofluids with 0.2 wt% PEG-POSS.	58
Figure 4.20 : Viscosity as a function of temperature for aqueous GNP (800 m ² /g) nanofluids with 0.2 wt% PEG-POSS.	59
Figure 4.21 : Viscosity as a function of shear rate for aqueous GNP (800 m ² /g) nanofluids with 0.3 wt% PEG-POSS.	59
Figure 4.22 : Viscosity as a function of temperature for aqueous GNP (800 m ² /g) nanofluids with 0.3 wt% PEG-POSS.	60
Figure 4.23 : Viscosity as a function of shear rate for aqueous GNP (530 m ² /g) nanofluids with no PEG-POSS.	61
Figure 4.24 : Viscosity as a function of temperature for aqueous GNP (530 m ² /g) nanofluids with no PEG-POSS.	61
Figure 4.25 : Viscosity as a function of shear rate for aqueous GNP (320 m ² /g) nanofluids with no PEG-POSS.	62
Figure 4.26 : Viscosity as a function of temperature for aqueous GNP (320 m ² /g) nanofluids with no PEG-POSS.	63
Figure 4.27 : Viscosity as a function of shear rate for aqueous 0.1 wt% GNP nanofluids with different surface areas and without PEG-POSS.	63
Figure 4.28 : Viscosity as a function of temperature for aqueous 0.1 wt% GNP nanofluids with different surface areas and no PEG-POSS.	64

Figure 4.29 : Viscosity as a function of shear rate for aqueous 0.5 wt% GNP nanofluids with different surface areas and no PEG-POSS.....	65
Figure 4.30 : Viscosity as a function of temperature for aqueous 0.5 wt% GNP nanofluids with different surface areas and no PEG-POSS.....	65
Figure 4.31 : Viscosity as a function of shear rate for aqueous 1.0 wt% GNP nanofluids with different surface areas and no PEG-POSS.....	66
Figure 4.32 : Viscosity as a function of temperature for aqueous 1.0 wt% GNP nanofluids with different surface areas and no PEG-POSS.....	66
Figure 4.33 : Viscosity as a function of shear rate for aqueous 2.0 wt% GNP nanofluids with different surface areas and no PEG-POSS.....	67
Figure 4.34 : Viscosity as a function of temperature for aqueous 2.0 wt% GNP nanofluids with different surface areas and no PEG-POSS.....	67
Figure 4.35 : Viscosity as a function of shear rate for EG-based GNP (800 m ² /g) nanofluids with no PEG-POSS.....	68
Figure 4.36 : Viscosity as a function of temperature for EG-based GNP (800 m ² /g) nanofluids with no PEG-POSS.....	69
Figure 4.37 : Viscosity as a function of shear rate for EG-based GNP (800 m ² /g) nanofluids with 0.1 wt% PEG-POSS.....	69
Figure 4.38 : Viscosity as a function of temperature for EG-based GNP (800 m ² /g) nanofluids with 0.1 wt% PEG-POSS.....	70
Figure 4.39 : Viscosity as a function of shear rate for EG-based GNP (800 m ² /g) nanofluids with 0.2 wt% PEG-POSS.....	71
Figure 4.40 : Viscosity as a function of temperature for EG-based GNP (800 m ² /g) nanofluids with 0.2 wt% PEG-POSS.....	71
Figure 4.41 : Viscosity as a function of shear rate for EG-based GNP (800 m ² /g) nanofluids with 0.3 wt% PEG-POSS.....	72
Figure 4.42 : Viscosity as a function of temperature for EG-based GNP (800 m ² /g) nanofluids with 0.3 wt% PEG-POSS.....	73
Figure 4.43 : Viscosity as a function of shear rate for EG-based GNP (530 m ² /g) nanofluids with no PEG-POSS.....	73
Figure 4.44 : Viscosity as a function of temperature for EG-based GNP (530 m ² /g) nanofluids with no PEG-POSS.....	74
Figure 4.45 : Viscosity as a function of shear rate for EG-based GNP (320 m ² /g) nanofluids with no PEG-POSS.....	75
Figure 4.46 : Viscosity as a function of temperature for EG-based GNP (320 m ² /g) nanofluids with no PEG-POSS.....	75
Figure 4.47 : Viscosity as a function of shear rate for EG-based 0.1 wt% GNP nanofluids with different surface areas and no PEG-POSS.....	76
Figure 4.48 : Viscosity as a function of temperature for EG-based 0.1 wt% GNP nanofluids with different surface areas and no PEG-POSS.....	76
Figure 4.49 : Viscosity as a function of shear rate for EG-based 0.5 wt% GNP nanofluids with different surface areas and no PEG-POSS.....	77
Figure 4.50 : Viscosity as a function of temperature for EG-based 0.5 wt% GNP nanofluids with different surface areas and no PEG-POSS.....	78
Figure 4.51 : Viscosity as a function of shear rate for EG-based 1.0 wt% GNP nanofluids with different surface areas and no PEG-POSS.....	78
Figure 4.52 : Viscosity as a function of temperature for EG-based 1.0 wt% GNP nanofluids with different surface areas and no PEG-POSS.....	79
Figure 4.53 : Viscosity as a function of shear rate for EG-based 0.0 wt% GNP nanofluids with different surface areas and no PEG-POSS.....	80

Figure 4.54 : Viscosity as a function of temperature for EG-based 2.0 wt% GNP nanofluids with different surface areas and no PEG-POSS.	80
Figure 4.55 : Viscosity as a function of shear rate for aqueous SWCNT nanofluids with no PEG-POSS.	81
Figure 4.56 : Viscosity as a function of temperature for aqueous SWCNT nanofluids with no PEG-POSS.	82
Figure 4.57 : Viscosity as a function of shear rate for aqueous SWCNT nanofluids with 0.1 wt% PEG-POSS.	82
Figure 4.58 : Viscosity as a function of temperature for aqueous SWCNT nanofluids with 0.1 wt% PEG-POSS.	83
Figure 4.59 : Viscosity as a function of shear rate for aqueous SWCNT nanofluids with 0.2 wt% PEG-POSS.	83
Figure 4.60 : Viscosity as a function of temperature for aqueous SWCNT nanofluids with 0.2 wt% PEG-POSS.	84
Figure 4.61 : Relative viscosity as a function of GNP concentration for aqueous nanofluids.	85
Figure 4.62 : Relative viscosity as a function of GNP concentration for EG-based nanofluids.	85
Figure 4.63 : Relative viscosity as a function of SWCNT concentration for aqueous nanofluids.	86
Figure 4.64 : Thermal conductivity enhancement as a function of PEG-POSS concentration for aqueous nanofluids at different GNP (800 m ² /g) concentrations.	87
Figure 4.65 : Thermal conductivity enhancement as a function of surface area of GNP for aqueous nanofluids without PEG-POSS at different GNP concentrations.	88
Figure 4.66 : Thermal conductivity enhancement as a function of PEG-POSS concentration for EG-based nanofluids at different GNP (800 m ² /g) concentrations.	89
Figure 4.67 : Thermal conductivity enhancement as a function of surface area of GNP for EG-based nanofluids without PEG-POSS at different GNP concentrations.	90
Figure 4.68 : Thermal conductivity enhancement as a function of PEG-POSS concentration for aqueous nanofluids at different SWCNT concentrations and ultrasonication time.	91
Figure 4.69 : Thermal conductivity enhancement as a function of PEG-POSS concentration for oil-based nanofluids at different GNP (800 m ² /g) concentrations.	92
Figure 4.70 : Thermal conductivity enhancement as a function of surface area of GNP for oil-based nanofluids without PEG-POSS at different GNP concentrations.	93
Figure 4.71 : Contact angle as a function of 800 m ² /g GNP concentration for aqueous nanofluids with PEG-POSS at different concentrations.	94
Figure 4.72 : Contact angle as a function of GNP concentration with different surface areas for aqueous nanofluids without PEG-POSS.	95
Figure 4.73 : Contact angle as a function of 800 m ² /g GNP concentration for EG-based nanofluids with PEG-POSS at different concentrations.	95
Figure 4.74 : Contact angle as a function of GNP concentration with different surface areas for EG-based nanofluids without PEG-POSS.	96

Figure 4.75 : Contact angle as a function of 800 m ² /g GNP concentration for oil-based nanofluids with PEG-POSS at different concentrations..	97
Figure 4.76 : Contact angle as a function of GNP concentration with different surface areas for oil-based nanofluids without PEG-POSS.	97
Figure 4.77 : Contact angle as a function of SWCNT concentration for aqueous nanofluids with PEG-POSS at different concentrations.	98
Figure 4.78 : Surface tension as a function of 800 m ² /g GNP concentration for aqueous nanofluids with PEG-POSS at different concentrations.	99
Figure 4.79 : Surface tension as a function of GNP concentration with different surface areas for aqueous nanofluids with no PEG-POSS.	100
Figure 4.80 : Surface tension as a function of GNP concentration with different surface areas for EG-based nanofluids with no PEG-POSS.	100
Figure 4.81 : Surface tension as a function of 800 m ² /g GNP concentration for EG-based nanofluids with PEG-POSS different concentrations.	101
Figure 4.82 : Surface tension as a function of SWCNT concentration for aqueous nanofluids with PEG-POSS at different concentrations.	102
Figure 4.83 : Surface tension as a function of 800 m ² /g GNP concentration for oil-based nanofluids with PEG-POSS different concentrations.	103
Figure 4.84 : Surface tension as a function of GNP concentration with different surface areas for oil-based nanofluids with no PEG-POSS.	103

PREPARATION AND CHARACTERIZATION OF CARBON-BASED NANOFLUIDS

ABSTRACT

Nanofluids are produced by the addition of nano-sized particles to the base fluid in order to increase the thermal conductivity of heat transfer fluids. Preparation of stable nanofluids with high thermal conductivity is a very complex process and their usage in heat transfer applications are related to many important parameters from the stability of nanofluids to their viscosity. Optimization of these parameters is essential for the practical use of nanofluids. The objectives of this study are to successfully prepare carbon-based nanofluids while investigating the stability mechanisms and to determine thermal, rheological, and surface properties of those nanofluids.

In this context, carbon-based nanofluids were produced through ultrasound technology in the presence of polyethylene glycol-derived polyhedral oligomeric silsesquioxane (PEG-POSS) as a stabilizer, for the first time in literature. Graphene nanoplatelets (GNP) with three different surface areas and single-walled carbon nanotubes (SWCNT) were used as nanoparticles; while distilled water, ethylene glycol (EG), and compressor oil were used as base fluids. Stability evaluations were carried out by Ultraviolet-Visible (UV-Vis) spectrophotometry and zeta potential measuring device (Zetasizer Nano). The aqueous 1.0 wt% SWCNT nanofluid with 0.1 wt% PEG-POSS had the highest zeta potential value of -68.2 mV. Thermal conductivity measurements were carried out by 3ω method. The maximum increase of 32% in thermal conductivity was measured for EG-based nanofluids having 2.0 wt% GNP and 0.3 wt% PEG-POSS. The increase of thermal conductivity in EG-based nanofluids was observed to be directly proportional to the amount of PEG-POSS.

KARBON BAZLI NANOAKIŞKANLARIN HAZIRLANMASI VE KARAKTERİZASYONU

ÖZET

Çok çeşitli uygulama alanına sahip olan nanoakışkanlar, ısı transferi sistemlerinde, kullanılan akışkanların ısıl iletkenlik katsayısını arttırmak amacıyla baz akışkanın içerisine, ısıl iletkenliği yüksek nano boyutlarda parçacıklar katılmasıyla üretilirler. Nanoakışkanların hazırlanması, hazırlanan nanoakışkanın ısıl iletkenliğinin artırılması her ne kadar basit görünse de çok karmaşık bir sistemdir. Nanoakışkanların ısıl iletkenliğinin artması ve ısı transferi uygulamalarında kullanılabilirliği, hazırlanan nanoakışkanın kararlılığından, viskozitesine kadar birçok önemli parametre ile bağlantılıdır. Nanoakışkanların pratikte kullanımı için bu parametrelerin optimizasyonu elzemdir. Bu tezin amacı, kararlı nanoakışkanların hazırlanması, ısıl iletkenliklerinin, reolojisinin ve yüzey özelliklerinin belirlenmesidir.

Bu bağlamda karbon bazlı nanoakışkanlar, literatürde ilk kez stabilizatör olarak kullanılan polietilen glikol türevi polihedral oligomerik silseskuokzan (PEG-POSS) varlığında ultrasonikasyon teknolojisi ile hazırlanmıştır. Baz akışkan olarak su, etilen glikol (EG) ve kompresör yağı kullanılan bu projede, nanoparçacık olarak farklı yüzey alanlarına sahip grafen nanoplateletler (GNP) ve tek duvarlı karbon nanotüpler (SWCNT) kullanılmıştır. Kararlılık değerlendirmesi için UV-Vis Spektrofotometrisi ve Zeta Potansiyeli ölçümleri yapılmıştır. En yüksek zeta potansiyeli -68,2 mV ile su bazlı, kütlece %0,1 PEG-POSS ve %1,0 SWCNT içeren nanoakışkana aittir. Isıl iletkenlik ölçümleri 3ω yöntemiyle gerçekleştirilmiştir. En yüksek ısıl iletkenlik artışı kütlece %0,3 PEG-POSS ve %2,0 GNP içeren EG bazlı nanoakışkanlar için ölçülmüştür ve bu değer %32'dir. EG bazlı nanoakışkanlarda PEG-POSS kullanımı ile ısıl iletkenlik artışının doğru orantılı olduğu gözlemlenmiştir.

1. INTRODUCTION

Nanotechnology was first introduced by Richard Feynman with the famous phrase as "There is plenty of room at the bottom." on December 29, 1959, in a speech to the American Physical Society. Feynman, who is considered as the father of nanotechnology, did not use the word nanotechnology in his speech, but years later it was understood that he described nanotechnology [1]. Another important person after Feynman is Norio Taniguchi and with his article published in 1974, the concept of nanotechnology was introduced for the first time in the world. The word nano comes from the Greek word 'nannos' which means dwarf. Today, nano is used as a technical unit of measurement and is one-billionth of any unit. Nanotechnology refers to the construction of structures, materials, and tools by special methods and techniques at the atomic and molecular scale and the ability of measuring, estimating, monitoring, and constructing activities at the nanoscale and the ability to benefit from some basic features of nanoscale. In 1981, molecules were imaged at the nanometer level with a Scanning Tunneling Microscope (STM), invented by Gerd Karl Binnig and Heinrich Rohrer. Atomic Force Microscope (AFM) was discovered shortly after the invention of the STM [2]. These inventions have significantly accelerated the development of nanotechnology. Many years after Maxwell's idea of incorporating micron and millimetric metal particles into the fluids in 1873 to enhance the thermal and electrical conduction of a fluid, Japanese scientist Iijima discovered carbon nanotubes (CNT). In 1995, Choi and his colleagues used CNTs in their study called as nanofluids [3;4]. High-performance nanofluids are prepared by adding nanoparticles such as metallic nanoparticles, carbon nanotubes, graphene to conventional coolants such as distilled water and ethylene glycol (EG). These nanoparticle-containing liquids have the following advantages over macroparticle-containing liquids:

- Better thermal conductivity than base fluids,
- Having a wear-resistant coating surface due to nanoparticles that can easily penetrate the contact area,

- No need for induction time to achieve the desired tribological properties due to their efficiency at ambient temperature in the application areas,
- Better thermophysical properties [5].

The most important issue for nanofluids with many advantages is that nanoparticles cannot remain stable in the fluid for a long time. The reason for the nanoparticles to settle in the liquid phase is the high reactivity due to the large surface area of the nanoparticles, the strong Van der Waals bonds between them, and the density difference between the nanoparticles and the base fluid [6]. For this reason, the most important challenge in the production of nanofluids is to keep balance between stability and thermal conductivity. Furthermore, it should be noted that nanoparticle structures vary based on production parameters such as temperature, pH, ultrasonication, microwave irradiation, and concentration.

The stability of nanofluids depends on some properties of nanoparticles and base fluids. According to Stoke's law, the sedimentation rate decreases with the reduction of the nanoparticle size, the decrease in density difference between the nanoparticle and the base fluid, and the increase in the viscosity of the base fluid. The stability of nanofluids can be determined by characterization methods such as zeta potential measurement, UV-Vis spectrophotometry, STM, SEM [7-9].

The most popular and economical method to solve the stability problem is the usage of surfactants. Due to their hydrophobic tail and hydrophilic head, surfactants reduce the interfacial tension of nanoparticles and base fluid. Water-soluble surfactants should be selected for nanofluids in which polar solvents are used as base fluids. Precipitation and agglomeration problems are encountered as a result of the wrong choice of surfactant; hence, important thermophysical properties of nanofluids such as viscosity, thermal conductivity, and specific heat are affected [10].

The base fluids used in this study are distilled water, ethylene glycol, and compressor oil, conventionally known as heat transfer fluid. Graphene nanoplatelet (GNP) and single-walled carbon nanotubes (SWCNT) with different surface areas were used as nanoparticles. Polyethylene glycol derivative polyhedral oligomeric silsesquioxane (PEG-POSS), which was not previously used as a stabilizer in the preparation of nanofluidics, was used for the first time in this study to ensure the stability of the nanofluid. Aqueous nanofluids containing SWCNT were ultrasonicated for 50 min and

100 min. UV-Vis Spectrophotometry and Zetasizer Nano for zeta potential measurement were used for stability evaluation. In this thesis, due to the opacity of carbon-based nanofluids, the effect of nanoparticle concentration on zeta potential was investigated by different processes such as centrifugation and dilution of samples. The usage of different carbon based nanoparticles, various concentrations of surface active agent, and 3 different base fluids; studying the other factors (e.g. pH, ultrasonication time etc.) affecting the thermal, rheological, and surface properties of nanofluids in heat transfer systems has made this project a multi-faceted and successful work.

1.1 Graphene

Graphene is a two-dimensional carbon element allotrope in the form of a honeycomb with a single atomic thickness, 0.142 nm long C—C bonds [11]. Graphene is an interesting material due to its high electron mobility at room temperature (250.000 cm²/ Vs), high surface area (theoretically 2600 m²/g) [12;13], and extremely good mechanical properties such as 1 TPa elastic modulus [14]. Transparent conductive electrodes, sensors, composites, solar cells, energy storage devices, and lithium-ion batteries are some of the applications of graphene.

For safe and trouble-free operation of electronic components, the removal of excess heat is essential. In this context, carbon allotropes such as graphite, diamond, carbon nanotube and graphene show promise with high thermal conductivity. The thermal conductivity of the monolayer graphene can reach up to 5000 W/m.K at room temperature [15].

Graphene has a high thermal conductivity, can be easily synthesized, requires less heat transfer fluid to remove a certain amount of heat, has low corrosion-clogging and erosion properties, has a lower coefficient of friction, has a larger surface area-volume ratio and therefore it has many advantages over other nanoparticles with its large increase in chemical reactivity and thermal conductivity [16;17]. Due to its superior properties, graphene nanoparticles are the preferred cause for heat transfer applications, but stable graphene containing nanofluid production is a challenging process. Frequent clustering problems cause clogging in micro heat transfer devices.

1.2 Carbon Nanotubes

Carbon nanotubes (CNT) are the folded form of graphene [18]. CNTs, which are allotropes of carbon element, are named according to the number of nanotubes they contain:

- Single-Walled Carbon Nanotube (SWCNT): It is formed by rolling a single layer of graphene on itself and has a diameter of 1-2 nm.
- Double-Walled Carbon Nanotube (DWCNT): It consists of two concentric carbon nanotubes in which the outer tube encloses the inner tube.
- Multi-Walled Carbon Nanotube (MWCNT): It consists of several layers rolling on itself with diameters ranging from 2 nm to 50 nm, depending on the number of nanotubes. The distance between the layers of these tubes is approximately 0.34 nm.

CNTs can also be divided into three groups, depending on the rolling direction:

1. Zig-Zag,
2. Chiral,
3. Armchair.

The folding direction (chirality) determines the properties of the electrical conductivity of CNTs. Even small changes in the diameter of CNTs lead to the conversion of their conductivity from metallic to semiconductor [19].

Since the first synthesis in 1991, CNTs are used as an additive for polymers, metallic and ceramic surfaces due to their good properties such as lightweight ($\sim 1.34 \text{ g/cm}^3$), high surface areas (theoretically $50\text{-}1315 \text{ m}^2/\text{g}$), good elastic modulus ($>1 \text{ TPa}$), and good conductivity [18;20-23]. CNTs have 100 times more tensile strength ($\sim 100 \text{ GPa}$) than steel and show thermal and electrical properties close to copper [24;25]. In their study, Kim et al. measured the thermal conductivity of MWCNTs at room temperature as 3000 W/m.K . They also stated that the thermal conductivity of the bulk MWCNTs was at least twice as high as that of the individual ones [26]. A similar study with SWCNTs indicated that the increase in thermal conductivity values in the bulk was greater than 2000 W/m.K [27]. Thermal conductivity varies depending on the atomic arrangement of carbon nanotubes, tube diameter, amount of structural defect, impurities they have [28-30].

Intermolecular interactions of CNTs lead to agglomeration. This makes dispersing difficult in polymeric media and solvents. Therefore, purification and functionalization of CNTs are critical for dispersion and reactivity. Purification removes unwanted particles from the synthesis process and functionalization brings a functional group into the side chains or ends of the CNTs [31]. It is also known that functionalization methods that ensure good distribution of CNTs reduce toxicity. For this purpose, non-covalent functionalization and covalent functionalization methods ensure that the CNTs are distributed in the medium.

Some important surfactants, such as polyethylene glycol, sodium dodecyl sulfate, and dodecyl-benzene sodium sulfonate, are widely used to reduce the agglomeration tendency of CNTs in water and other solvents. The presence of benzene rings ensures efficient dispersion of CNTs. The stacking interactions of benzene rings on CNT surfaces are thought to increase the adsorption rate of surfactants. Ultrasonication, one of the physical dispersion methods using vibration energy, is an effective method for overcoming the intermolecular attractive forces of CNTs and reducing the tendency of agglomeration [32].

Carbon nanotubes are used in different applications in various fields, including medicine, energy, environment, and sensors, as shown in Figure 1.1.

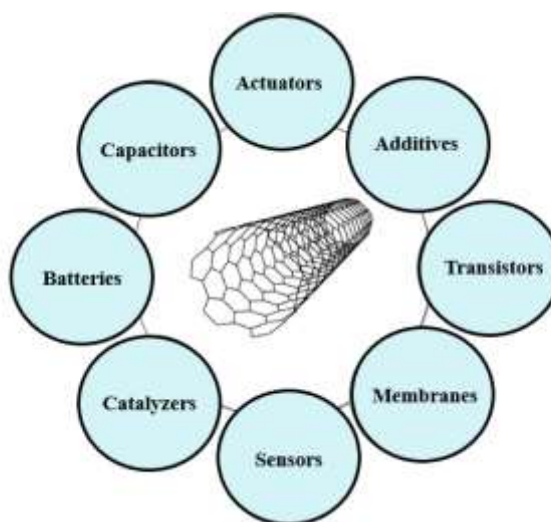


Figure 1.1 : Some applications of carbon nanotubes, re-drawn from [32].

1.3 Polyhedral Oligomeric Silsesquioxane (POSS)

Silsesquioxanes are structures having the empirical formula $\text{RSiO}_{1.5}$, containing hydrogen or organic functional radical groups such as alkyl, alkylene, aryl, and arylene

[33]. The name Silsesquioxane is derived from the word 'sesqui' which means 'one and a half' in Latin, starting from 1.5 oxygen atoms in its empirical formula. The first oligomeric organosilsesquioxanes $(\text{CH}_3\text{SiO}_{1.5})_n$ were produced in 1946 by hydrolysis of methyl trichlorosilane and dimethylchlorosilane [34]. As shown in Figure 1.2, silsesquioxanes can be randomly arranged, ladder, cage, or partially cage [35].

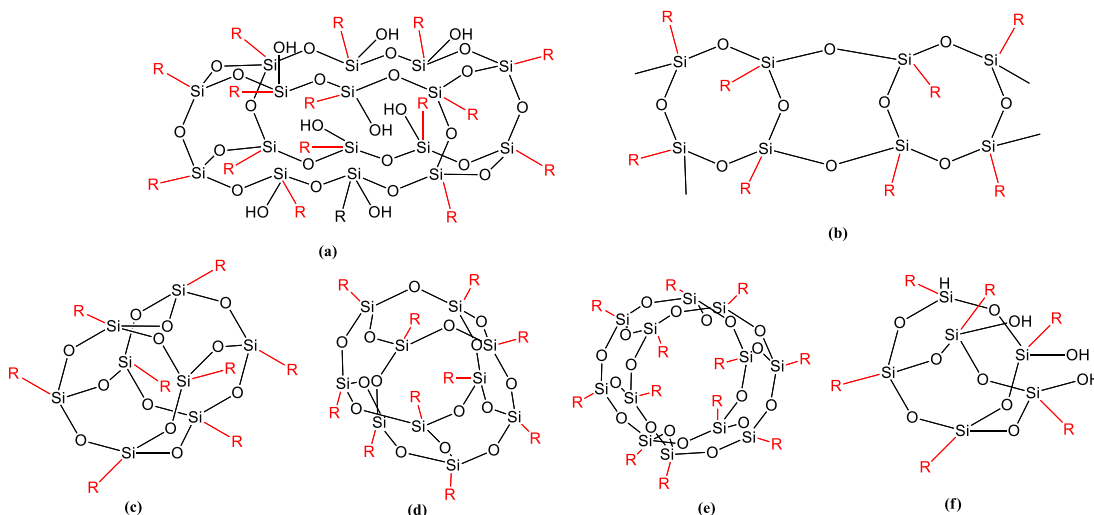


Figure 1.2 : Silsesquioxanes (a) randomly arranged; (b) ladder; (c), (d), and (e) cage; (f) partially cage.

Cage silsesquioxanes are often referred to as polyhedral oligomeric silsesquioxanes (POSS). Researches have shown that the use of POSS molecules in polymeric composites increases the strength and stiffness but does not alter lightness and ductility. POSS molecules are also known to reduce flammability and viscosity of polymeric composites [36]. Additionally, POSS can be dispersed by chemical bonding into the polymer or by physical mixing. The compatibility of POSS and polymer depends on the compatibility of the group bound to the structure of POSS with the polymer. In nanocomposite studies, nonionic POSS derivatives are generally used in order to increase the distribution of nanoparticles. The small molecular size of these particles has a positive effect on the dispersion process [37]. Figure 1.3 shows the chemical structure of polyethylene glycol (PEG)-POSS. It is known that PEG-POSS can form spherical micelles with an average diameter of 200 nm in aqueous systems [38].

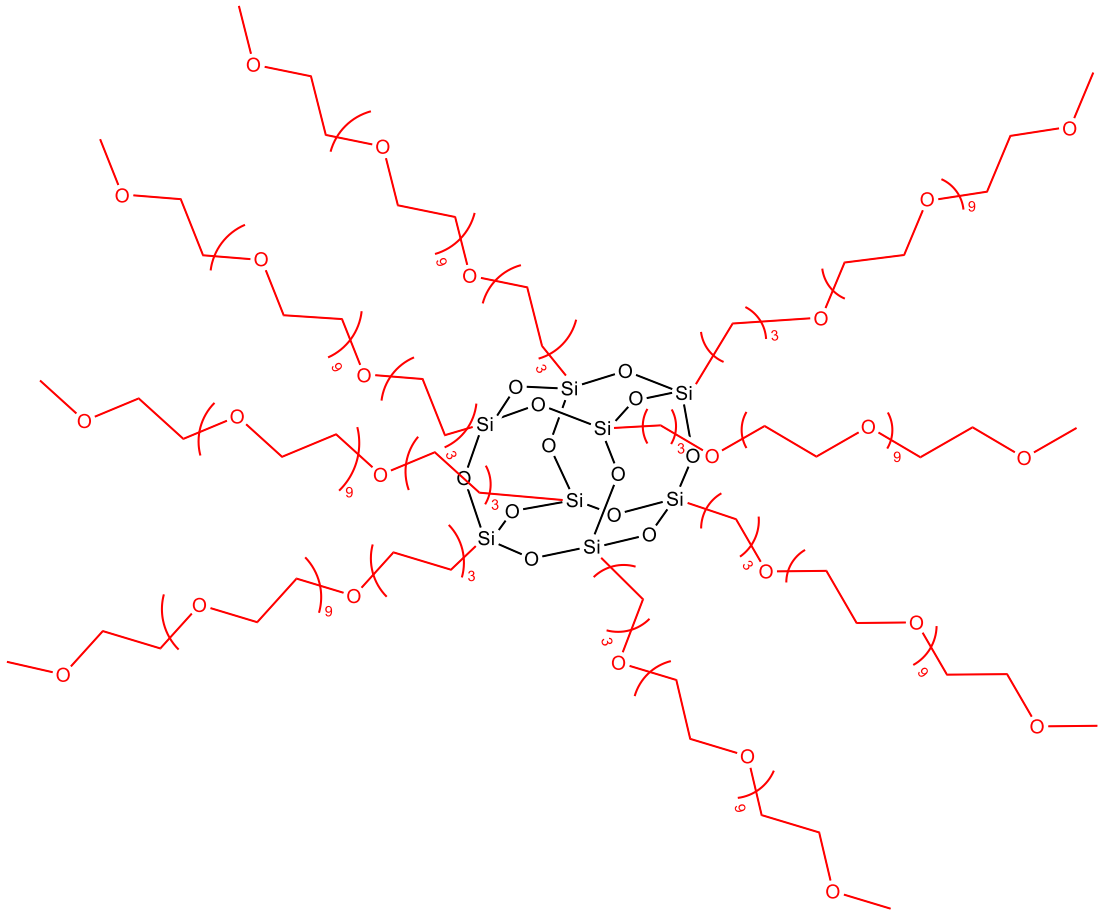


Figure 1.3 : Chemical structure of PEG-POSS.

1.4 Stability of Nanofluids and Zeta Potential

The state of the particles in the dispersion is determined by the interactions between the particles as well as the interactions between the particle and the base fluid. Dispersion stability is best explained by Derjaguin, Landau, Verwey, and Overbeek (DLVO) theory. The DLVO theory is mainly concerned with Van der Waals attractive forces of two particles in the water and the primary repulsive forces caused by the electrical charge of the particles [39].

Van der Waals attractive forces;

$$V_A = \frac{-A}{12} \left[\frac{1}{x(x+2)} + \frac{1}{(x+1)^2} + 2 \ln \frac{x(x+2)}{(x+1)^2} \right] \quad (1.1)$$

$x = \frac{H}{2r}$ expressed in Equation 1.1, H is the distance between the surfaces of two nanoparticles, r is the radius of nanoparticles. A is Hamaker constant. This constant is related to the attraction potential of the particles in a medium formed between each other and the medium. If the interaction of nanoparticle with the medium is high, the

stability of the dispersion will increase as it reduces the interaction between other nanoparticles. In addition, the formation of Electrical Double Layer (EDL) forms a repulsion force between nanoparticles against Van der Waals attractive forces and is an important parameter for dispersion stability. The potential difference between the two charged particles is shown in Equation 1.2.

$$V_R = \epsilon r \Psi_0^2 \ln(1 + \exp(-\kappa H)) \quad (1.2)$$

ϵ is the dielectric constant of the medium, Ψ_0 is the surface charge of nanoparticles, κ is the length of Debye and is expressed in Equation 1.3.

$$\kappa = \frac{8\pi n e^2 z^2}{\epsilon K T} \quad (1.3)$$

n represents the number of ions per cm^2 , e represents the electrical charge, and z represents the counter ions and forms an energy barrier against Van der Waals attraction, which causes the agglomeration of nanoparticles. If Van der Waals attraction overcomes the potential in the EDL, the particles will begin to agglomerate and collapse.

As shown in Figure 1.4, the region where the particles and counter ions are strongly bonded to each other is the Stern Layer, and the region where the counter ions are scattered around the particle is Diffuse Layer. When a particle is subjected to an effect such as gravitational force or magnetic forces, it acts like a single particle with all the ions around it in a region called the slipping plane. The electrical charge of the slipping plane is called the zeta potential. The magnitude of the zeta potential is a measure of the stability of the colloidal system. The greater the positive or negative the magnitude of the zeta potential of dispersion, the more the particles will tend to repel each other. This prevents clustering, agglomeration, and precipitation of the particles in the dispersion.

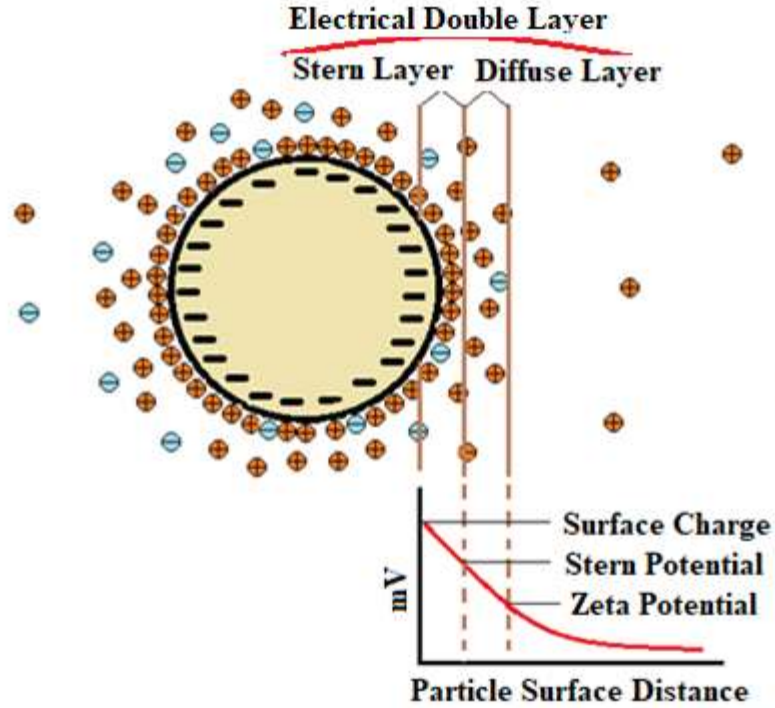


Figure 1.4 : EDL regions and electrical potentials of a particle (adapted from [40]).

For a dispersion to be considered stable, the zeta potential value must be greater than the absolute 30 mV. The most important factor affecting the zeta potential is pH. When the zeta potential is plotted against the pH values by changing the ion equilibria of dispersion, the pH value where the zeta potential is measured as 0 is called an isoelectric point. The further the pH of the dispersion is from this point, the more stable the dispersion is. This pH value is 3.1 for GNP dispersions [6].

When an electric field is applied to dispersion with charged particles, the particles move towards the oppositely charged electrode of the charge they have. This movement is called electrophoresis. The viscous forces in the dispersion tend to interfere with this movement and when they are in equilibrium with the force exerted by the electric field, the particles begin to move at a constant speed. This velocity is called electrophoretic mobility and depends on the magnitude of the applied electric field, the dielectric coefficient and viscosity of the medium, and the zeta potential of the dispersion. Electrophoretic mobility is found by the Henry Equation below.

$$U_E = \frac{2\epsilon z f(\kappa a)}{3\eta} \quad (1.4)$$

In Equation 1.4, electrophoretic mobility U_E , dielectric coefficient ϵ , zeta potential ζ and, viscosity η are shown. According to the Smoluchowski approach, for aqueous media and dispersions with an average electrolyte concentration, the $f(\kappa a)$ value is taken into account as 1.5. For dispersions with low dielectric coefficients, the Huckel approach is used, where $f(\kappa a)$ is taken as 1.0. As shown in Figure 1.5, the electrophoretic mobility of the ions moving to the opposite charged electrode is measured by Laser Doppler Velocimetry (LDV). The zeta potential of the dispersions whose electrophoretic mobility is measured by LDV is obtained by the Smoluchowski or Huckel approach.

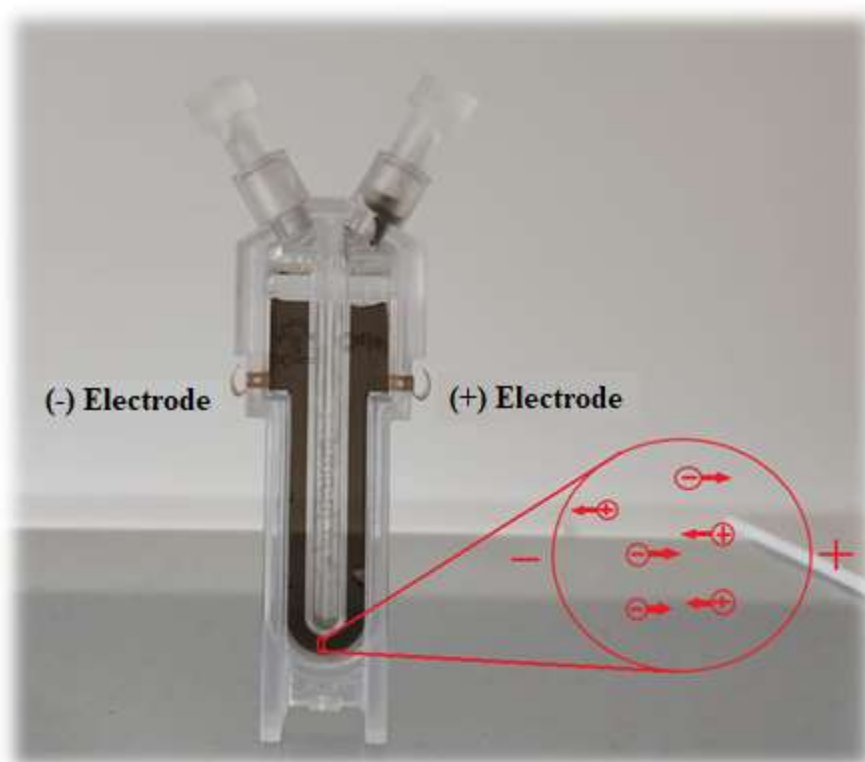


Figure 1.5 : Zetasizer Nano device cuvette, electrodes, and direction of movement of charged ions.

1.5 Determination of Stability by UV-Vis Spectrophotometry

A molecule or ion absorbs light in an environment where it is visible or exposed to ultraviolet light and performs electron transitions. Due to the extra energy provided by the light, the electrons in the molecule jump to a higher energy state than the current steady states. The orbital of excited electrons are determined by the wave function. These transitions are characteristic and are six types, as shown in Figure 1.6. If the light wavelength is low, the orbital level is large [41].

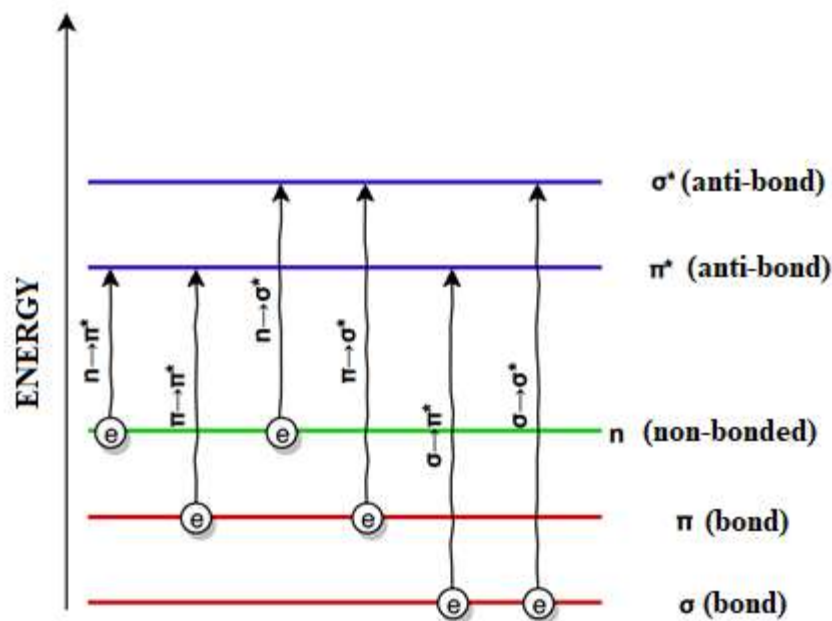


Figure 1.6 : Possible electron transitions (energy increases from left to right).

UV-Vis spectrophotometry is based on the principle of absorption of monochromatic light in the ultraviolet (10-380 nm) or visible region (380-780 nm) by the compounds in the solution. UV-Vis spectrophotometry is a simple, fast, low-cost and consistent method of quantitative analysis. Transitions at specific wavelengths can be used to identify molecules or inorganic ions and complexes in solution.

The image of UV-Vis spectrophotometry working principle is given in Figure 1.7. While deuterium lamps are used as UV sources, tungsten lamps are used for the visible zone. The light from the source is reduced to a specific wavelength by the lenses in the monochromator. This light beam is sent to the sample and the data obtained with the beam scattered from the sample detected by the detector is transferred to the computer.

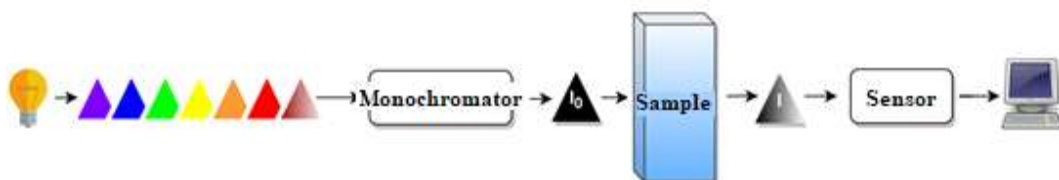


Figure 1.7 : Working principle of UV-Vis Spectrophotometry.

The transmittance value of the sample is the ratio of the scattered beam to the incident light.

$$T = \frac{I}{I_0} \quad (1.5)$$

The relationship between light transmittance and absorbance is calculated by Equation 1.6.

$$A = \log T \quad (1.6)$$

According to Beer Lambert's law, Equation 1.7, the absorbance of a solution varies depending on the concentration of the solution and the beam path of light.

$$A = \epsilon bc = \log \frac{I_0}{I} \quad (1.7)$$

The absorbance of sample A given in the Beer Lambert equation, ϵ molar absorption coefficient [$\text{L}\cdot\text{mol}^{-1}\text{cm}^{-1}$], b light path [cm], c sample concentration [$\text{mol}\cdot\text{L}^{-1}$], I_0 is the intensity of incident light and I is the intensity of incident light [42]. The Molar absorption coefficient found in the Beer Lambert equation is constant for each solution and does not change with concentration. Therefore, when graph of absorbance at a specific wavelength versus concentration of a solution is drawn, since the slope will be linear, the unknown concentration of sample of the same solution can be found by UV-Vis spectrophotometry. UV-Vis spectrophotometry applications are quite wide. It is mainly used for qualitative and quantitative analysis such as enzyme analysis, molecular weight determination. It is often a preferred method for applications of analytical chemistry such as quantitative determination of metal ions, highly conjugated organic compounds and biological macromolecules. The analysis is generally suitable for solutions, but solids and gases can also be examined [43]. In addition, UV-Vis spectrophotometry is widely used to determine the stability of nanofluids containing metallic and carbon-derived nanoparticles and surfactants and to investigate the precipitation performance [7-9].

1.6 Theory of 3 ω Method

The thermal probe with a length of $2l$ and a radius r , which serves as both a heater and a thermometer, is immersed in the dispersion. The wire of the thermal probe is excited by alternating current, $I(t) = I_0 \cos(\omega t)$. The temperature $\theta(f, t)$ has component 2ω proportional to the power $I^2(t)R_0$. 2ω and $2f$ notations are used since thermal generation occurs at the second harmonic of the modulated excitation current. Since the metal wire withstands high thermal conductivity and is very thin in the radial direction, it can be assumed that $\theta(f, t)$ is the same across the cross-sectional area. The electrical resistance $R(t)$ of the metal wire oscillates at a frequency of 2ω , Equation 1.8.

$$R(t) = R_0[1 + r_{el}\theta_{2\omega} \cos(2\omega t - \varphi)] \quad (1.8)$$

The voltage of the wire is given in Equation 1.9.

$$V(t) = I(t)R(t) = I_0 R_0 \left\{ \cos(\omega t) + \frac{1}{2} r_{el} \theta_{2\omega} [\cos(\omega t - \varphi) \cos(3\omega t - \varphi)] \right\} \quad (1.9)$$

The expression 3ω is a combination of the current ω and the resistance change of 2ω :

$$V_{3\omega}(f) = \frac{I_0 R_0 (2l)}{2} r_{el} \theta_{2\omega} \quad (1.10)$$

For the thermal probe, the stored heat is negligible at frequencies as low as 1 kHz and all electrical power is assumed to be transmitted to the liquid by transmission. The temperature, in this case, is given in Equation 1.11.

$$\theta_{2\omega} = P_{2\omega} \frac{Z_s}{2} = \frac{I_0^2 \rho_{el} (2l) Z_s}{2\pi r^2} \frac{Z_s}{2} \quad (1.11)$$

In this expression, ρ_{el} is the density and Z_s is the thermal resistance between the liquid sample and the half-length wire. Since it is more appropriate to use dimensionless resistance, F factor is given in the Equation 1.12 [44].

$$F = \frac{Z_s}{Z_p} = \frac{Z_s / 2\pi r l}{l / (\pi r^2 k_p)} = \frac{k_p r}{2l^2} Z_s \quad (1.12)$$

Z_s [m^2/W] is the specific heat resistance of the interface. Z_p is the thermal resistance of the half-length wire in the axial direction, and end-point supports are regarded as endless heat sources. If $F \ll 1$, the heat losses at the support points of the wire can be omitted. When Equation 1.12 is set,

$$V_{3\omega_{eff}}(f) = \left(\frac{l_{eff}l}{\pi r^2}\right)^3 C_M F(f) \quad (1.13)$$

is obtained and $C_M = \rho_{el}^2 r_{el} / k_p$ is the material benefit indicator of the wire used [45].

Alternating current solution of temperature rise $\theta(r, f)$ realized by linear heat source in infinite and homogeneous medium is periodically excited at cylindrical coordinates.

The temperature for unit power, $P_{2\omega}/l$ [W/m] is

$$\theta(r, f) = \frac{P_{2\omega}/l}{2\pi k_s} K_0(\sigma_s r) \quad (1.13)$$

obtained by Equation 1.13 [46]. K_0 is the zero-order Bessel function. The complex variable is $\sigma_s r = (1 + i)/\mu_s$ and $\mu_s = [\alpha_s \pi^{-1} (2f)^{-1}]^{1/2}$ refers to the heat dissipation in the medium at a frequency of $2f$ and $\alpha_s = k/\rho c$ is the coefficient of thermal dissipation. In the case of low frequency, $r/\mu_s \ll 1$, the Equation 1.14 is obtained by $K_0(\sigma_s r)$ expansion.

$$\theta_{2\omega} = -\frac{P_{2\omega}}{2\pi k_s l} \left(\gamma + \ln \frac{\sigma_s r}{2} \right) \quad (1.14)$$

$\gamma = 0.5772$ and it is Euler constant. When Equation 1.14 rearranged

$$\theta_{2\omega} = -\frac{P_{2\omega}}{2\pi k_s l} \left(\ln \frac{\mu_s}{1,2594r} - i \frac{\pi}{4} \right) \quad (1.15)$$

is obtained [47] and with $z_s = 2\pi r l \theta_{2\omega} / P_{2\omega}$, the F factor becomes:

$$F = \frac{k_p r^2}{2k_s l^2} \left(\ln \frac{\mu_s}{1,2594r} - i \frac{\pi}{4} \right) \quad (1.16)$$

The F factor is inversely proportional to the thermal conductivity k_s of the liquid. The real part is used to determine the thermal conductivity of solids. The relationship between the nanofluid and pure water by data reduction method is given in Equation 1.17.

$$\frac{k_s}{k_w} = \frac{Im(F_w)}{Im(F_s)} \quad (1.17)$$

S sub-index represents liquid dispersion and W sub-index represents pure water.

1.7 Rheology Measurements

Rheology is a science that examines the flow behavior of complex viscoelastic materials with both solid and liquid properties, depending on force, deformation and time. The term rheology is derived from the words 'rheos', which means work, and 'logos', which means science [48]. Rheological knowledge is very important for fluid mechanics, petroleum-refinery applications, drilling operations, polymer science, mining, food (chocolate) production applications. Rheological behaviors play an important role in determining flow characteristics such as required pumping power and pressure analysis in the flow channel [49].

Regardless of solid and liquid, all materials are deformed under stress. The amount of deformation may vary according to the tensile strength, speed, and direction of force, viscosity of the material. Viscosity refers to the resistance of fluids to flow. Most fluids require a small amount of stress for the flow start [50]. Fluids below this critical stress level, called yield stress, behave as solids and do not show yielding [51].

Fluids are classified in two ways as Newtonian and non-Newtonian. In Newtonian fluids, there is a linear relationship between the applied shear stress and the deformation rate. Such fluids have a constant viscosity at a constant temperature. If the viscosity changes depending on the applied shear stress, the fluid is defined as non-Newtonian and the relationship between shear stress and deformation rate is distorted from linearity. In the graph shown in Figure 1.8 (a), fluids with increased shear stress and viscosity show shear thickening or dilatant flow behavior. In the graph shown in Figure 1.8 (b), fluids whose shear stress increases while viscosity decreases show shear thinning or pseudoplastic behavior [49].

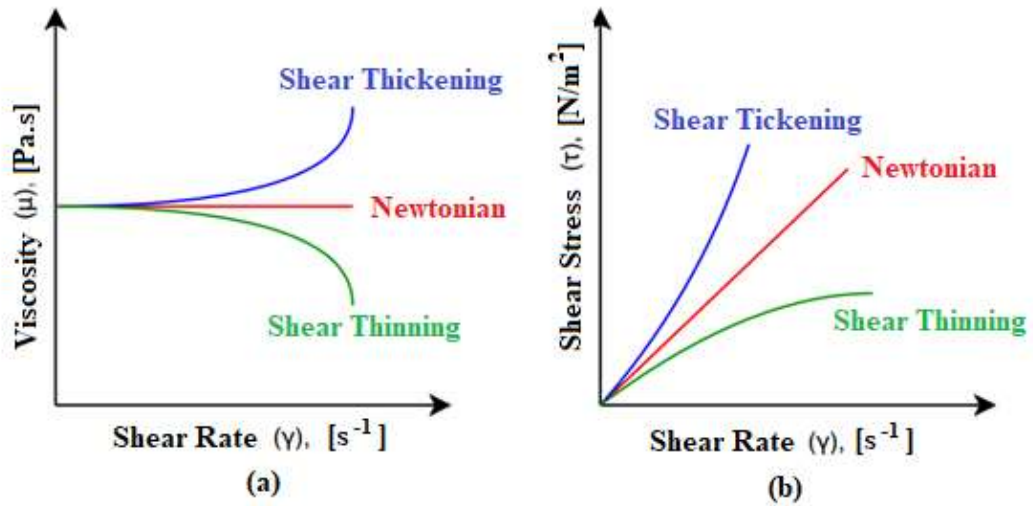


Figure 1.8 : Viscosity versus shear rate (a) and shear stress vs shear rate (b) plots of different fluid types.

For nanofluid applications, rheological properties need to be well analyzed. In most cases, the flow characteristics of the suspensions and dispersions vary with the addition of a small amount of solid particles. In nanofluids, the thermal conductivity and viscosity value increase as the nanoparticle concentration increases. The increase in viscosity causes negative effects such as pressure drop in the flow channel, erosion on the surface of the channel, an increase in the required pumping power. Therefore, an ideal nanofluid should have a low viscosity while showing high thermal conductivity [52].

There are two types of devices for rheology analysis. The viscometer is a device mainly used to measure viscosity. The rheometer is used for measuring rheological properties in a wider range of conditions. There are two common methods for rheometric measurements of fluid systems: capillary and rotational. In the capillary method, the flow of the test liquid is carried out by means of externally applied pressure or by spontaneous hydrostatic effect through a narrow tube. The flow rate varies depending on the viscosity of the liquid. Capillary measurements are considered the most accurate way to determine the viscosity of the Newtonian and some non-Newtonian fluids. This method, which is generally simpler in design, is cheaper than the rotational method. There are two types of capillary analysis methods: Glass Capillary Viscometer and Extrusion Capillary Viscometer. Polymer solutions, ceramic slurries, foodstuffs, inks, and coatings can be analyzed by this method.

In the rotational method, the test fluid is subjected to shear forces continuously, between one or both rotating surfaces. These devices can apply shear to the sample for an unlimited period of time. In this way, the behavior of the liquid under temporary or controlled rheometric conditions can be monitored. Rotational methods may also include oscillation and normal stress tests to characterize the viscoelastic properties of the samples. Rotational measurements are divided into two categories as stress-controlled or speed controlled (Brookfield type). In stress-controlled measurements, a constant torque is applied to produce rotation and the rotation speed is determined. The shear rate is obtained from the rotational speed with the help of the chosen rotating shaft in geometry according to the sample type, given in Figure 1.9. In speed-controlled measurements, the rotational speed is constant and the torque generated by the sample is determined using a suitable stress detection device, such as a torsion spring or strain gauge.

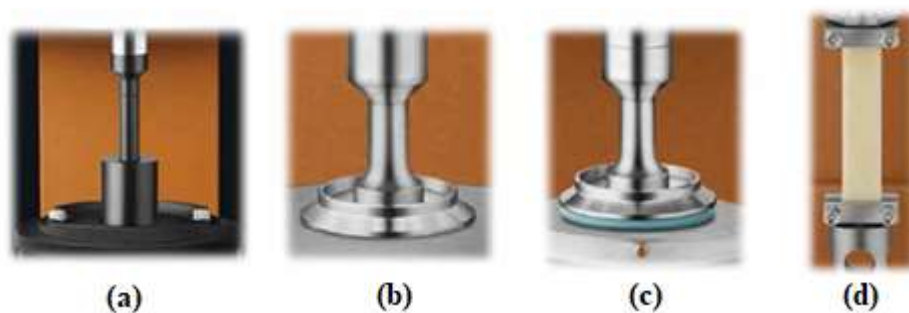


Figure 1.9 : Shaft types (a) concentric cylinder, (b) cone, (c) parallel plate and (d) torsion.

Some devices are capable of operating both stress-controlled and speed-controlled modes. They can also analyze at different temperature conditions. In general, rotational methods are more suitable for measuring concentrated suspensions, gels, and pastes, but are less sensitive than capillary methods [53].

1.8 Contact Angle and Surface Tension

Wetting behavior of liquids on solid surfaces is measured with a goniometer. The goniometer essentially consists of a light source, a syringe, a high-resolution camera, the plane on which it will be placed, and computer components. The device can measure the angle of contact with the sessile drop method while measuring the surface tension with the pendant drop method shown in Figure 1.10. In the pendant drop

method, the liquid to be analyzed is dropped onto the solid surface by means of a metal needle syringe. The image of micron size drop is recorded with a high-resolution camera and transferred to a computer. Afterward, the related equations are solved by means of the software in the device and the contact angle value is reflected the user. These simple and convenient instruments, which require several μL of liquid and surface for analysis, can measure static and dynamic contact angles. On the other hand, due to the smallness of the liquid and the substrate, impurities can affect the result relatively further.

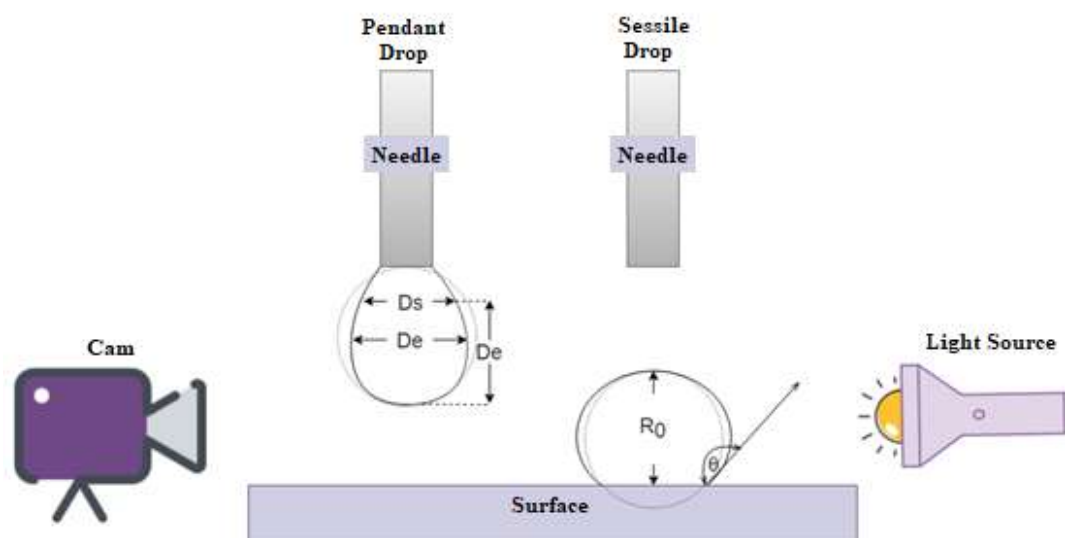


Figure 1.10 : Pendant drop and sessile drop methods.

The Young's Equation, Equation 1.18, defines the relationship between the contact angle and the free energies of the solid, liquid and gas phases in thermodynamical equilibrium. The Young's Equation is only applied to uniform solid surfaces that do not interact with the fluid to be measured with homogeneously dispersed liquids. Wenzel and Cassie-Baxter equations should be used for rough surfaces [54]. The three equilibrium phases and the contact angle are shown in Figure 1.11. The term wettability describes the contact between a liquid and a solid surface and is the result of intermolecular interactions that occur when the surfaces are combined. The contact angle gives information about the wettability and surface energy of the material. Materials with a contact angle of more than 150, more than 90, and less than 90 degrees are classified as super-hydrophobic, hydrophobic, and hydrophilic, respectively.

$$\cos\theta = \frac{\gamma_{\text{solid-air}} - \gamma_{\text{solid-liquid}}}{\gamma_{\text{liquid-air}}} \quad (1.18)$$

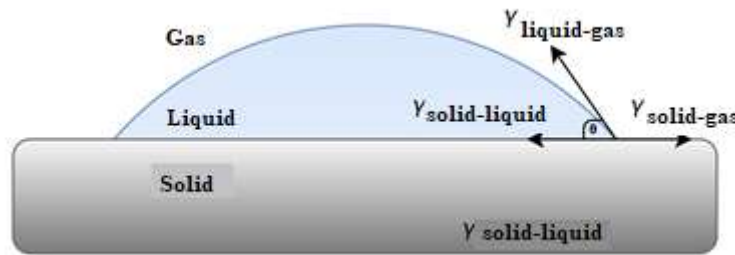


Figure 1.11 : Contact angle between droplet and surface.

The Young-Dupre equality, given in Equation 1.19, shows the relationship between contact angle and adhesion. In the equation W_A refers to the adhesion force. According to the equation, for perfect wetting, the $\cos \theta$ must be zero.

$$W_A = \gamma_{\text{liquid-air}}(1 + \cos \theta) \quad (1.19)$$

In order to achieve wettability, a decrease in contact angle, i.e. an increase in adhesion stress and surface roughness, must be achieved. Both effects cause a significant decrease in contact angle. In addition, the contact angle varies depending on droplet size and gravity. Therefore, a unique and precise criterion for measuring surface wettability cannot be determined. It is known that the contact angle is used to determine the adhesion quality of protective and decorative coatings and polymer composite structures. There are no consistent studies in the literature on the direct effect of the size and concentration of nanoparticles dispersed in a liquid on the contact angle [55].

Although there are many methods for surface tension analysis, pendant drop method is widely used because of its practicality and consistent results. The surface tensions of various fluids such as polymers, liquid crystals, and other low molecular weight liquids are measured using this method [56]. In this method, the surface tension value is calculated by using the diameter at the peak-midpoint of the drop that is allowed to fall free at the needle tip and the density difference between the liquid and the medium. The way the drop falls is related to the effects between surface tension or interface tension and gravitational force. The interfacial tension between the internal and external phase causes a pressure increase inside the drop. The drop is deformed by the

effect of hydrostatic pressure and gravity generated. The curvature of the drop interface also changes in the vertical direction. The drop takes on the characteristic pear shape given in Figure 1.12. The degree of deviation from the sphericity is given by the ratio between the weight of the drop and the surface tension. The pendant drop method is expressed by the Young Laplace equation as follows:

$$\Delta P = \gamma \left(\frac{1}{R_1} + \frac{1}{R_2} \right) = \Delta \rho g z \quad (1.20)$$

In Equation 1.20, ΔP is the pressure difference, γ is the surface tension, R_1 and R_2 are the fundamental curvature radii ($R_1 = R_2 = R_0$ for the drop peak), $\Delta \rho$ is the density difference between the medium and the liquid, g is the gravity acceleration, z is the drop height.

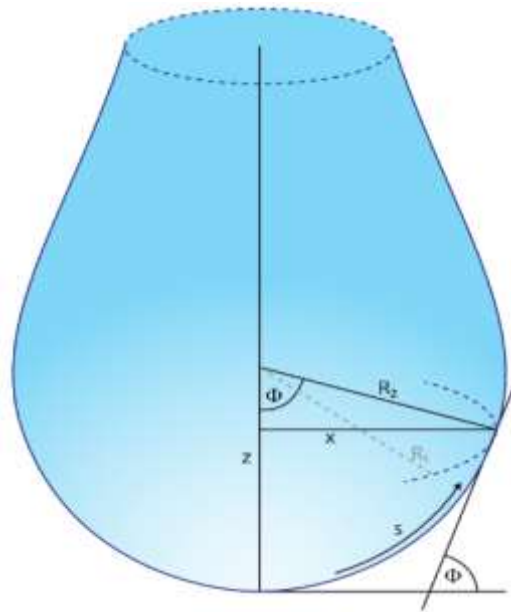


Figure 1.12 : Variables used in surface tension calculation according to the hanging drop method (from Kruss Scientific).

The Young-Laplace equation can be applied if the droplet is spherical. Bond Number (shape factor) with zero boundary conditions should be used in order to calculate the pressure difference and to solve multi-dimensional differential equations. With the Bond Number, the equation with a dimensionless variable can be written using the top radius of the drop.

$$B_0 = \frac{\Delta \rho g R_0^2}{\gamma} \quad (1.21)$$

In Equation 1.21, B_0 and $\Delta\rho$ represent the Bond number and the density difference between the medium and the liquid, respectively. Additionally, ρ is the gravitational acceleration, R_0 and γ are peak diameter and surface tension, respectively.

Today's devices can calculate these equations automatically and give solution directly thanks to the points they mark around the drop image with the software they contain. The drop shape on the image is spherically simulated during analysis. The basic curvature diameters are calculated by comparing the deformed drop and the spherical drop (by analyzing the shadow). The bond number is generated over curvature diameters. The difference between the media and liquid density values entered into the device is taken. The gravitational acceleration and peak diameter values are also written to the equation to obtain the unknown surface tension value [57].

2. LITERATURE SURVEY

Detailed nanofluid studies accelerated approximately 120 years after the revealed of Maxwell's theory of increasing thermal and electrical conductivity in suspensions. The first study on the use of carbon nanotubes in nanofluids is carried out by Choi et al. (2001) [58]. The thermal conductivity of dispersions containing MWCNT as nanoparticles and poly α olefin as base fluid were investigated. The increase in thermal conductivity of dispersions containing 1.0% by volume of nanoparticles has been reported as 160%. Although this abnormal increase was well above the theoretical expectations, a nonlinear correlation between nanotube concentration and thermal conductivity was obtained [58].

Xie et al. (2003) in their study, MWCNT nanoparticles dispersed in three different base fluids (distilled water, EG, and decene) with the help of sonicator. Due to its hydrophobic nature, nanoparticles were added to distilled water and EG after being functionalized with oxygen-carrying functional groups. In decene based nanofluids, oleyamine was used as a surfactant. Thermal conductivity measurements were performed by transient hot wire (THW) method. The maximum thermal conductivity increases for distilled water, EG and decene based nanofluids containing 1.0% by volume MWCNT are 7, 12.7 and 19.6%, respectively [59].

Assael et al. (2004) used distilled water as the base fluid and MWCNT as the nanoparticle. Sodium dodecyl sulfate (SDS) was used as a surfactant for the stability of nanofluids and its content is 0.1 wt%. Ultrasonication was chosen as the dispersion preparation technique. The maximum thermal conductivity increase measured by THW is 38% for MWCNT of 0.6 vol% [60].

In their study, Liu et al. (2005) used MWCNT and engine oil, 5 vol% n-hydroxy succinimide as a surfactant. After dispersing the base fluids and nanoparticles with a magnetic stirrer, homogeneity of dispersions was achieved by ultrasonication. The

maximum increase in thermal conductivity, measured using the modified THW method, is 30% for 2.0 vol% MWCNT dispersions [61].

Assael et al. (2005), used distilled water as base fluid, MWCNT as a nanofluid, as well as cetyl trimethyl ammonium bromide (CTAB) and Nanospense AQ as surfactants. THW was used as the thermal conductivity measurement method. The 34% increase in thermal conductivity obtained in dispersions containing 0.6 vol% MWCNT and CTAB was recorded as maximum [62].

Assael et al. (2006), in another study, have prepared distilled aqueous nanofluids containing MWCNT. Different surfactants were studied, 1 vol% CTAB, 0.35 vol% SDS and Triton-X were used. Ultrasonication was preferred for homogenization of nanofluids. The thermal conductivity increases measured by the THW method were 34%, 21% and 13% for dispersions containing CTAB, SDS and Triton-X with 0.6 vol% MWCNT, respectively [63].

Ding et al. (2006) used distilled water and CNT in their studies. 0.25 vol% Gum Arabic was used as a surfactant and ultrasonic bath was preferred for the preparation of dispersions. KD2 Pro method was used for thermal conductivity measurement. The maximum increase in thermal conductivity is 25% for dispersions containing 0.5 wt% CNT [49].

Hwang et al. (2006) used MWCNT as nanoparticles, as the base fluid distilled water and SDS as a surfactant, in their nanofluid study. The nanofluids were kept in ultrasonication for 2 hours to homogenize. The maximum increase in thermal conductivity measurements by the THW method is 11% for dispersions containing 1.0 vol% MWCNT [64].

Hwang et al. (2006) in another research, studied with MWCNT, fullerene, copper oxide, silicon dioxide, and silver as nanoparticles. Various base fluids such as distilled water, EG, silicone oil, poly α olefin were used and SDS was used as a surfactant. Ultrasonication was performed for 2 hours to obtain a homogeneous dispersion. THW method was used to measure the increase in thermal conductivity. The maximum increase in thermal conductivity was recorded as 7% for dispersions containing 1.0 vol% MWCNT [65].

Chen et al. (2008) used MWCNT as nanoparticle, EG and distilled water as base fluid. In this study, thermal conductivity was measured by THW, which was not use

surfactant but functionalized nanoparticles with potassium hydroxide. The dispersions using nanoparticles functionalized with potassium hydroxide precipitated after 5 minutes. Subsequently, distilled water and EG-based nanofluids containing nanoparticles modified by mechanochemical reaction method were prepared. For 1.0 vol% MWCNT nanofluids, the maximum thermal conductivity increases were 12% and 17.5% for distilled water and EG, respectively [66].

In their study, Amrollahi et al. (2008) used EG as the base fluid and chose SWCNT as the nanoparticle. The nanofluids were ultrasonicated to disperse the nanoparticles in the base fluid. In this study, which was not use surfactant, the parallel plate method was used for thermal conductivity measurement. The maximum thermal conductivity increase was 20% for dispersions containing 2.5 vol% SWCNT [67].

Nanda et al. (2008) used poly α olefin and EG as base fluid and SWCNT as nanoparticles. To ensure stability, acid treatment was used and $-\text{COOH}$ groups were added to SWCNT. Maximum thermal conductivity increases were 12% and 35% for EG and poly α olein dispersions containing 1.1 vol% SWCNT, respectively [68].

In their study, Glory et al. (2008) used MWCNT as nanoparticle, distilled water was used as the base fluid. In addition, Gum Arabic was added to the nanofluids to ensure stability. Ultrasonication was performed before and after the addition of Gum Arabic at different times. Visual observation method and UV-Vis spectrophotometry were used for stability measurements. While 20 minutes of ultrasonication dispersions could not remain stable, 50 minutes of ultrasonication samples were stable for 5 days. In this study, the parallel plate method was used as a thermal conductivity measurement method. Maximum thermal conductivity increase was recorded as 64% in dispersions containing 3.0 wt% MWCNT [69].

Chen and Xie (2009), while using MWCNT as nanoparticle, chose silicon oil as the base fluid. $\text{C}-\text{O}-\text{C}$, $\text{C}=\text{O}$, and $\text{O}-\text{H}$ functional groups were added to the nanoparticles by acid treatment. Subsequently, shear dispersion technology was used to obtain dispersion by adding base fluid. Hexamethyldisilazane was used as a surface active agent and THW was used as a thermal conductivity measurement method. For dispersions containing 1.0 vol% MWCNT, the maximum increase in thermal conductivity measured as 19% was recorded [70].

Jha and Ramaprabhu (2009) prepared hybrid nanofluids consisting of Ag and MWCNT in their study. The MWCNTs rendered hydrophilic by treatment with acid was coated with Ag. While distilled water was used as the base fluid, thermal conductivity measurements were performed with the KD2 Pro method. They measured the maximum increase in thermal conductivity as 37.3% in dispersions containing 0.03 vol% nanoparticles [71].

Kim et al. (2010) prepared distilled aqueous MWCNT nanofluids. MWCNTs functionalized by plasma treatment were performed ultrasonication for 15 minutes after addition to the base fluid. Thermal conductivity measurements were made by the THW method. The maximum increase in these measurements was recorded as 25% in dispersions containing 0.01 vol% MWCNT [26].

Liu et al. (2011) used EG base fluid and MWCNT nanoparticles in their study. In this study, without any surfactant, the maximum thermal conductivity increase was measured as 12.4% for MWCNT dispersions of 1.0 vol%. The thermal conductivity measurement method used was THW [72].

Aravind et al. (2011) used distilled water and EG as the base fluid and MWCNT as nanoparticles. To improve dispersion stability, functional groups were added to the surface of the nanoparticles by acid treatment. Functionalized nanoparticles were added to the base fluids and ultrasonication was performed for about 40 minutes to obtain nanofluids. The thermal conductivity increases measured using the THW method were 33% and 40% for distilled water and EG nanofluids, containing 0.03 vol% MWCNT, respectively [73].

Harish et al. (2012) used sodium deoxycholate to increase the stability in dispersions prepared with SWCNT and EG. The pH of the nanofluids waited in the ultrasonic bath for 90 minutes was recorded as 7. The maximum value of the thermal conductivity increase measured by THW is 14.8% for the dispersion containing 0.2 vol% SWCNT [74].

Ma et al. (2013) chose functionalized GNP as nanoparticle and silicone oil as the base fluid. First, the functionalized nanoparticles were dispersed in acetone and kept in an ultrasonic bath. The obtained dispersion was combined with silicone oil and allowed to stand in the ultrasonic bath for a further 6 hours. To determine the stability of the prepared nanofluids, precipitation observation and UV-Vis spectrophotometry were

used. Nanofluids were found to be stable for 256 hours. THW method was used to measure thermal conductivity. The maximum thermal conductivity increase was measured as 18.9% in dispersions prepared at different nanoparticle concentrations from 0.01 wt% to 0.07 wt% [75].

Hadadian et al. (2014) used graphene oxide as nanoparticle and distilled water as base fluid to investigate the stability of nanofluids. Precipitation observation, zeta potential measurement, and UV-Vis spectroscopy were used to determine the stability. In this study, without any stabilizers, it was observed that the nanofluids were stable for 60 days [76].

Hemmat Esfe et al. (2015) used DWCNT and ZnO in a ratio of 1:1 by volume as nanoparticles. EG and distilled water, which were mixed by mass in a ratio of 60:40, were selected as the base fluid. While the ultrasonic bath is used for homogenization of nanofluids, KD2 Pro is used as the thermal conductivity measurement method. The maximum thermal conductivity increase is 33% for a 1.0 vol% nanoparticle concentration [77].

The first study of surface tension of GNP based nanofluids was made by Zheng (2015). The relationship between surface tension and different mass ratio (0.02%, 0.04%, 0.06%, 0.08%, and 0.10%), temperature (between 20 and 60°C), different nanoparticle size (between 14-80 nm) were investigated. Surface tension was measured according to the Du-Nouy ring method. Experimental results showed that as the mass ratio of nanoparticles increased, the surface tension of the nanofluids increased. However, the surface tension of the nanofluids with maximum concentration increased by only 2.9% compared to deionized water. The surface tension of nanofluids decreased with temperature rise and nanoparticle size decrease. The type of oxide used in the study and the experimental process for the dispersion of nanoparticles in water have not been explained in detail [78].

Kamatchi et al. (2015), prepared aqueous nanofluids with different concentrations of synthesized reduced graphene oxide (rGO) (0.01, 0.1 and 0.3 g/L). In this study, thermal conductivity, viscosity, and surface tension (according to maximum bubble pressure method) were investigated depending on the concentration and temperature. Surface tension values of 0.1 and 0.3 g/L rGO concentrations were higher than deionized water. However, since the distance between the particles at the liquid-gas

interface was sufficiently large for 0.01 g/L rGO concentration, no significant difference was observed on the result. This trend is explained by the increase in surface energy seen by the accumulation of rGO nanoparticles with Van der Waals interactions at the liquid-gas interface [79].

Ahmed et al. (2016) investigated the effect of volume concentration and temperature change of nanoparticle on the surface tension of aqueous graphene nanofluids according to maximum bubble pressure method. They reported that the surface tension of nanofluids decreased with increasing volume concentration and temperature. Surface tension values showed a decrease of approximately 3.3% per 10°C increase. The average decrease in surface tension for the 0.05% increase in volume concentration was found to be 14.18%. The increase in the volume of graphene showing hydrophobic characteristics increased the nanoparticle absorption at the liquid-gas interface, while the molecular interactions between the fluid molecules and the nanoparticles weakened with temperature. In addition, the direct effect of SDBS used as a surfactant on the surface tension of nanofluid was not investigated in this study [80].

Kumar and Milanova (2009) investigated the effect of SDBS on surface tension, measured with bubble pressure method, of aqueous nanofluids containing 0.1% by volume of SWCNT. They stated that the surfactant content in water reduces the surface tension. After the concentration of surfactant adsorbed on the nanotube surface exceeded the critical value, the surface tension decreased [81].

Tanvir and Qiao (2012) measured the surface tension, with pendant drop method, of nanofluids having 0.1-10 wt% MWCNT dispersed in deionized water and ethanol without surfactant at room temperature. In the study, it was stated that the surface tension of aqueous nanofluids increased with the increase in nanotube concentration. For ethanol-based nanofluids, surface tension values decreased by up to 2% and thereafter increased. They attributed the results to the increase in electrostatic force between the particles and polymer groups bound to the surfactant layer between a particle and the surrounding fluid. Agglomeration at high concentrations reduced the surface tension [82].

As seen in the literature, the method used in nano-fluid and thermal conductivity studies is mostly THW. Antoniadis et al. (2016) determined that in their paper, the

thermal conductivity values measured by THW method were very different in different studies with the same parameters. While it was stated in the literature that there was chaos about this issue, they proposed some necessary criteria for accuracy of THW [83].

Alasli et al. (2018) did not use any surfactants while using MWCNT and low viscosity mineral oil. By ultrasonication, dispersion of nanoparticles was achieved and re-dispersion property of nanofluids was revealed. The highest value in thermal conductivity increases measured using the 3ω method was 5% for a sample with 0.3 wt% nanoparticle [84].

The thermal conductivity increase results measured by the 3ω method are lower but more realistic than the data obtained from other methods. Therefore, the 3ω method was used in this thesis for thermal conductivity measurement. It is clear in the literature that although the studies on thermal conductivity have been carried out frequently, the stability of nanofluids has not yet been elucidated. In the published studies, the determination of stability is performed by zeta potential measurement, UV-Vis spectrophotometry, and visual observation method and the details of these measurements are not shared. Due to the dark and opaque state of carbon-based nanofluids, zeta potential and UV-Vis spectroscopy measurements are challenging research issue.

3. EXPERIMENTAL

In this thesis, distilled water, ethylene glycol (EG) and compressor oil were used as base fluids. EG was purchased from Sigma Aldrich (USA). Compressor oil (JOMO FREOL S8P) was supplied from JX Nippon Oil & Energy (Japan). Having 800 m²/g, 530 m²/g, and 320 m²/g surface areas GNPs nanoparticles were provided from Nanografi (Istanbul, Turkey). Another nanoparticle SWCNT (TUBALL Matrix, Beta 302) was obtained from OcSiAl (USA). PEG-POSS (PG-1190), used as a stabilizer, was purchased from Hybrid Plastics (USA). Ammonia anhydrous $\geq 99.98\%$ used for pH adjustment was purchased from Sigma Aldrich. The properties of base fluids, nanoparticles, and stabilizer are shown in Tables 3.1, 3.2 and 3.3, respectively.

Table 3.1 : Material properties of nanoparticles.

GNP		SWCNT	
Appearance	Black Powder	Appearance	Black Powder
Carbon Content	> 99.5%	Carbon Content	> 75%
Density	0.2-0.4 g/cm ³	Particle Diameter	< 2 nm
Specific Surface Area	320, 530, and 800 m ² /g	Length	5-10 μ m
Particle Diameter	3 μ m		
Thickness	1.5 nm		

Table 3.2 : Material properties of base fluids.

Ethylene Glycol		Compressor Oil	
Appearance	Colorless, liquid	Appearance	Light yellow, liquid
Melting, Freezing Point	-12.9°C	Melting, Freezing Point	-35.0°C
Boiling Point	195°C, 1 atm	Boiling Point	-
Flash Point	111°C (closed cup)	Flash Point	160°C (open cup)
Vapor Pressure	0.11 atm	Vapor Pressure	0.11 atm
Relative Density	1.130 g/cm ³	Relative Density	0.868 g/cm ³ , 15°C
Viscosity	16.5 cP, 25°C	Viscosity	-

Table 3.3 : Material properties of PEG-POSS.

PEG-POSS	
Appearance	Colorless, liquid
Molecular Weight	~5576 g/mol
Viscosity	280 cP, 25°C
Thermal Stability	5% weight loss at 250°C
Solvent Stability	Water, alcohols

3.1 Preparation of Nanofluids

Two-step method was applied in the preparation of nanofluids. For the preparation of the dispersions, the ultrasonicator (UP400S, Hielscher Ultrasonics GmbH, Teltow, Germany), shown in Figure 3.1, adjusted to 0.5 cycles and 50% amplitude, was used. In the preparation of the nanofluids, 100 mL volume borosilicate glass bottles were used and 50 mL of base fluid was used for the nanofluids.



Figure 3.1 : Preparation of nanofluids with Hielscher ultrasonication device.

3.1.1 Preparation of aqueous nanofluids

In aqueous nanofluids, GNP with different surface areas (320, 530, and 800 m²/g) and SWCNT were used as nanoparticles (Table 3.4). PEG-POSS was only used as a stabilizer in nanofluids containing 0.1, 0.5, 1.0, and 2.0 wt% GNP with a surface area of 800 m²/g, shown in Table 3.5. In addition to dispersions containing 0.1, 0.2, and 0.3 wt% PEG-POSS, nanofluids without PEG-POSS were also produced as control samples.

The nanoparticle concentrations of aqueous SWCNT nanofluids were 0.1, 0.5, 1.0 and 2.0 wt%. The total of 12 dispersions were prepared with no PEG-POSS and with 0.1 and 0.2 wt% PEG-POSS, ultrasonication was performed for 50 minutes. Ultrasonication time was determined as a parameter in aqueous SWCNT nanofluids, and 100 minutes of ultrasonication was conducted in addition to 50-minute samples.

In the preparation of all nanofluids, nanoparticles were added into distilled water and ultrasonicated for 10 minutes. In the case of nanofluids containing PEG-POSS, first PEG-POSS and distilled water were ultrasonicated for 5 minutes, then nanoparticles were added and an additional 10 minutes of ultrasonication was performed. The purpose of pre-ultrasonication is to provide nanoparticle homogeneity prior to pH measurement. Previous studies have shown the effect of pH on stability due to electrokinetic properties [6]. For pH adjustment, 0.1 M NH₄OH solution was prepared. The pH of the pre-sonicated nanofluids was measured with Innolab Multi 9310 pH meter. Then, the required amount of NH₄OH solution was added to maintain the pH in the range of 8-8.5. All measurements were performed at approximately 25°C. Later, nanofluids were ultrasonicated for 50 and 100 min. To prevent overheating, the ice bath was used during ultrasound process.

Table 3.4 : Aqueous SWCNT nanofluids based on the nanoparticle concentration, stabilizer concentration, and ultrasonication time.

SWCNT Concentration [wt%]	PEG-POSS Concentration [wt%]	Ultrasonication Time [min]
0.1	0	50
0.1	0.1	50
0.1	0.2	50
0.5	0	50
0.5	0.1	50
0.5	0.2	50
1	0	50
1	0.1	50
1	0.2	50
2	0	50
2	0.1	50
2	0.2	50
0.1	0	100
0.1	0.1	100
0.1	0.2	100
0.5	0	100
0.5	0.1	100
0.5	0.2	100
1.0	0	100
1.0	0.1	100
1.0	0.2	100
2.0	0	100
2.0	0.1	100
2.0	0.2	100

Table 3.5 : Aqueous GNP nanofluids based on the nanoparticle surface area and concentration, stabilizer concentration, and ultrasonication time.

GNP		PEG-POSS Concentration [wt%]	Ultrasonication Time [min]
Surface Area [m ² /g]	Concentration [wt%]		
320	0.1	0	50
	0.5	0	50
	1.0	0	50
	2.0	0	50
530	0.1	0	50
	0.5	0	50
	1.0	0	50
	2.0	0	50
800	0.1	0	50
	0.1	0.1	50
	0.1	0.2	50
	0.1	0.3	50
	0.5	0	50
	0.5	0.1	50
	0.5	0.2	50
	0.5	0.3	50
	1.0	0	50
	1.0	0.1	50
	1.0	0.2	50
	1.0	0.3	50
	2.0	0	50
	2.0	0.1	50
2.0	0.2	50	
2.0	0.3	50	

3.1.2 Preparation of EG-based nanofluids

In EG-based nanofluids, GNP with different surface areas (320, 530, and 800 m²/g) was used as nanoparticles. PEG-POSS was only used as a stabilizer in nanofluids containing 0.1, 0.5, 1.0, and 2.0 wt% GNP with a surface area of 800 m²/g, shown in Table 3.6. In addition to dispersions containing 0.1, 0.2, and 0.3 wt% PEG-POSS, nanofluids without PEG-POSS were also produced as control samples.

In the preparation of all nanofluids, nanoparticles were added into EG and ultrasonicated for 10 minutes. In the case of nanofluids containing PEG-POSS, first PEG-POSS and EG were ultrasonicated for 5 minutes, then nanoparticles were added and an additional 10 minutes of ultrasonication was performed. For pH adjustment, 0.1 M NH₄OH solution was prepared. The pH of the pre-sonicated nanofluids was measured with Innolab Multi 9310 pH meter. Then, the required amount of NH₄OH solution was added to maintain the pH in the range of 8-8.5. All measurements were performed at approximately 25°C. Later, nanofluids were ultrasonicated for 50 min. To prevent overheating, the ice bath was used during ultrasound process.

3.1.3 Preparation of compressor oil-based nanofluids

In oil-based nanofluids, GNP with different surface areas (320, 530, and 800 m²/g) was used as nanoparticles. PEG-POSS was only used as a stabilizer in nanofluids containing 0.1, 0.5, 1.0, and 2.0 wt% GNP with a surface area of 800 m²/g, shown in Table 3.7. In addition to dispersions containing 0.1, 0.2, and 0.3 wt% PEG-POSS, nanofluids without PEG-POSS were also produced as control samples.

In the preparation of all nanofluids, nanoparticles were added into compressor oil and ultrasonicated for 10 minutes. In the case of nanofluids containing PEG-POSS, first PEG-POSS and compressor oil were ultrasonicated for 5 minutes, then nanoparticles were added and an additional 10 minutes of ultrasonication was performed. For pH adjustment, 0.1 M NH₄OH solution was prepared. The pH of the pre-sonicated nanofluids was measured with Innolab Multi 9310 pH meter. Then, the required amount of NH₄OH solution was added to maintain the pH in the range of 8-8.5. All measurements were performed at approximately 25°C. Later, nanofluids were ultrasonicated for 50 min. To prevent overheating, the ice bath was used during ultrasound process.

Table 3.6 : EG based nanofluids according to the nanoparticle and stabilizer concentrations.

GNP		PEG-POSS Concentration [wt%]	Ultrasonication Time [min]
Surface Area [m ² /g]	Concentration [wt%]		
320	0.1	0	50
	0.5	0	50
	1.0	0	50
	2.0	0	50
530	0.1	0	50
	0.5	0	50
	1.0	0	50
	2.0	0	50
800	0.1	0	50
	0.1	0.1	50
	0.1	0.2	50
	0.1	0.3	50
	0.5	0	50
	0.5	0.1	50
	0.5	0.2	50
	0.5	0.3	50
	1.0	0	50
	1.0	0.1	50
	1.0	0.2	50
	1.0	0.3	50
	2.0	0	50
	2.0	0.1	50
2.0	0.2	50	
2.0	0.3	50	

Table 3.7 : Oil-based nanofluids according to the nanoparticle and stabilizer concentrations.

GNP		PEG-POSS Concentration [wt%]	Ultrasonication Time [min]
Surface Area [m ² /g]	Concentration [wt%]		
320	0.1	0	50
	0.5	0	50
	1.0	0	50
	2.0	0	50
530	0.1	0	50
	0.5	0	50
	1.0	0	50
	2.0	0	50
800	0.1	0	50
	0.1	0.1	50
	0.1	0.2	50
	0.1	0.3	50
	0.5	0	50
	0.5	0.1	50
	0.5	0.2	50
	0.5	0.3	50
	1.0	0	50
	1.0	0.1	50
	1.0	0.2	50
	1.0	0.3	50
	2.0	0	50
	2.0	0.1	50
2.0	0.2	50	
2.0	0.3	50	

3.2 Characterization of Nanofluids

Zeta potential measurement and UV-Vis spectrophotometer were used to evaluate the stability of nanofluids. Contact angle and surface tension measurements were performed for wettability assessment. In addition, rheometer was used to investigate the flow properties of nanofluids and the 3ω method was used to determine the thermal conductivity constant.

3.2.1 Zeta potential measurement

The Zetasizer Nano ZS 90 device, shown in Figure 3.2, was used for zeta potential measurement. This device can measure the zeta potential of particles with a diameter between 3.8 nm-100 μm . Zeta potential measurement method is Electrophoretic Light Scattering (ELS). In this method, the dispersions are exposed to laser light at a certain frequency and the electric field generated in the device determines the movement of the nanoparticles. The shifts in the frequency and phase of the laser light depend on the movement of the nanoparticles. By detecting these shifts, the zeta potential value is calculated by measuring the electrophoretic mobility of the nanoparticles.

The minimum sample volume required for measurement is 150 μL . The most critical point in zeta potential measurement is the concentration of sample. The minimum concentration value depends on the particle in the sample. In order to measure the zeta potential, the laser light should be dispersed in the sample, depending on the optical properties of the particle and the polydispersity of the particle size distribution. Because of the high refractive index of carbon-based nanoparticles, the scattering level of the laser light were high; thus, the samples had to be diluted in order to take measurements. Samples were centrifuged at 1350 rpm for 3 hours instead of dilution to avoid disrupting the ion balance of the dispersions. The supernatant of the centrifuged samples was taken and zeta potential measurement was performed. Dilution with ultra-distilled water was performed for the samples of which zeta potential measurements could not be taken due to the high concentration of nanoparticles, despite centrifugation. The images of a sample with high concentration and with adjusted concentration in the zeta potential cuvette are given in Figure 3.3 (a) and (b), respectively.



Figure 3.2 : Malvern Zetasizer Nano ZS 90 device.



(a)

(b)

Figure 3.3 : Samples with high concentration (a) and adjusted concentration (b) for zeta potential measurement.

3.2.2 UV-Vis spectrophotometry

For UV-Vis measurements, Perkin Elmer brand LAMBDA 950 model spectrophotometer was used, shown in Figure 3.4. The wavelength range was selected as 200-1100 nm and absorbance versus wavelength graphs were plotted. Before taking measurements, samples were diluted at different ratios such as 1:20, 1:100, 1:300

based on the concentrations of the samples. Therefore, the absorbance values were expanded with the dilution ratio, in order to obtain actual absorbances of the samples.



Figure 3.4 : Perkin Elmer, LAMBDA 950 UV-Vis Spectrophotometer.

3.2.3 Rheology measurements

Rheology measurements were carried out using TA Instruments, Hybrid Rheometer Discovery HR-2, shown in Figure 3.5. Concentric cylinder cell in low viscosity to medium viscosity samples was used during the measurements. In rheology study, two different step of measurements were performed: shear flow ramps and temperature ramps at a constant shear flow. For shear flow effect, experiments were performed between 0.1 and 1000 s^{-1} . To observed temperature influence on viscosity, temperature increased from 25°C to 60°C with 5°C/min, at a constant shear rate of 200 s^{-1} .



Figure 3.5 : TA Instruments, HR-2 rheometer.

3.2.4 3ω thermal conductivity measurement method

Thermal conductivity measurements were taken with the laboratory type 3ω set up given in Figure 3.6 consisting of a thermal probe, Wheatstone bridge, phase lock-in amplifier, and buffer amplifier. There is a nickel wire with a length of $2l = 19.0$ mm and a diameter of $d = 50$ μm at the tip of the thermal probe, which is completely immersed in the nanofluid and operates simultaneously as a heater and thermometer. A sine output current (AC) at $f/2$ frequency is applied to this wire shown in Figure 3.7. To obtain a good signal-to-noise ratio, the first harmonic (1ω) is canceled by a Wheatstone bridge arrangement. The third harmonic (3ω) selection is made from the differential signal along the bridge by the Stanford SR-850 phase-locked amplifier set to the same frequency.

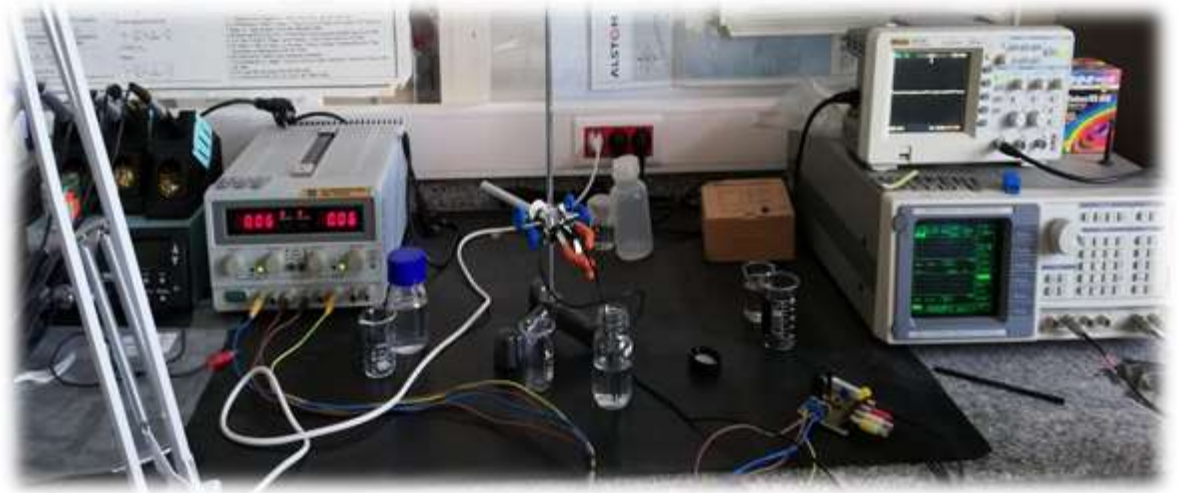


Figure 3.6 : Lab-made 3ω set-up.



Figure 3.7 : Thermal probe operating both as heater and thermometer.

3.2.5 Contact angle and surface tension measurements

The Attention Theta Lite Goniometer (Biolin Scientific AB, Vastra Frolunda, Sweden), given in Figure 3.8, was used for contact angle and surface tension analyses. The experiments were performed at 25°C and the borosilicate microscope slide was chosen as a contact surface. Before each measurement, the glass contact surface was cleaned with ethanol and distilled water. According to Young's Equation, the contact angle and surface tension values were calculated with the sessile drop method and pendant drop method, respectively. For both analyses, recordings were taken for 10 seconds at 12 images per second. Five trials were performed for each sample and the average results were given with standard deviations.

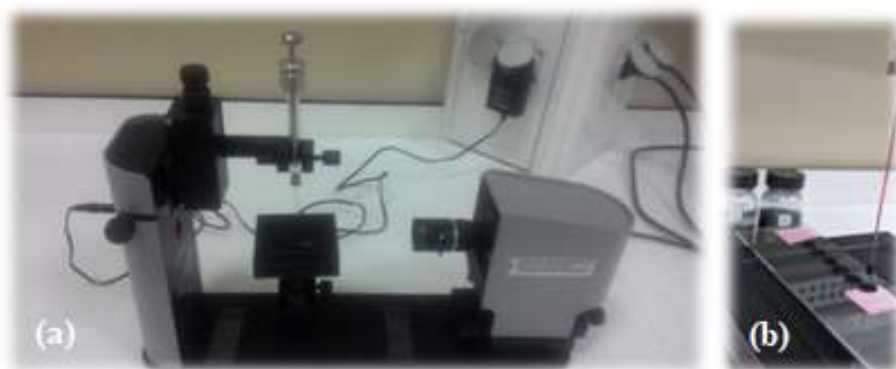


Figure 3.8 : Surface tension (a) and contact angle (b) measurements performed with a goniometer.

4. RESULTS AND DISCUSSION

The main objective of the current study was to prepare stable nanofluids with high thermal conductivity imparted by the presence of carbon nanoparticles. In addition, this study was carried out to investigate the stability mechanisms, along with rheological, and surface properties of nanofluids. Accordingly, a systematic characterization was conducted to acquire more detailed information about carbon-based nanofluids.

4.1 Stability Evaluation of Nanofluids

In heat transfer applications, the stability of nanofluids is an important criterion because it directly affects thermal conductivity and viscosity. Nanoparticles attract each other due to strong Van der Waals forces; therefore, they tend to agglomerate and collapse [85]. In this thesis, zeta potential and UV-Vis spectrophotometry measurements were conducted for stability evaluation.

4.1.1 Results of zeta potential measurements

Zeta potential measurements of aqueous GNP (800 m²/g) nanofluids, without PEG-POSS and with 0.1, 0.2, and 0.3 wt% PEG-POSS, are given in Figure 4.1. The 0.1 wt% GNP dispersion with no PEG-POSS showed a zeta potential of -42.7 mV. With increase in nanoparticle concentration (0.5, 1.0, and 2.0 wt%), the zeta potential values (-33.2, -33.3, and -35.6 mV) decreased. This is because of the fact that the distance between nanoparticles diminished, resulting in higher Van der Waals attraction forces given in Equation 1.1. In 1.0 wt% GNP dispersions containing 0.1 wt% PEG-POSS, the decrease in zeta potential was observed with the increase of nanoparticle concentration, due to PEG-POSS acting as a nonionic surfactant. With the absence of electrical charges on the molecules, the use of PEG-POSS led to a reduction in zeta potential.

On the other hand, the zeta potential increase in 1.0 wt% GNP dispersions with 0.2 and 0.3 wt% PEG-POSS resulted from saturated PEG-POSS concentration, covering

the surface area of nanoparticle. With the increase of nanoparticle concentration to 2.0 wt%, this saturation deteriorated and zeta potential decreased.

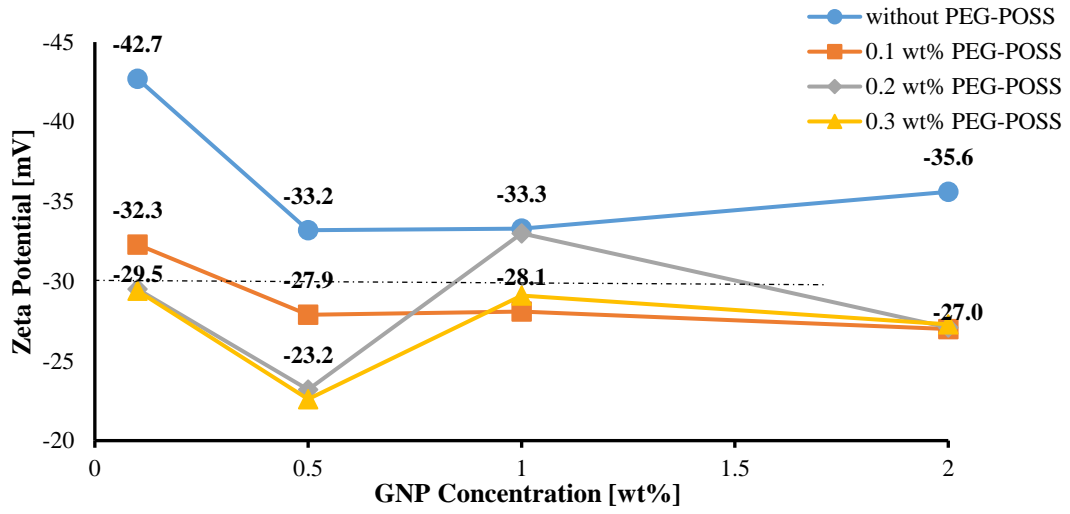


Figure 4.1 : Zeta potential as a function of GNP (800 m²/g) concentration for aqueous nanofluids at different PEG-POSS concentrations.

Zeta potential as a function of GNP concentration (320, 530, and 800 m²/g) for aqueous nanofluids prepared without PEG-POSS is given in Figure 4.2. Zeta potential of 800 m²/g GNP nanofluids decreased with an increase in nanoparticle concentration. Due to the higher density with lower surface area (320 and 530 m²/g) of nanoparticles, the Hamaker constant and Van der Waals forces increased as stated in Equation 1.1; thus, zeta potential decreased. In addition, with the higher density of the nanoparticle, the gravitational force acting on the particle increased.

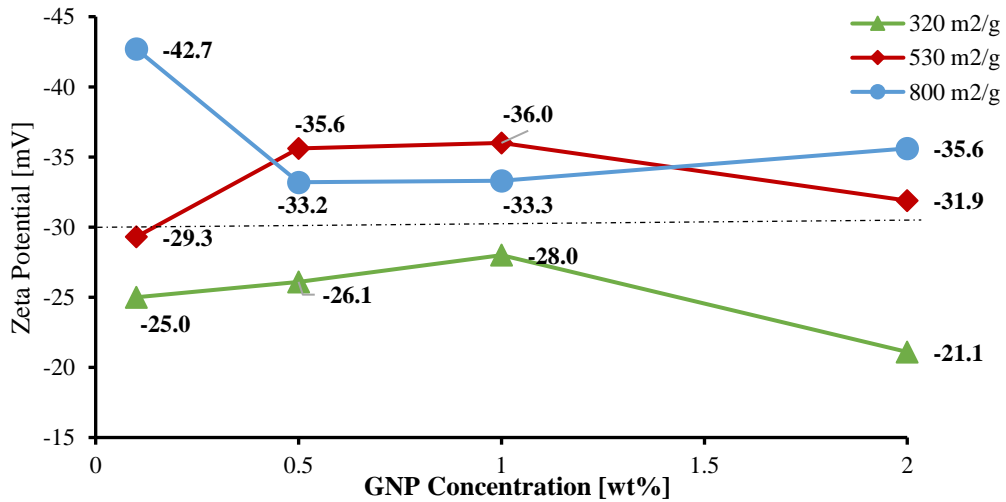


Figure 4.2 : Zeta potential as a function of GNP concentration (320, 530, and 800 m²/g) for aqueous nanofluids without PEG-POSS.

Zeta potential as a function of SWCNT concentration for aqueous nanofluids at different PEG-POSS concentrations is given in Figure 4.3. All zeta potential values above -30 mV proved good colloidal stability of nanofluids. The zeta potential of SWCNT nanofluids is better because the material properties given in Table 3.1 are smaller in radius and length than in GNPs and therefore the aggregation number is smaller. The small aggregation number means that the number of stabilizer molecules required for coating a SWCNT nanoparticle is less [86].

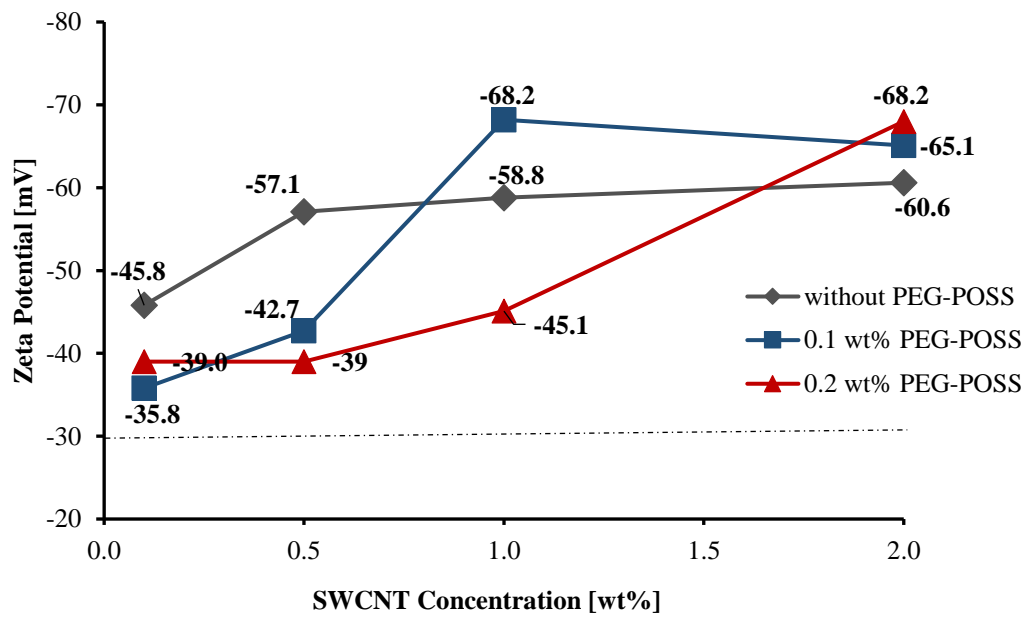


Figure 4.3 : Zeta potential as a function of SWCNT concentration for aqueous nanofluids at different PEG-POSS concentrations.

Zeta potential as a function of GNP (800 m²/g) concentration for EG-based nanofluids at different PEG-POSS concentrations is given in Figure 4.4. Lower zeta potential values were observed in EG-based nanofluids than those in aqueous ones due to the lower dielectric constant of EG [85]. As claimed in Equation 1.2, a decrease in the dielectric constant of the base fluid led to a decrease in the repulsive forces.

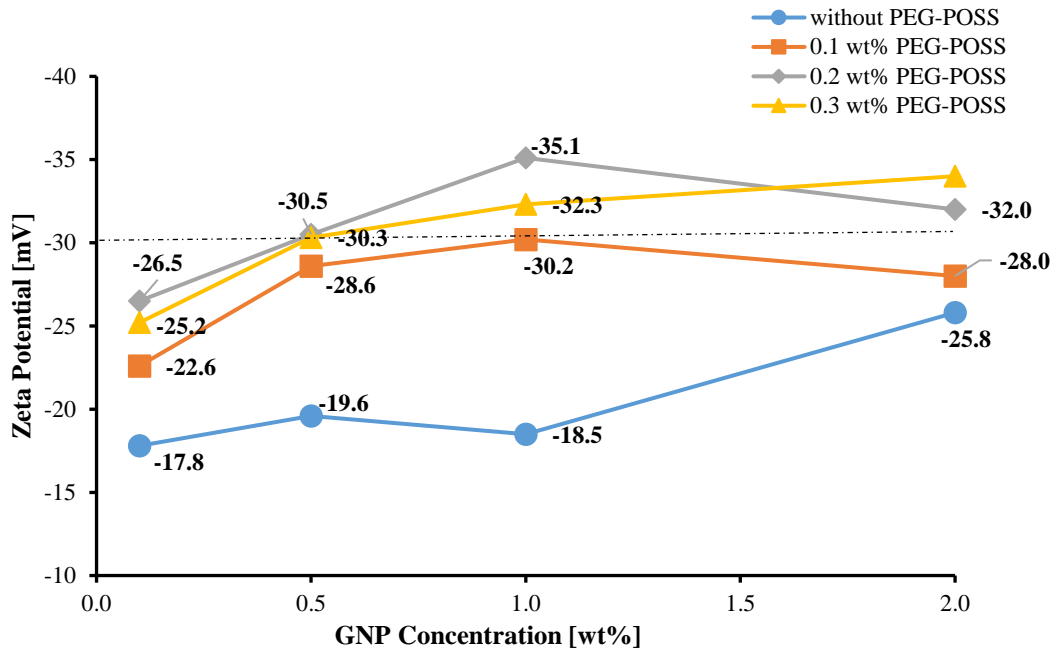


Figure 4.4 : Zeta potential as a function of GNP ($800 \text{ m}^2/\text{g}$) concentration for EG-based nanofluids at different PEG-POSS concentrations.

4.1.2 Determination of relative concentration of nanofluids by UV-Vis spectrophotometry

Spectral analyses like UV-Vis spectrophotometry have often been preferred methods for determining the stability of nanofluids. In UV-Vis, the absorption band of the nanoparticle should be between 190-1100 nm [85].

UV-Vis measurements of aqueous SWCNT and GNP ($800 \text{ m}^2/\text{g}$) nanofluids at different PEG-POSS concentrations were performed. Sarsam et al. (2016) diluted 0.1 wt% GNP nanofluids with distilled water at a ratio of 1:20, before taking measurements [87]. In our study, highly concentrated dispersions of 2.0 wt% nanoparticle were diluted with distilled water at a ratio of 1:300 for proper measurements. The UV-Vis measurements of GNP (320 and $530 \text{ m}^2/\text{g}$) nanofluids could not be performed due to the visible phase separation and the sedimentation of the samples. Likewise, UV-Vis measurements of both EG-based and oil-based GNP ($800 \text{ m}^2/\text{g}$) nanofluids were not carried out, since those viscous base fluids (i.e. EG and compressor oil) could not be diluted properly. All absorbance values were expanded with dilution ratio according to Beer Lambert's Law given in Equation 1.7.

Figures 4.5, 4.6, 4.7, and 4.8 show the UV-Vis spectra of aqueous GNP ($800 \text{ m}^2/\text{g}$) nanofluids at different PEG-POSS concentrations. In previous studies, the absorption

band of the GNP was noted to be around 280-290 nm [6;87]. In this study, the absorption band of GNP was observed between 300 and 305 nm. The difference about 15 nm might be due to the impurities of GNP supplied from Nanografi or the sensitivity of UV-Vis spectrophotometer.

As the nanoparticle concentration increased in Figure 4.5, the absorbance values also increased as predicted in the Beer-Lambert Equation. The increase in the absorbance at the same rate of nanoparticle concentration indicated a proper distribution of nanoparticles. In Figures 4.6, 4.7, and 4.8, the increase in absorbance values was more proportional for the samples with PEG-POSS, which provides better distribution of nanoparticles.

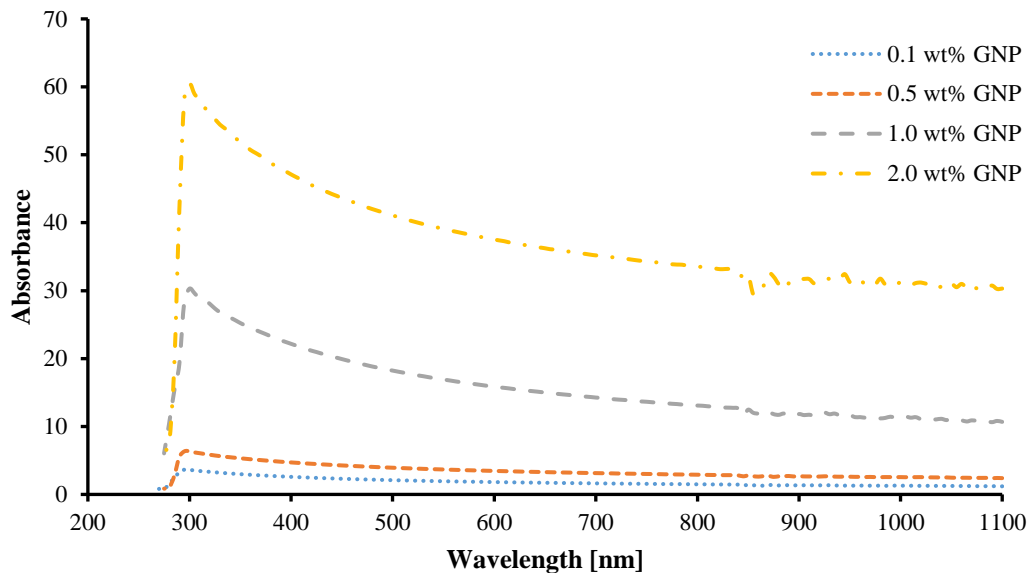


Figure 4.5 : UV-Vis Spectra of aqueous nanofluids at different GNP (800 m²/g) concentrations with no PEG-POSS.

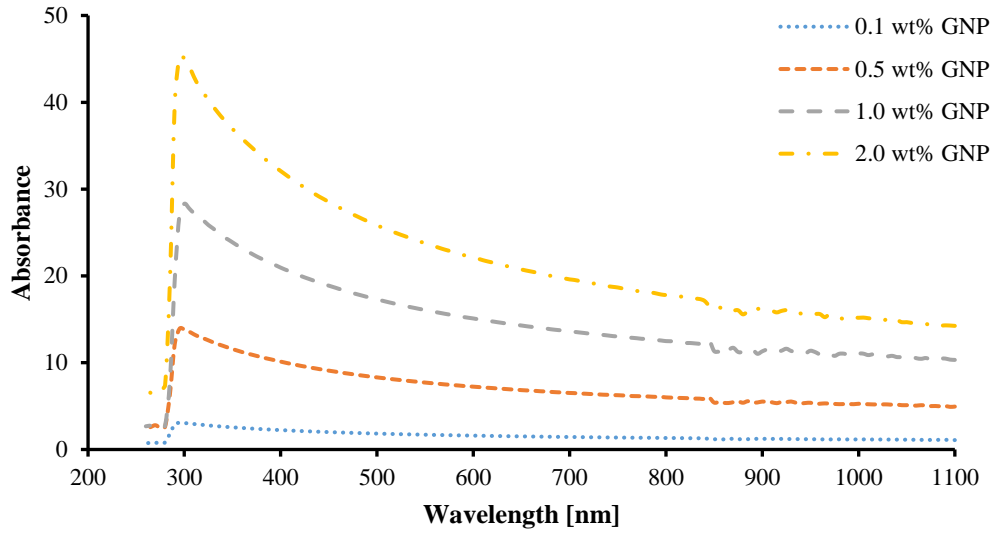


Figure 4.6 : UV-Vis Spectra of aqueous nanofluids at different GNP ($800 \text{ m}^2/\text{g}$) concentrations with 0.1 wt% PEG-POSS.

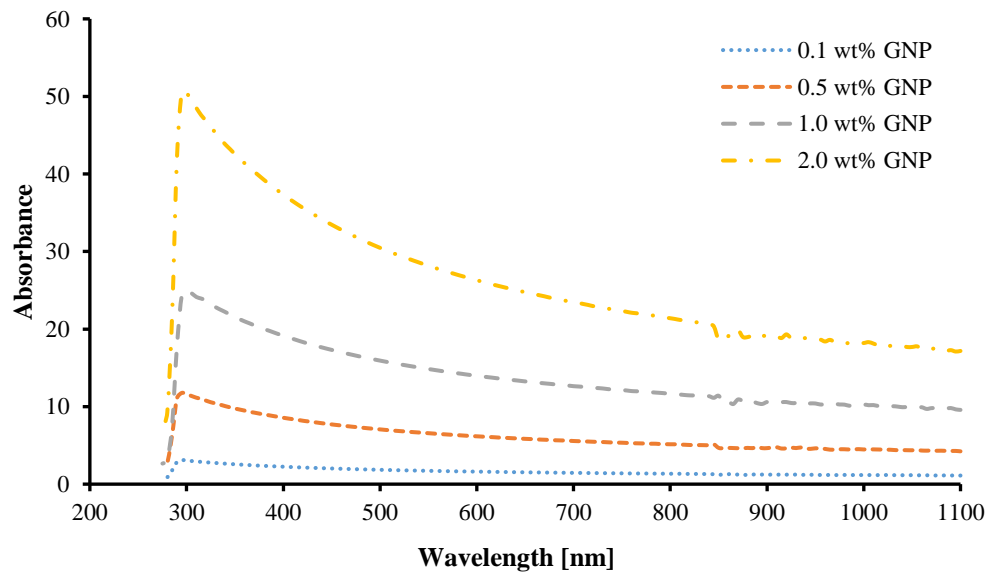


Figure 4.7 : UV-Vis Spectra of aqueous nanofluids at different GNP ($800 \text{ m}^2/\text{g}$) concentrations with 0.2 wt% PEG-POSS.

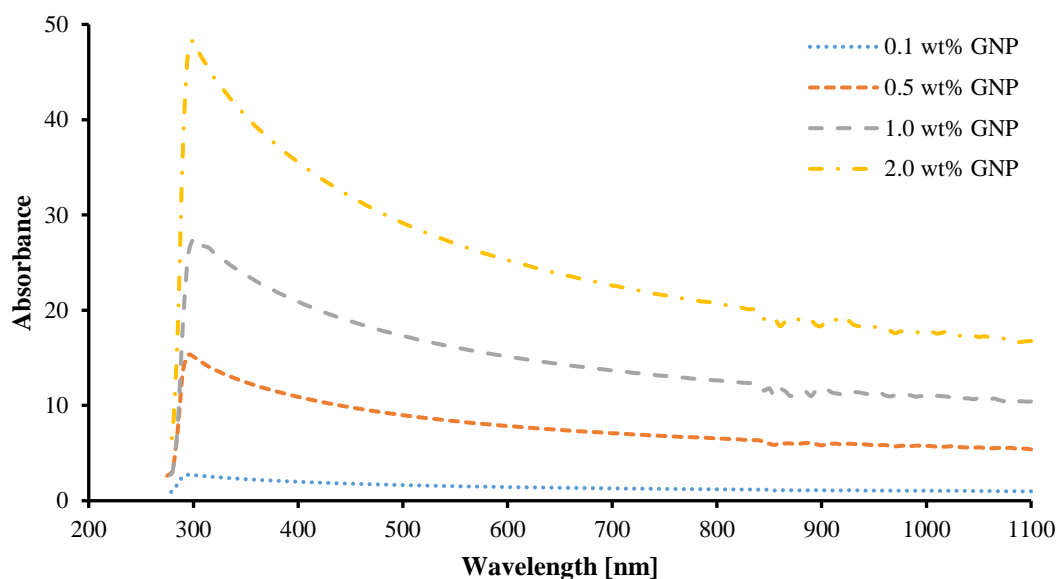
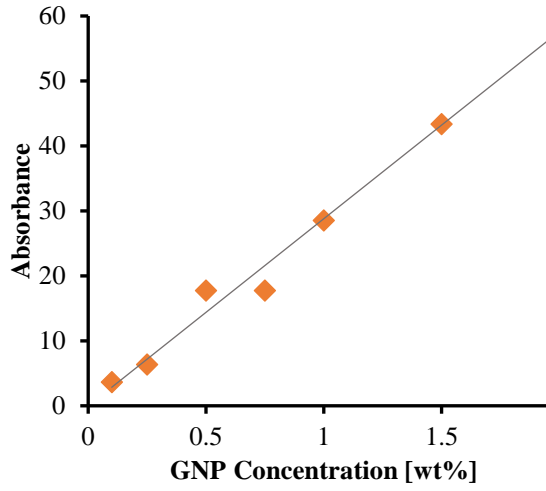


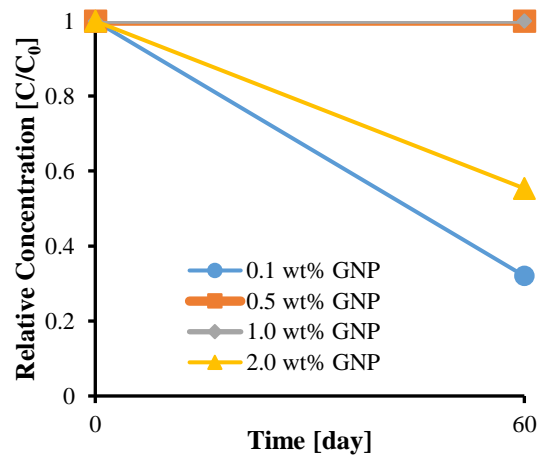
Figure 4.8 : UV-Vis Spectra of aqueous nanofluids at different GNP (800 m²/g) concentrations with 0.3 wt% PEG-POSS.

Based on Beer-Lambert Equation, the absorbance and concentration values of a material are directly proportional with each other. Accordingly, if the graph of absorbance versus at different concentrations is drawn, when the absorbance value is obtained by UV-Vis measurement at any time, the unknown nanofluid concentration value can be found by reading the corresponding concentration in the calibration graph. In order to determine the concentration values of the nanofluids prepared at the end of 60 days, calibration graphs were drawn.

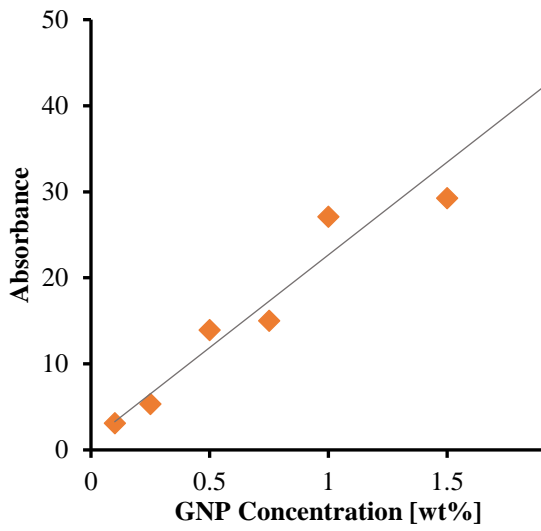
The calibration graphs are shown in Figures 4.9 (a), (b), (c), and (d); relative concentration versus time graphs are given in (e), (f), (g), and (h). As given in Figure 4.9 (e), after 60 days, the relative concentrations of nanofluids without PEG-POSS and having 0.1 wt% and 2.0 wt% GNP are 0.32 and 0.55, respectively. The zeta potential values of these samples were measured as -42.7 and -35.6 mV, respectively. When the zeta potential values are examined, it can be accepted that these samples were stable but their stabilities were decreased after 60 days. It was also observed that the samples had different precipitation rates regardless of the nanoparticle concentration. This situation has been recorded in the literature by different researchers [6;87;88].



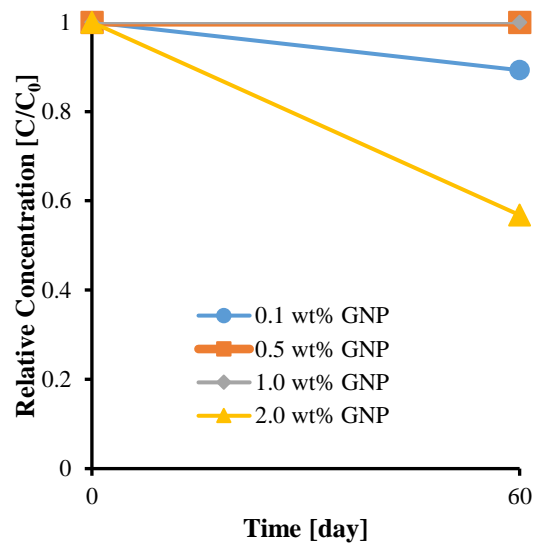
(a)



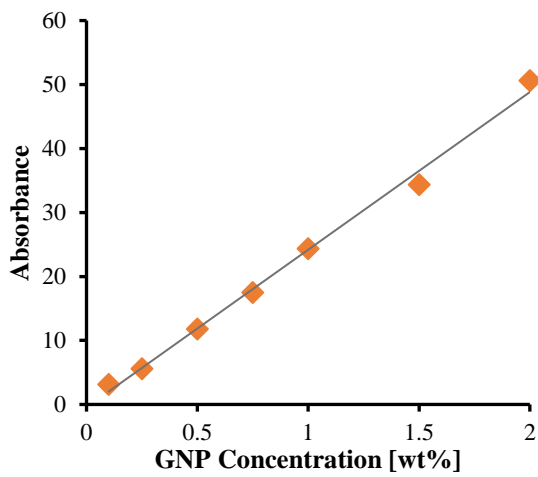
(e)



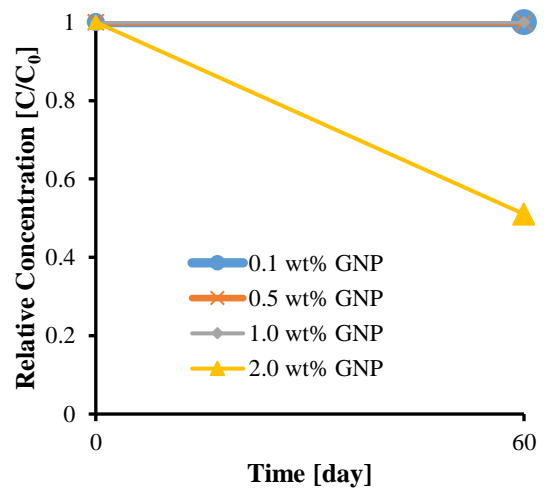
(b)



(f)



(c)



(g)

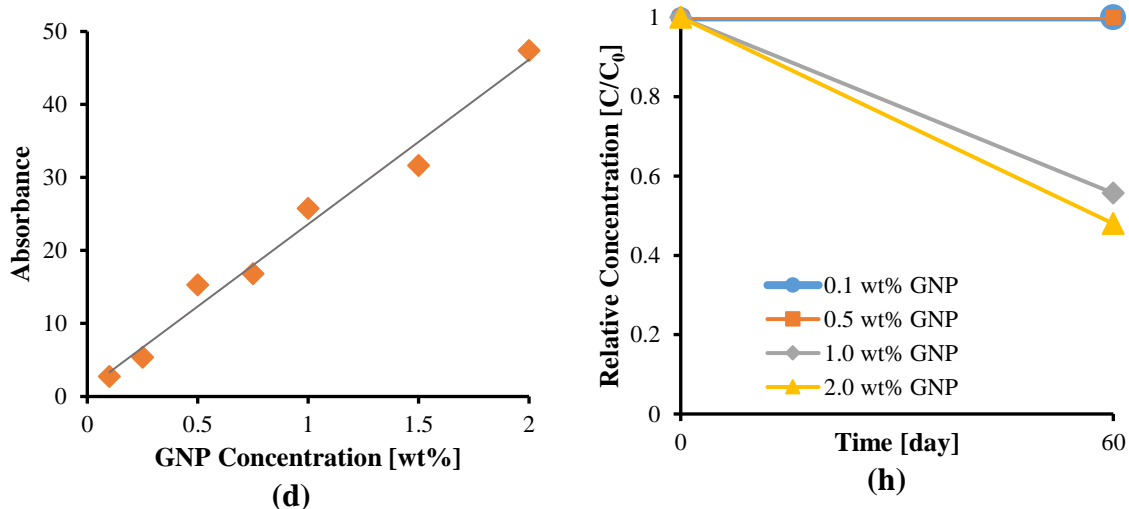


Figure 4.9 : Calibration graphs of GNP ($800 \text{ m}^2/\text{g}$) nanofluids with (a) no PEG-POSS, (b) 0.1 wt% PEG-POSS, (c) 0.2 wt% PEG-POSS, and (d) 0.3 wt% PEG-POSS; relative concentration of GNP ($800 \text{ m}^2/\text{g}$) nanofluids with (e) no PEG-POSS, (f) 0.1 wt% PEG-POSS, (g) 0.2 wt% PEG-POSS, and (h) 0.3 wt% PEG-POSS at the end of the 60 days.

As for aqueous SWCNT nanofluids, the absorption bands were observed around 355 nm. Figures 4.10, 4.11, and 4.12 show the UV-Vis spectra of aqueous SWCNT nanofluids without PEG-POSS and with 0.1 and 0.2 wt% PEG-POSS, respectively. In these spectra, absorbance values are proportional to the increase in nanoparticle concentration.

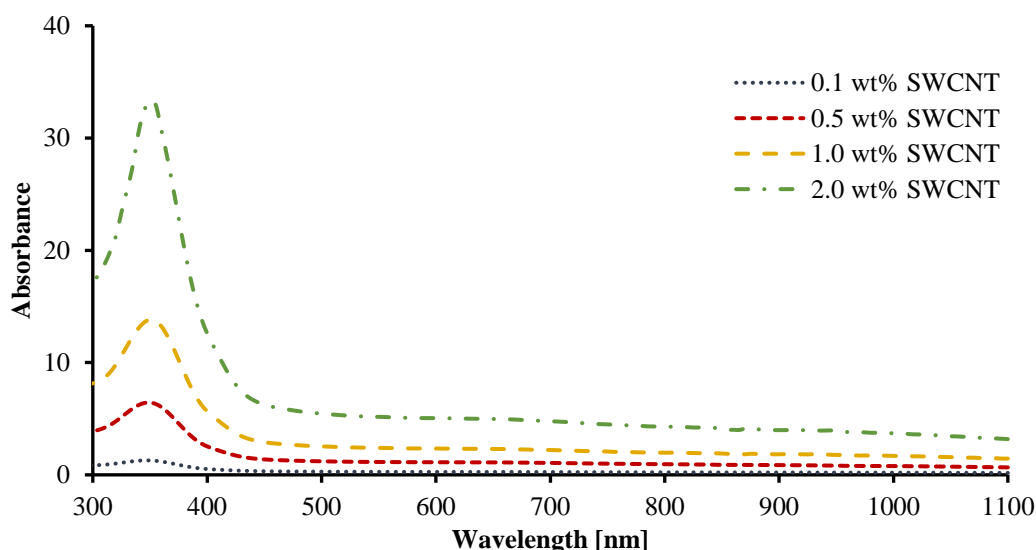


Figure 4.10 : UV-Vis Spectra of aqueous nanofluids at different SWCNT concentrations with no PEG-POSS.

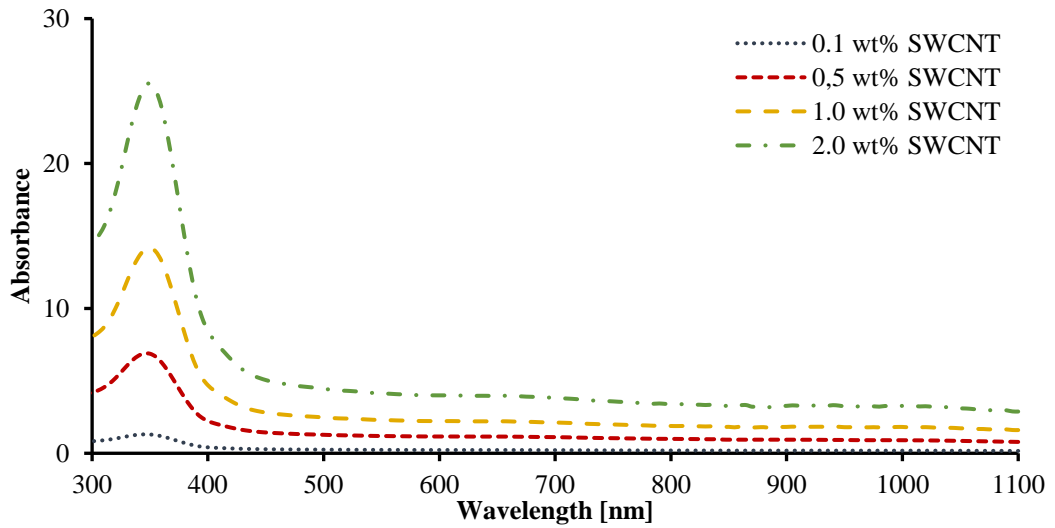


Figure 4.11 : UV-Vis Spectra of aqueous nanofluids at different SWCNT concentrations with 0.1 wt% PEG-POSS.

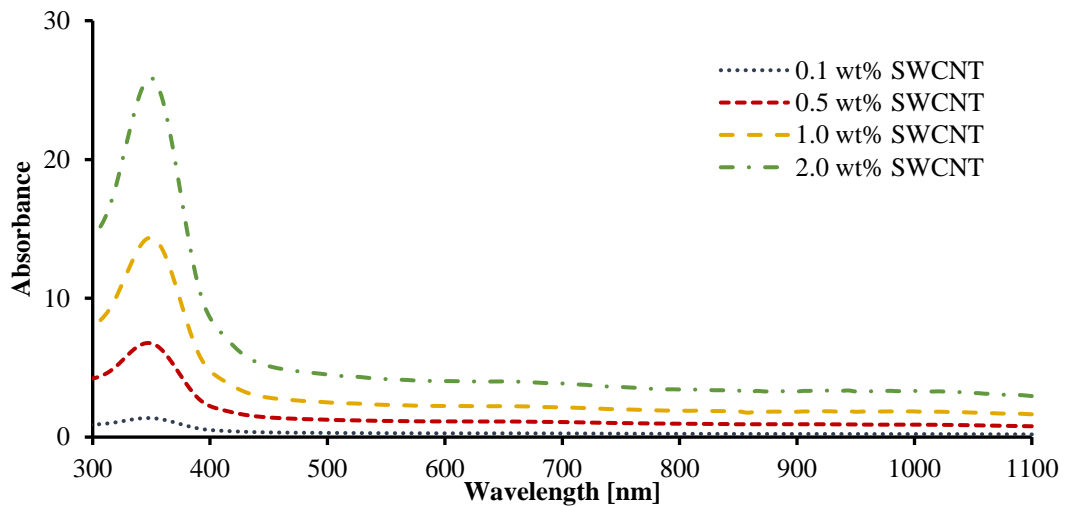


Figure 4.12 : UV-Vis Spectra of aqueous nanofluids at different SWCNT concentrations with 0.2 wt% PEG-POSS.

In the calibration graphs given in Figures 4.13 (a), (b) and (c), all data were very close to the linear trend line showing a good distribution [6]. The samples which sedimented the earliest, had the highest concentration of nanoparticles (2.0 wt%). This was supported by the zeta potential measurements of the SWCNT and GNP nanofluids. As previously mentioned, due to the different sedimentation rate, the aqueous 0.1 wt% SWCNT nanofluid with 0.2 wt% PEG-POSS showed the lowest relative concentration of 0.43.

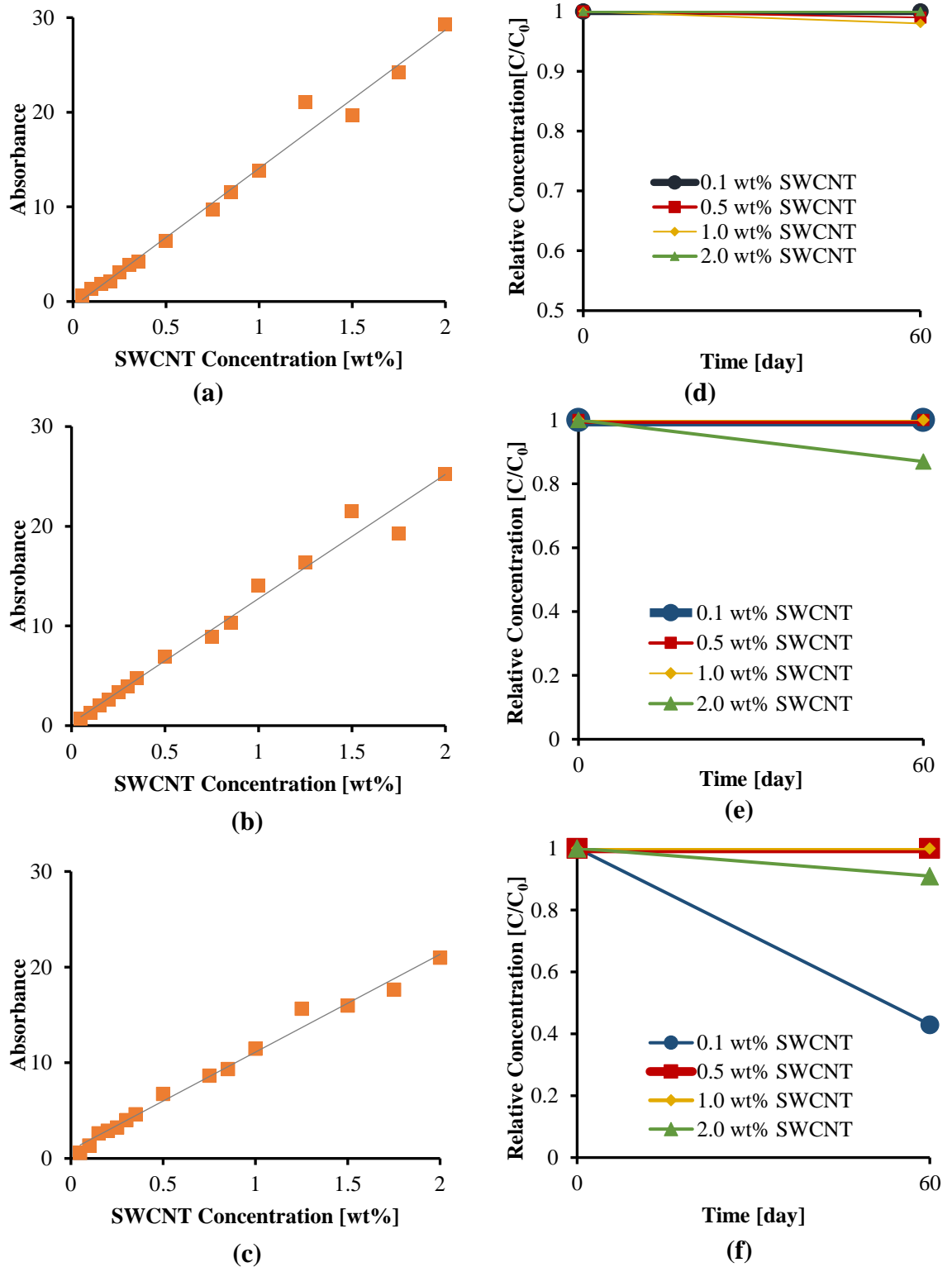


Figure 4.13 : Calibration graphs of SWCNT nanofluids with (a) no PEG-POSS, (b) 0.1 wt% PEG-POSS, and (c) 0.2 wt% PEG-POSS; relative concentration of SWCNT nanofluids with (d) no PEG-POSS, (e) 0.1 wt% PEG-POSS, and (f) 0.2 wt% PEG-POSS at the end of the 60 days.

Figure 4.14 (a) shows aqueous SWCNT nanofluids remaining stable for more than 18 months. Figure 4.14 (b) illustrates phase-separated samples, which were aqueous GNP (320 m²/g), EG-based GNP (320 m²/g), aqueous GNP (530 m²/g), and oil-based GNP (800 m²/g) nanofluids from left to right, respectively. In Figure 4.14 (c), aqueous GNP (320 m²/g) with re-dispersion ability were given.

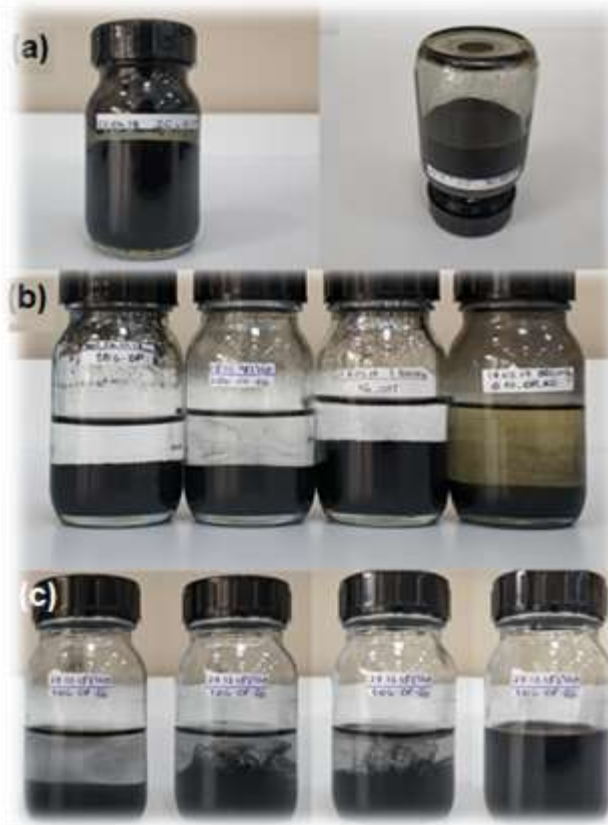


Figure 4.14 : Stable aqueous SWCNT samples (a), sedimented samples (b), re-dispersible samples.

4.2 Rheology Measurements

The viscosity of the nanofluid directly affects convection heat transfer and pump power [89]. Increase in viscosity causes a pressure drop in the system and increases the energy required for the pump and mixing processes.

Many parameters such as the method of nanofluid preparation, type of base fluid, process temperature, particle shape and size, nanoparticle concentration, shear rate, and use of surfactants affect the viscosity of nanofluids [90]. In addition, the stability of nanofluids plays an important role in improving the rheological properties of nanofluids.

In the current work, various parameters such as nanoparticles with different surface area and concentration, different base fluids and concentration, stabilizer effect, along with temperature and shear rate were studied in order to clarify the rheological behavior of the nanofluids. Figure 4.15 illustrates the shear rate versus viscosity change of aqueous GNP (800 m²/g) nanofluids with no PEG-POSS. In these measurements at constant temperature of 25°C, an increase in viscosity was observed with increasing nanoparticle concentration. With increase in concentration, the force applied on the fluid increases, resulting in higher internal shear stress. This causes increased viscosity.

The viscosity values of 0.1, 0.5, and 1.0 wt% GNP nanofluids were recorded close to each other, acting like Newtonian fluids. However, after shear rate of around 110 s⁻¹, higher viscosities were observed, showing a shear thickening behavior. Under the applied shear stress, the nanoparticles tend to line up in the fluid like a film layer. The increase in the shear rate after a certain value disrupts the packaged structure of the nanoparticles and more space is required for the display of the same lining up behavior again. The deterioration in the arrangement of nanoparticles leads to an increase in viscosity [91]. In the 2.0 wt% GNP nanofluid, viscosity reduction and shear thinning behavior were observed up to a shear rate of 340 s⁻¹. Shear thinning behavior of the sample having the highest nanoparticle concentration is an indication of agglomeration of the particles. This situation occurs when the agglomerated particles are separated into smaller particles under shear stress [91]. As shown in Figure 4.15, the shear thickening behavior after a shear rate of 340 s⁻¹ resulted from the lack of required space for nanoparticle sequencing and reordering.

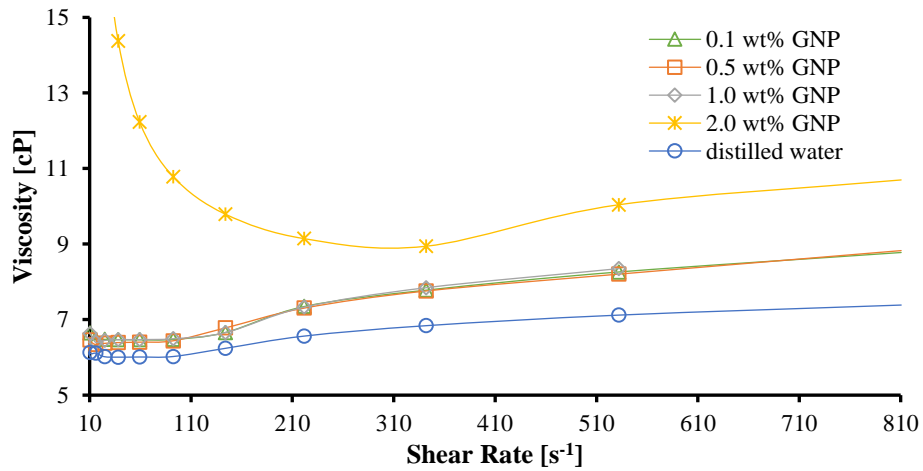


Figure 4.15 : Viscosity as a function of shear rate for aqueous GNP ($800 \text{ m}^2/\text{g}$) nanofluids with no PEG-POSS.

Figure 4.16 illustrates viscosity as a function of temperature (from 25°C to 60°C) for aqueous GNP ($800 \text{ m}^2/\text{g}$) with no PEG-POSS, under a constant shear rate of 200 s^{-1} . As temperature increases, intermolecular interactions weaken and viscosity of liquids decreases [92]. While the viscosities of nanofluids having 0.1, 0.5, and 1.0 wt% GNP decreased by approximately 0.2 cP, the viscosity of 2.0 wt% GNP nanofluid decreased by roughly 1 cP. As for the highest nanoparticle concentration of 2.0 wt%, a sharper reduction in viscosity was observed with increase in temperature.

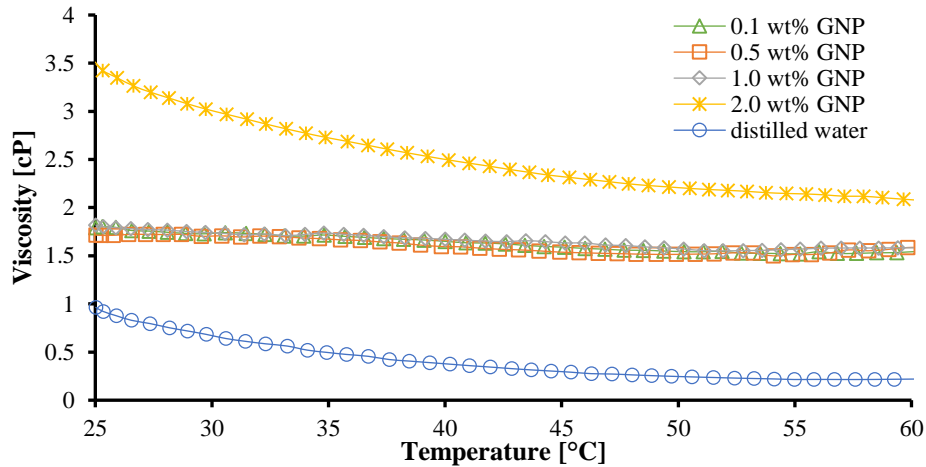


Figure 4.16 : Viscosity as a function of temperature for aqueous GNP ($800 \text{ m}^2/\text{g}$) nanofluids with no PEG-POSS.

Figures 4.17 and 4.18 show viscosity as a function of shear rate and viscosity as a function of temperature for aqueous GNP ($800 \text{ m}^2/\text{g}$) nanofluids with 0.1 wt% PEG-POSS, respectively. The addition of 0.1 wt% PEG-POSS did not have any effect on

the rheological behavior. The nanofluids containing 0.1, 0.5, and 1.0 wt% GNP had similar behavior at increasing shear rate and showed shear thickening behavior after a shear rate of about 150 s^{-1} . Aqueous 2.0 wt% GNP nanofluids showed shear thinning behavior at low shear rate region and shear thickening behavior after 340 s^{-1} .

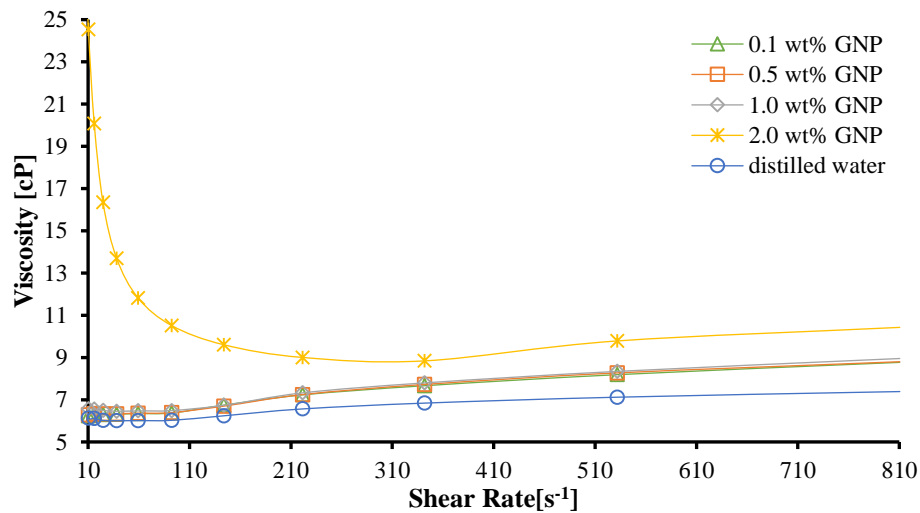


Figure 4.17 : Viscosity as a function of shear rate for aqueous GNP ($800 \text{ m}^2/\text{g}$) nanofluids with 0.1 wt% PEG-POSS.

In Figure 4.18, the viscosity of aqueous 0.1, 0.5, and 1.0 wt% GNP nanofluids had similar trend with respect to temperature. Since the increase in GNP concentration did not increase the viscosity much, the concentrated nanofluids were likely to be used in heat transfer systems. The viscosity of those nanofluids decreased by approximately 0.2 cP after a temperature increase of 35°C , while the viscosity of 2.0 wt% GNP nanofluids decreased by 1.5 cP.

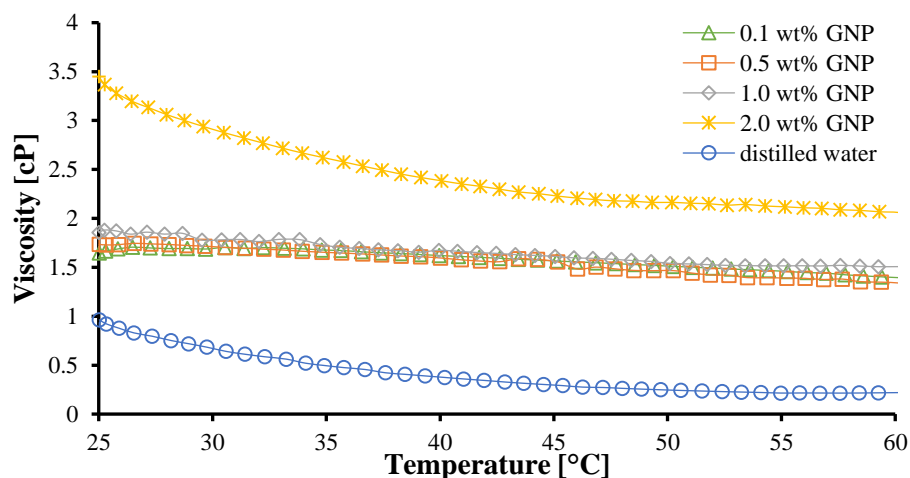


Figure 4.18 : Viscosity as a function of temperature for aqueous GNP ($800 \text{ m}^2/\text{g}$) nanofluids with 0.1 wt% PEG-POSS.

Figure 4.19 shows viscosity as a function of shear rate for aqueous GNP (800 m²/g) nanofluids with 0.2 wt% PEG-POSS. The 0.1 and 0.5 wt% GNP dispersions with 0.2 wt% PEG-POSS showed the same rheological behavior with dispersions having no PEG-POSS (Figure 4.15) and 0.1 wt% PEG-POSS (Figure 4.17). The shear thinning behavior of 1.0 wt% GNP sample up to shear rate of approximately 60 s⁻¹ and shear thickening behavior after 220 s⁻¹ were observed. As for 2.0 wt% GNP dispersion, shear thinning behavior continued up to a shear rate of 340 s⁻¹, followed by shear thickening at higher shear rate regions. The shear thinning behavior of 1.0 wt% GNP nanofluid up to 60 s⁻¹ indicated that particle agglomeration was less, as compared to 2.0 wt% GNP nanofluid showing shear thinning behavior up to 220 s⁻¹.

The viscosity as a function of temperature for aqueous GNP (800 m²/g) nanofluids with 0.2 wt% PEG-POSS is given in Figure 4.20. With a temperature increase of 35°C, the decrease in viscosity of 0.1 wt% and 0.5 wt% GNP samples were measured around 0.3 cP. For 1.0 wt% GNP nanofluid, the viscosity remained almost constant. The viscosity change in 2.0 wt% GNP nanofluid was 1.4 cP.

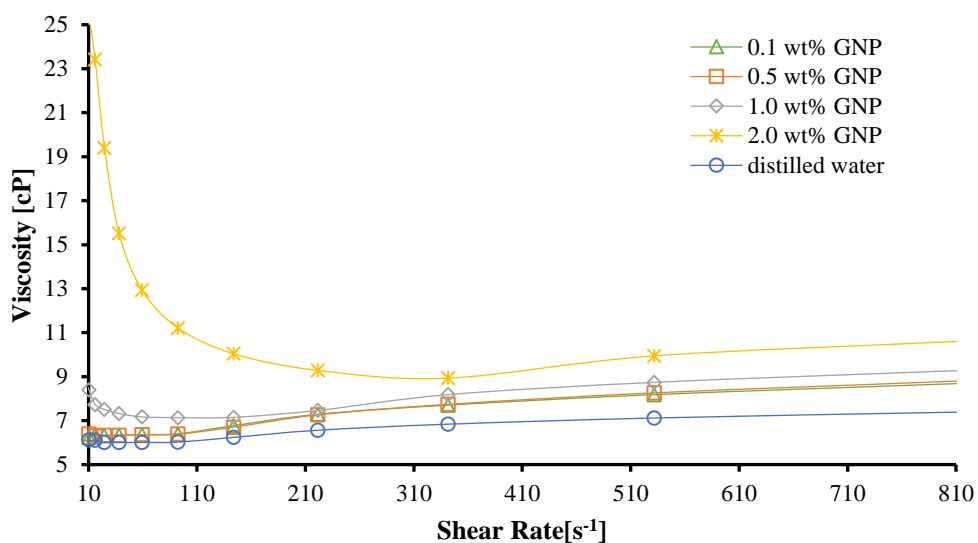


Figure 4.19 : Viscosity as a function of shear rate for aqueous GNP (800 m²/g) nanofluids with 0.2 wt% PEG-POSS.

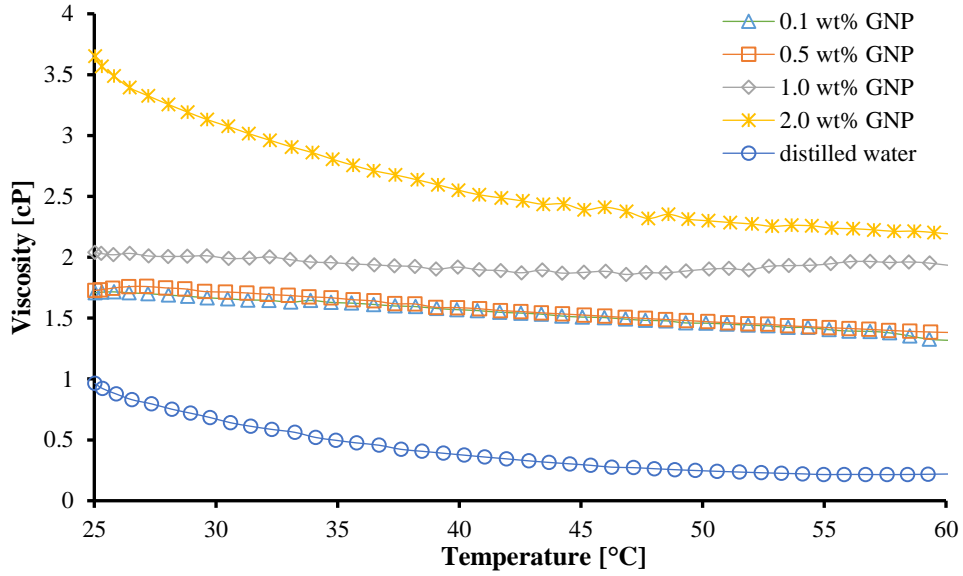


Figure 4.20 : Viscosity as a function of temperature for aqueous GNP ($800 \text{ m}^2/\text{g}$) nanofluids with 0.2 wt% PEG-POSS.

The viscosity as a function of shear rate for GNP ($800 \text{ m}^2/\text{g}$) nanofluids with 0.3 wt% PEG-POSS is given in Figure 4.21. The viscosity values were similar to the nanofluids with no PEG-POSS, with 0.1 wt% PEG-POSS, and 0.2 wt% PEG-POSS. The 0.1, 0.5, and 1.0 wt% GNP nanofluids showed shear thickening behavior after a shear rate of around 140 s^{-1} . In the 2.0 wt% GNP nanofluid, shear thinning behavior was observed up to 340 s^{-1} shear rate followed by shear thickening.

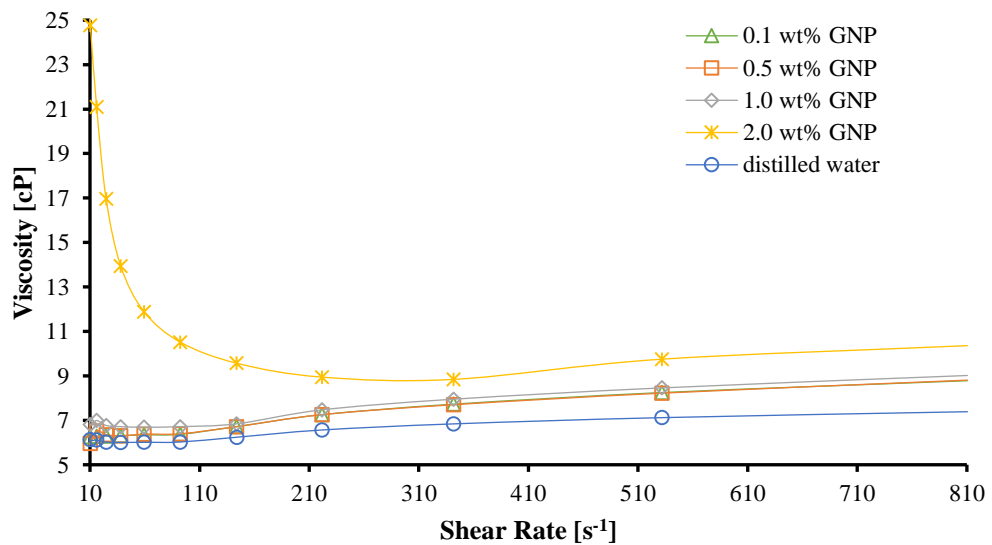


Figure 4.21 : Viscosity as a function of shear rate for aqueous GNP ($800 \text{ m}^2/\text{g}$) nanofluids with 0.3 wt% PEG-POSS.

In Figure 4.22, viscosity as a function of temperature for aqueous GNP (800 m²/g) with 0.2 wt% PEG-POSS showed a fluctuation at 1.0 wt% GNP sample. The increase in viscosity at 41°C and 52°C is indicative of the presence of unexpected flocculation and stability decrease of the dispersion. While the viscosity values of both 0.1 wt% and 0.5 wt% GNP nanofluids decreased by 0.35 cP at a temperature rise of 35°C, the viscosity reduction in 2.0 wt% GNP nanofluids was 1.4 cP.

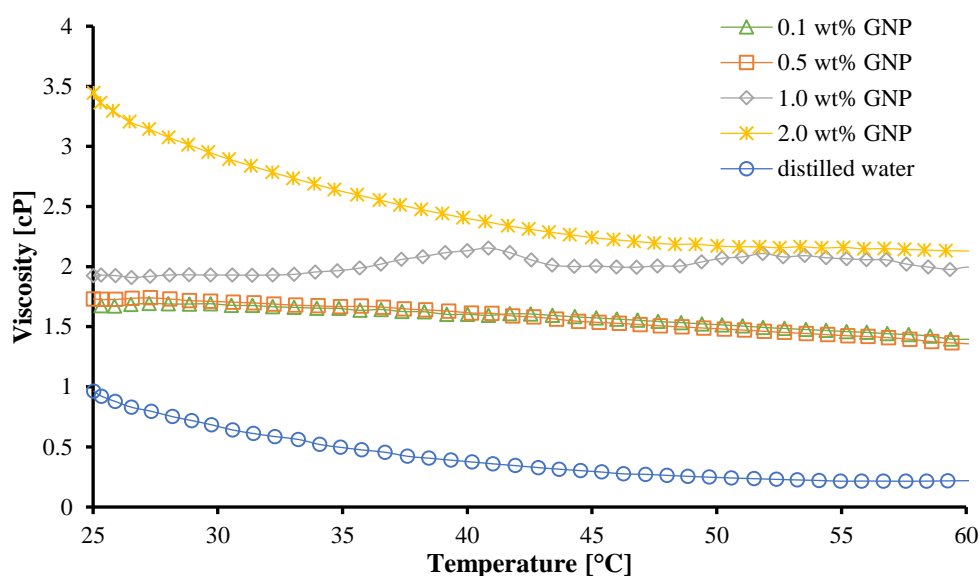


Figure 4.22 : Viscosity as a function of temperature for aqueous GNP (800 m²/g) nanofluids with 0.3 wt% PEG-POSS.

Figures 4.23 and 4.24 show viscosity as a function of shear rate and viscosity as a function of temperature for aqueous GNP (530 m²/g) nanofluids with no PEG-POSS, respectively. With increase in shear rate, viscosity change of 0.1 and 0.5 wt% GNP nanofluids were similar. The viscosity values measured as 6.3 cP at a shear rate of 140 s⁻¹ shear rate increased to 10 cP with increased shear rate. While the viscosity value of the 1.0 wt% GNP nanofluid was 15 cP at a shear rate of 10 s⁻¹, the viscosity decreased to 8 cP at a shear rate of 220 s⁻¹ due to increase in shear rate and reduction of the attraction forces between molecules. With an increase in shear rate, viscosity raised up to 10 cP. This was an indication that the viscosity decreased due to the separation of all agglomerated nanoparticles, and the nanofluid did not have the space required for reordering due to increased shear stress; later, shear thickening of nanofluids occurred. As for 2.0 wt% GNP nanofluid, the viscosity decreased from 34 cP to 10 cP in the shear thinning region of 10 s⁻¹ to 340 s⁻¹ in such a way that 2.0 wt% GNP nanofluid was proven to be less stable due to the nanoparticle agglomeration.

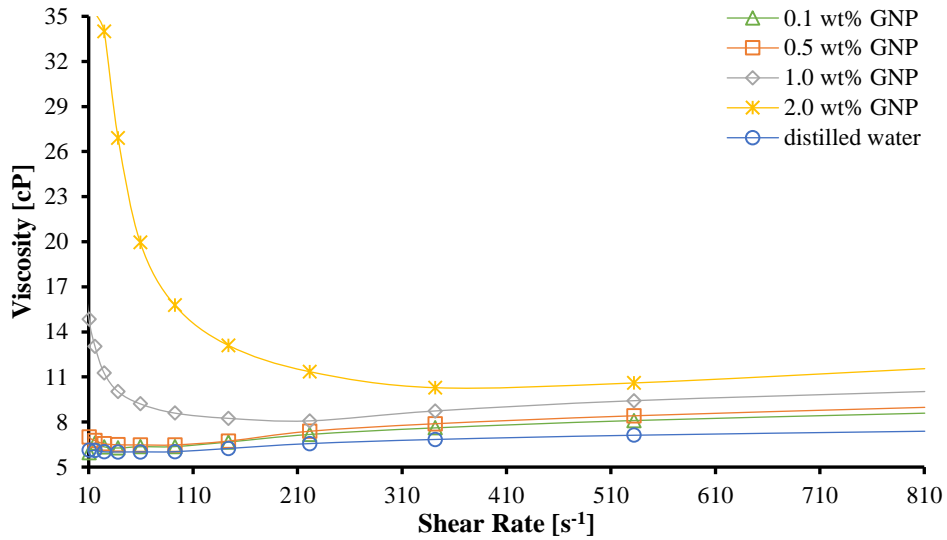


Figure 4.23 : Viscosity as a function of shear rate for aqueous GNP (530 m²/g) nanofluids with no PEG-POSS.

As in Figure 4.24, the viscosities of aqueous 0.1 wt% and 0.5 wt% GNP nanofluids were 1.64 and 2.0 cP, at 25°C, respectively. The viscosities decreased to 1.53 cP at 60°C. While the 1.0 wt% GNP nanofluid showed a viscosity of 2.65 cP at 25°C and 1.91 cP at 60°C, the 2.0 wt% GNP nanofluid had viscosities of 5.5 cP (25°C) and 2.77 cP (60°C). In addition to decrease in intermolecular interactions with rise in temperature, higher velocity of molecules leads to a reduction in viscosity [93]. Therefore, temperature increase on viscosity is more effective for concentrated nanofluids.

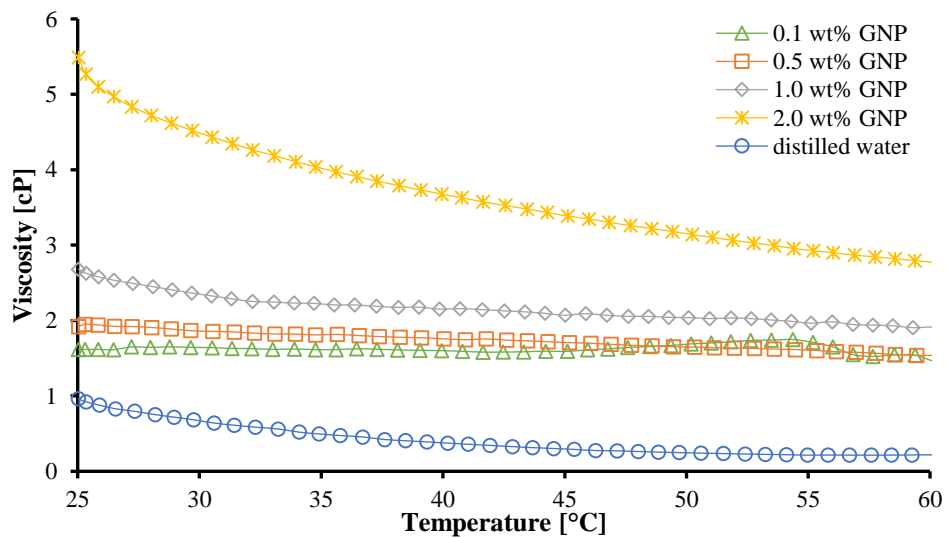


Figure 4.24 : Viscosity as a function of temperature for aqueous GNP (530 m²/g) nanofluids with no PEG-POSS.

Figure 4.25 illustrates the viscosity as a function of shear rate for aqueous GNP (320 m²/g) nanofluids, without PEG-POSS. Shear thinning behavior was observed in 0.5 wt% GNP nanofluid, which indicates nanofluids could not remain stable even at low concentrations. The shear thinning behavior of 0.5, 1.0 and 2.0 wt% GNP nanofluids continued up to shear rate of 140, 220 and 340 s⁻¹, respectively. For these nanofluids, the increase in nanoparticle concentration raised agglomeration and decreased stability.

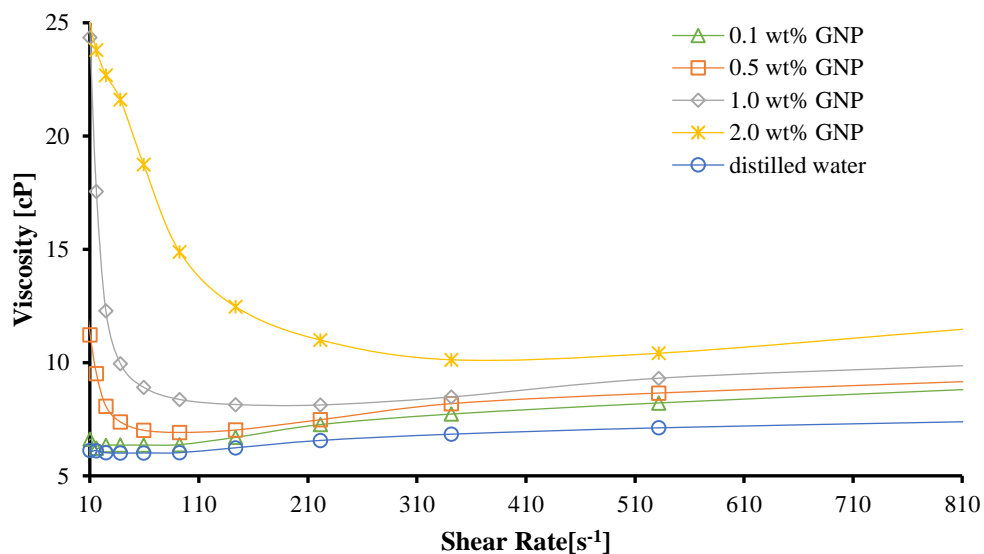


Figure 4.25 : Viscosity as a function of shear rate for aqueous GNP (320 m²/g) nanofluids with no PEG-POSS.

Viscosity as a function of temperature for aqueous GNP (320 m²/g) nanofluids with no PEG-POSS (Figure 4.26), the viscosity values of 0.1, 0.5, 1.0 and 2.0 wt% GNP nanofluids decreased by 0.22, 0.18, 0.9, and 3.2 cP, respectively. The reduction in viscosity increased with the rise of nanoparticle concentration.

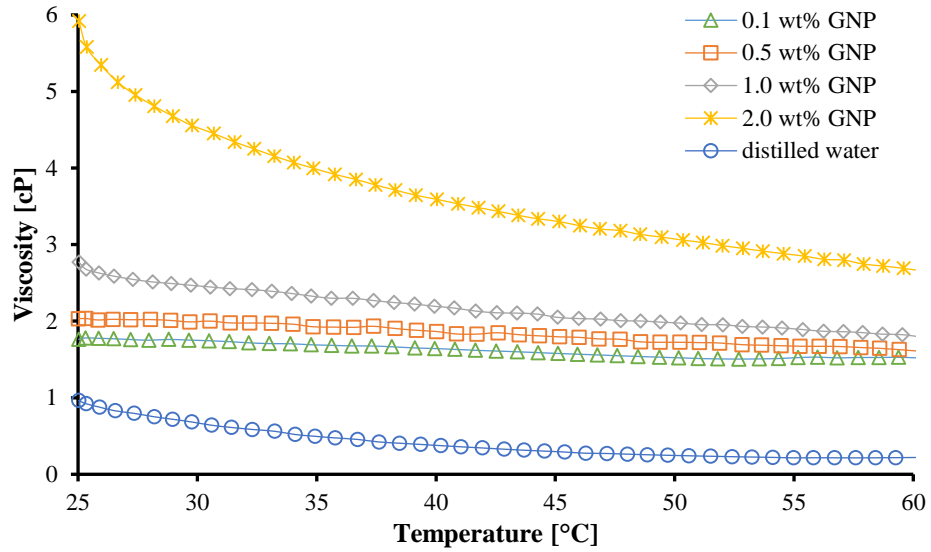


Figure 4.26 : Viscosity as a function of temperature for aqueous GNP (320 m²/g) nanofluids with no PEG-POSS.

Figure 4.27 illustrates viscosity versus shear rate graph of aqueous 0.1 wt% GNP (320, 500, and 800 m²/g) nanofluids with no PEG-POSS. Shear thickening behavior was observed for each nanofluid after a shear rate of 90 s⁻¹.

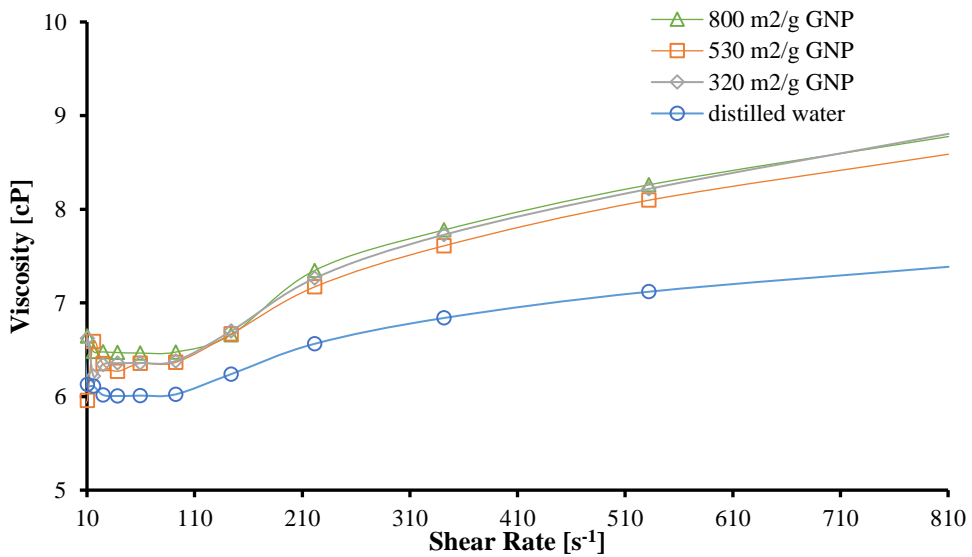


Figure 4.27 : Viscosity as a function of shear rate for aqueous 0.1 wt% GNP nanofluids with different surface areas and without PEG-POSS.

Viscosity as a function of temperature for aqueous 0.1 wt% GNP (320, 500, and 800 m²/g) nanofluids with no PEG-POSS is given in Figure 4.28. The viscosity values of nanofluids containing GNP with surface area of 320 and 800 m²/g had a similar trend.

Intermolecular attraction force, which decreased with a reduced surface area at low nanoparticle concentrations, did not have much effect on viscosity. As for 530 m²/g GNP nanofluid, showed both shear thickening and shear thinning behaviors between 45°C and 55°C due to the nanoparticle agglomeration in the nanofluid.

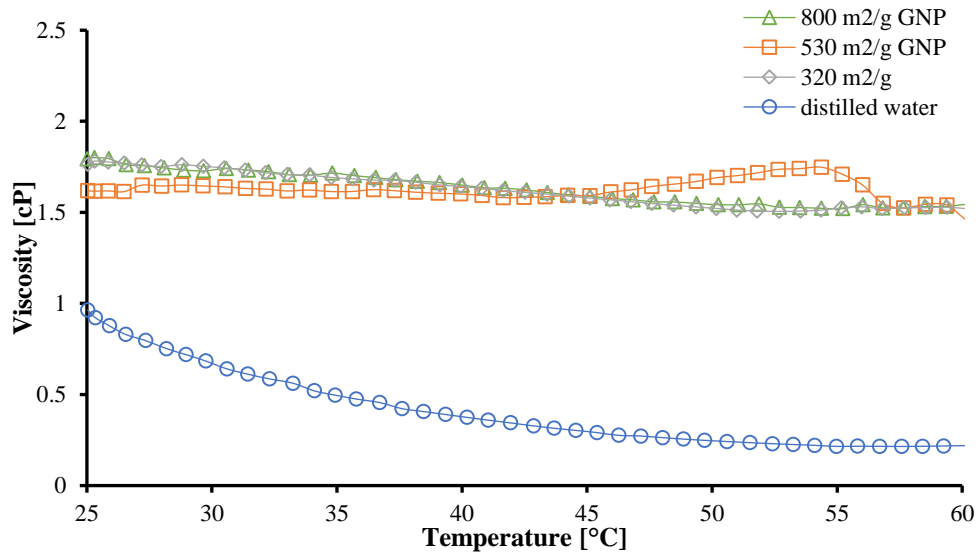


Figure 4.28 : Viscosity as a function of temperature for aqueous 0.1 wt% GNP nanofluids with different surface areas and without PEG-POSS.

Viscosity as a function of shear rate for 0.5 wt% GNP nanofluids with different surface area is given in Figure 4.29. Shear thinning behavior was observed for 320 m²/g and 530 m²/g GNP nanofluids up to a shear rate of about 90 and 140 s⁻¹, respectively. At the 320 m²/g GNP nanofluid, viscosity reduction of 4 cP was observed up to a shear rate of 90 s⁻¹, while a decrease of 1.1 cP was observed for 530 m²/g GNP nanofluid at shear rate of 140 s⁻¹. This was another indication that nanofluids having GNP with low surface area were less stable.

In Figure 4.30 showing viscosity as a function of temperature for GNP nanofluids with different surface areas, under the constant shear rate, the viscosity increased with the decrease in surface area of nanoparticles. Due to the high Van der Waals attractive forces between nanoparticles with lower surface area, the nanofluids were exposed to high shear stress at a constant shear rate, showed higher viscosity.

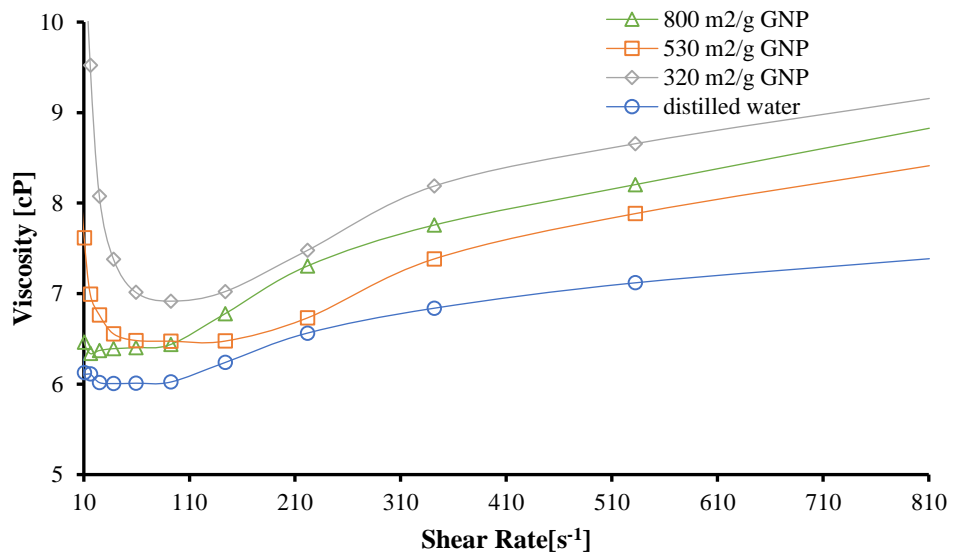


Figure 4.29 : Viscosity as a function of shear rate for aqueous 0.5 wt% GNP nanofluids with different surface areas and without PEG-POSS.

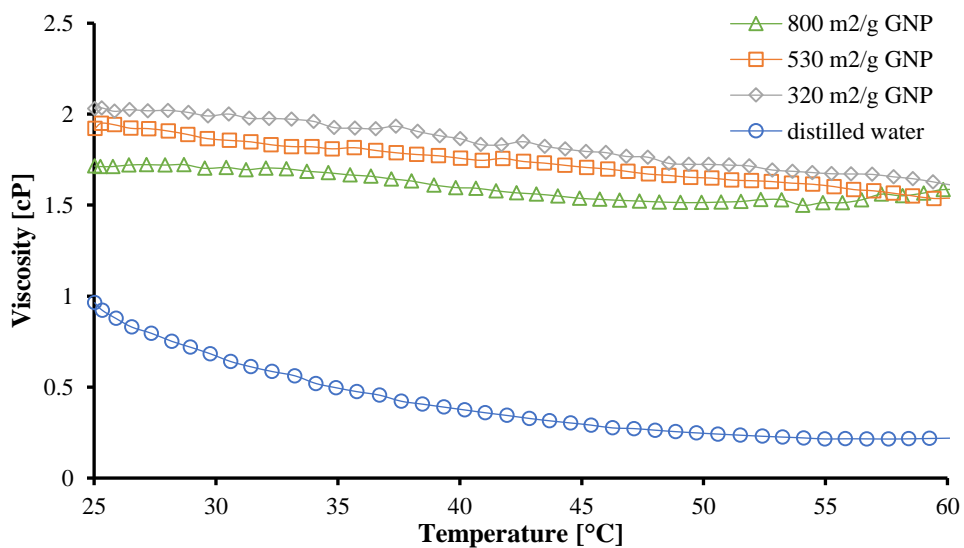


Figure 4.30 : Viscosity as a function of temperature for aqueous 0.5 wt% GNP nanofluids with different surface areas and without PEG-POSS.

In Figure 4.31, viscosity as a function of shear rate for 1.0 wt% GNP nanofluids with different surface area is given. The initial viscosities of nanofluids containing GNP with surface area of 320 m²/g and 530 m²/g were 25 and 15 cP, respectively. This is showed aggregation rises as the nanoparticle concentration increases. Shear thinning behavior was not observed in 800 m²/g GNP nanofluids due to their high stability. In viscosity versus temperature graph given in Figure 4.32, the viscosity of 800 m²/g GNP nanofluid was lower than the other samples at the same temperature and the viscosity

change of this sample was less depend on temperature. It shows that 800 m²/g GNP nanofluids were more stable.

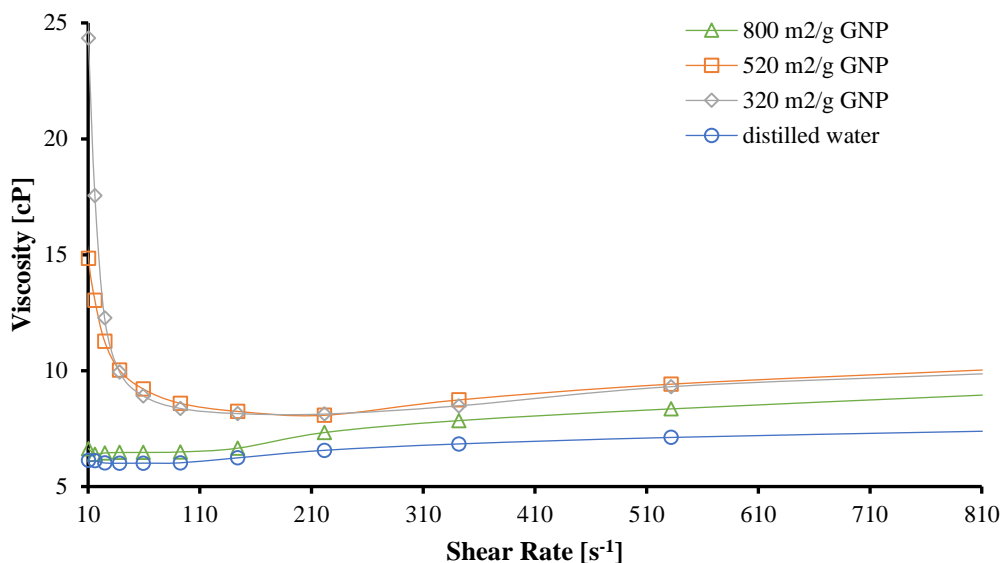


Figure 4.31 : Viscosity as a function of shear rate for aqueous 1.0 wt% GNP nanofluids with different surface areas and without PEG-POSS.

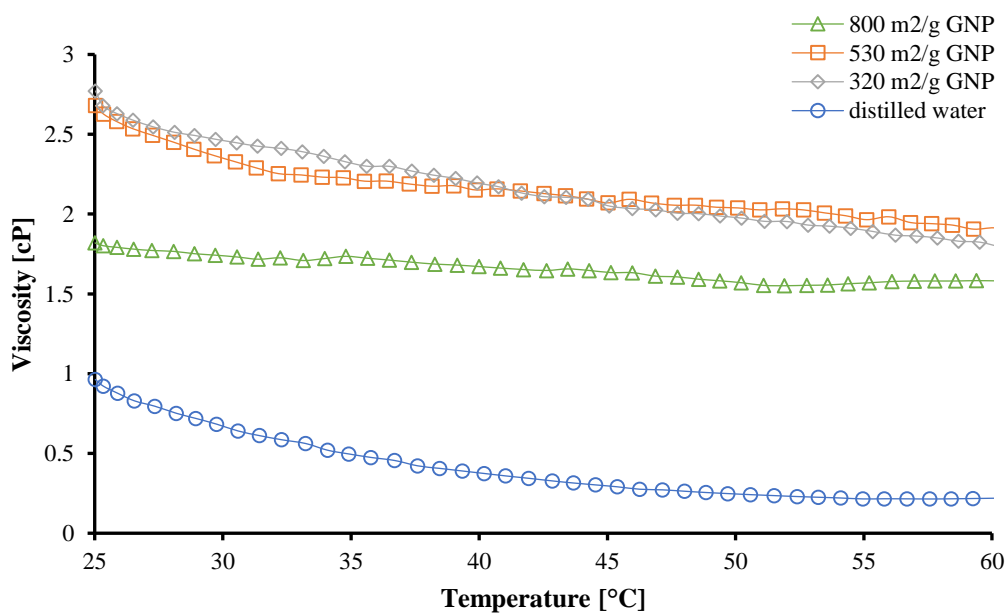


Figure 4.32 : Viscosity as a function of temperature for aqueous 1.0 wt% GNP nanofluids with different surface areas and without PEG-POSS.

Figure 4.33 illustrates viscosity as a function of shear rate for 2.0 wt% GNP nanofluids with the different surface areas. Due to the high stability of 800 m²/g GNP nanofluids, shear thickening was observed after the shear rate of 340 s⁻¹. The absence of shear thickening behavior in the 320 m²/g and 530 m²/g GNP nanofluids indicates nanoparticles still tend to agglomerate in the studied shear rate range [91].

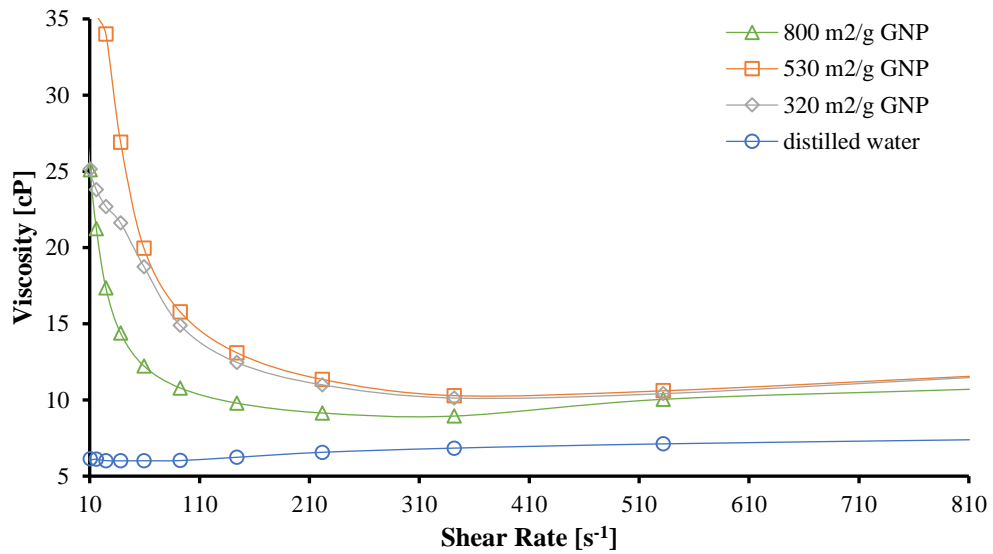


Figure 4.33 : Viscosity as a function of shear rate for aqueous 2.0 wt% GNP nanofluids with different surface areas and without PEG-POSS.

The viscosity as a function temperature for nanofluids having 2.0 wt% GNP with different surface areas is given in Figure 4.34. In these samples (having the highest nanoparticle concentration), the viscosity change of the samples with the highest surface area was found to be less than the others. So nanofluids having high surface area were more stable.

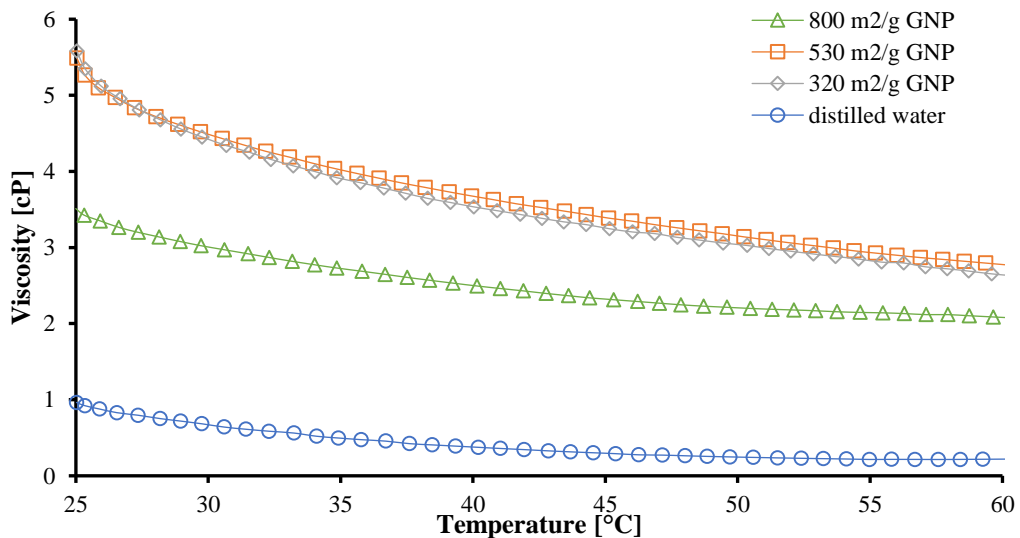


Figure 4.34 : Viscosity as a function of temperature for aqueous 2.0 wt% GNP nanofluids with different surface areas and without PEG-POSS.

Compared to that of aqueous nanofluids, the most important difference in the rheograms of EG-based nanofluids was that EG-based nanofluids showed lower viscosity than the base fluid EG. Figure 4.35 illustrates viscosity as a function of shear

rate for EG-based GNP ($800 \text{ m}^2/\text{g}$) nanofluids with no PEG-POSS. EG-base fluid exhibits Newtonian behavior with a viscosity value of 23 cP between 10 s^{-1} and 810 s^{-1} . While the viscosity of 0.1 wt% GNP nanofluid was about 22.5 cP, the viscosity of 0.5 and 1.0 wt% GNP nanofluids were 20.3 cP.

It has been reported in the literature, due to the lubricant effect for MWCNT-EG nanofluids have a lower viscosity than the base fluid [66]. In addition, another reason why the GNP-EG nanofluids have a lower viscosity than the base fluid is the addition of NH_4OH solution to nanofluids during pH adjustment, in this thesis. Shear thinning behavior was observed at having the highest nanoparticle concentration of 2.0 wt% GNP nanofluid with an increase in shear rate. With shear rate increase from 10 s^{-1} to 810 s^{-1} , 25 cP viscosity reduction was observed. Shear thickening behavior was not observed due to the formation of agglomeration and distribution of these agglomerated particles in studied shear rate range.

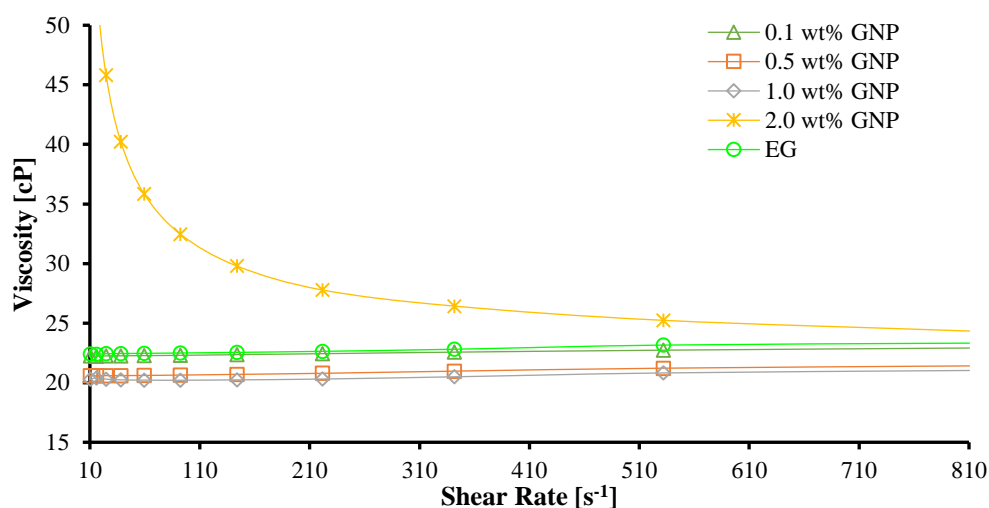


Figure 4.35 : Viscosity as a function of shear rate for EG-based GNP ($800 \text{ m}^2/\text{g}$) nanofluids with without PEG-POSS.

Viscosity as a function of temperature for EG-based GNP ($800 \text{ m}^2/\text{g}$) nanofluids with no PEG-POSS is given in Figure 4.36. In this graph, as in Figure 4.35, viscosities were lower than the base fluid, except for 2.0 wt% GNP nanofluids. For all samples, including the base fluid, temperature increased from 25°C to 60°C , resulted in a 11 cP reduction in viscosity.

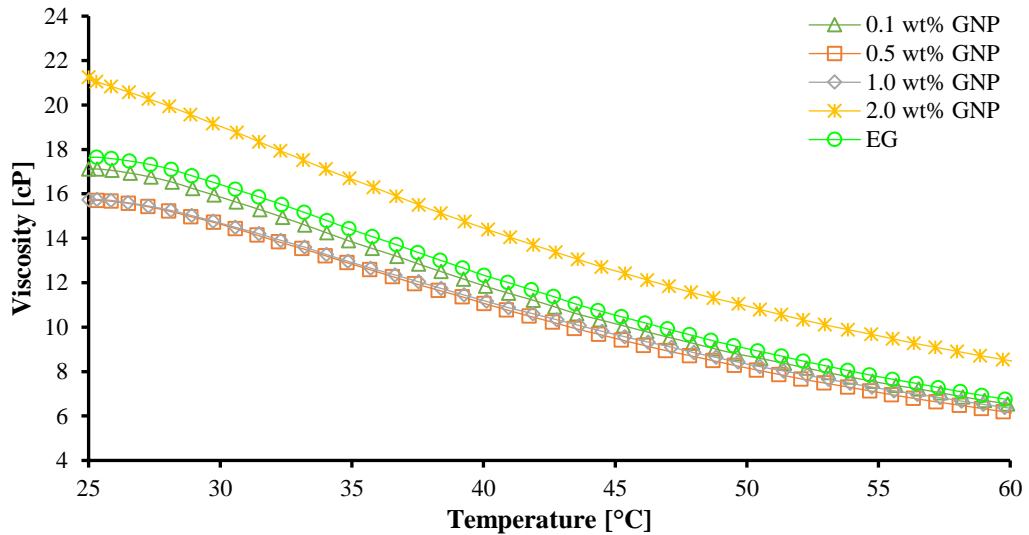


Figure 4.36 : Viscosity as a function of temperature for EG-based GNP ($800 \text{ m}^2/\text{g}$) nanofluids with no PEG-POSS.

Viscosity versus shear rate graph of EG-based $800 \text{ m}^2/\text{g}$ GNP nanofluids with 0.1 wt% PEG-POSS is given in Figure 4.37. The viscosity of 0.1 wt% GNP nanofluid, had the same values as the base fluid and was measured about 22.5 cP. With the effect of NH_4OH added during the preparation of nanofluids and the effect of PEG-POSS, the viscosities of 0.5 and 1.0 wt% GNP nanofluids were lower than base fluid and around 17 and 16 cP, respectively. The viscosity of 1.0 wt% GNP nanofluid was reduced up to 4 cP from 10 s^{-1} to 220 s^{-1} . In the 2.0% GNP nanofluid shear thinning behavior was observed until 810 s^{-1} and a viscosity decreased about 30 cP.

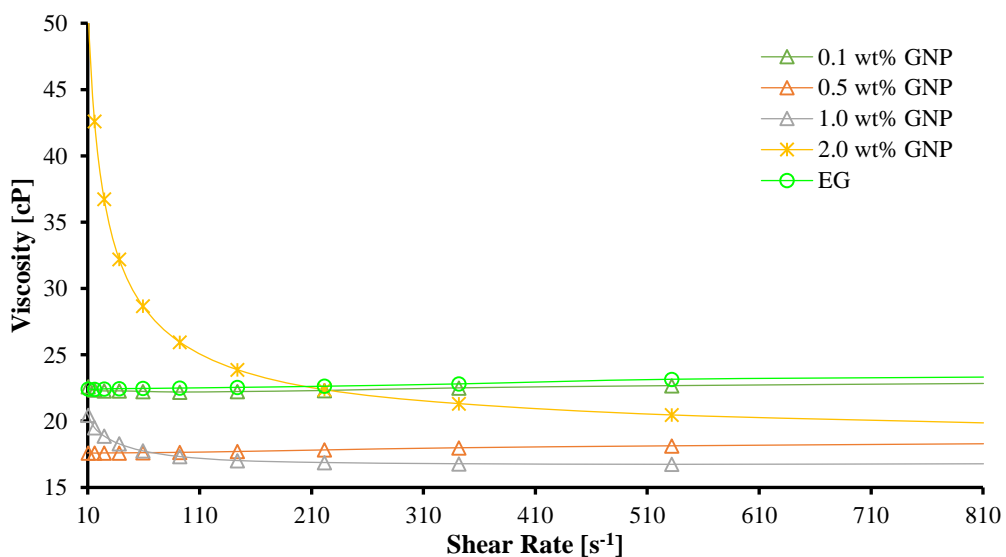


Figure 4.37 : Viscosity as a function of shear rate for EG-based GNP ($800 \text{ m}^2/\text{g}$) nanofluids with 0.1 wt% PEG-POSS.

Viscosity as a function of temperature for EG-based GNP (800 m²/g) nanofluids with 0.1 wt% PEG-POSS, at a constant shear rate of 200 s⁻¹ is given in Figure 4.38. With the temperature rising from 25°C to 60°C, a decrease in viscosity of about 9 cP was observed in all nanofluids. The lowest viscosity value belonged to 1.0 wt% GNP nanofluid and the highest viscosity value belonged to the base fluid. The absence of a tendency between the high viscosity values and the nanoparticle concentration was due to the addition of different amount of NH₄OH to the nanofluids.

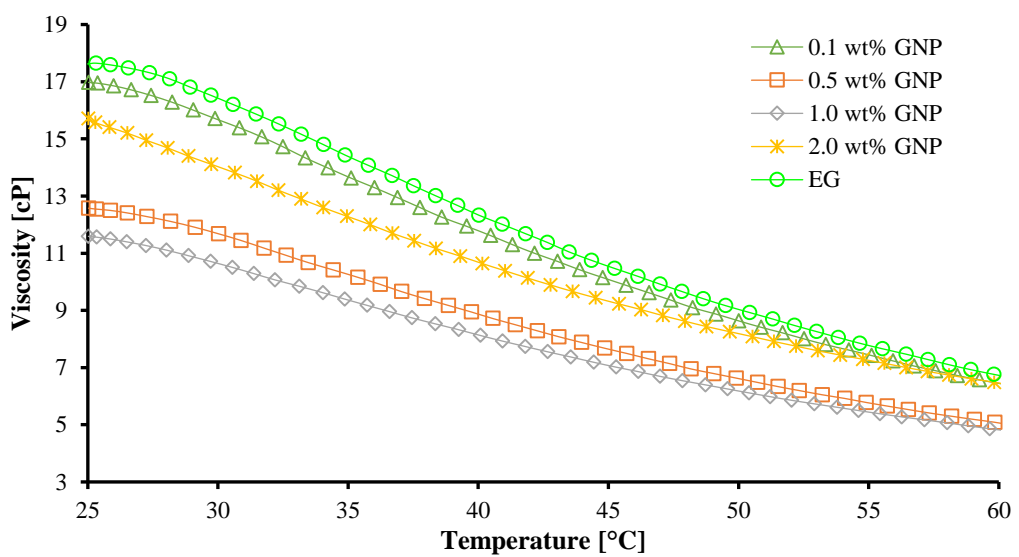


Figure 4.38 : Viscosity as a function of temperature for EG-based GNP (800 m²/g) nanofluids with 0.1 wt% PEG-POSS.

Viscosity as a function of shear rate for EG-based GNP (800 m²/g) nanofluids with 0.2 wt% PEG-POSS, is given in Figure 4.39. The viscosities of 0.1 to 0.5 and 1.0 wt% GNP nanofluids were measured as approximately 21 and 17 cP, respectively. With the increase in PEG-POSS concentration, the viscosity of 2.0 wt% GNP nanofluid decreased to about 45 cP at 10 s⁻¹ and reduced up to 17 cP, at shear rate of 810 s⁻¹.

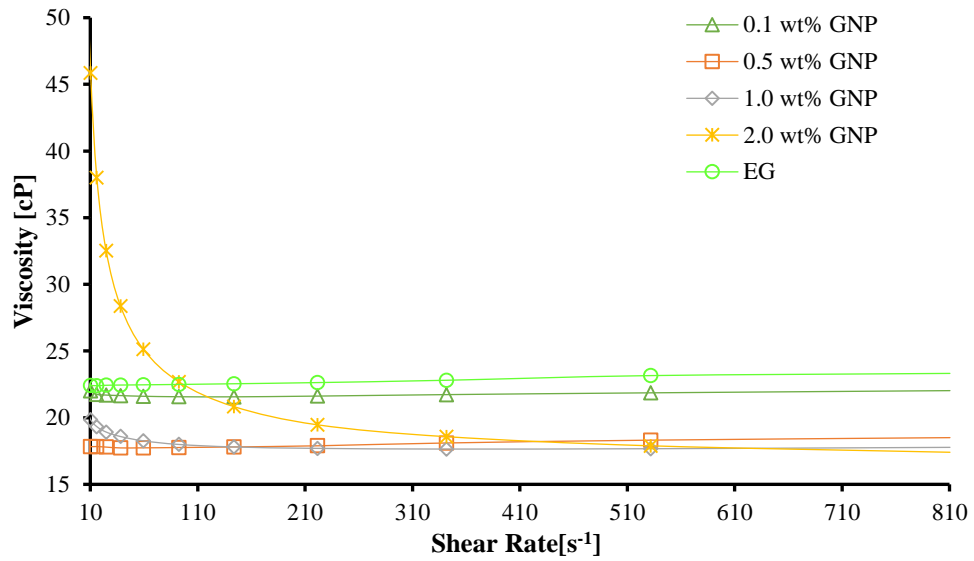


Figure 4.39 : Viscosity as a function of shear rate for EG-based GNP ($800 \text{ m}^2/\text{g}$) nanofluids with 0.2 wt% PEG-POSS.

In the temperature change and viscosity graph is given in Figure 4.40, the highest viscosity values belonged for EG base fluid. The viscosity of 2.0 wt% GNP nanofluid having 0.2 wt% PEG-POSS showed a decrease compared to other PEG-POSS concentrations. The viscosity values of both 0.5, 1.0 and 2.0 wt% GNP nanofluids were 13 cP and 5.7 cP at 25°C and 60°C , respectively. For 0.1 wt% GNP nanofluids, these values were 16.3 cP and 6.7 cP at 25°C and 60°C , respectively.

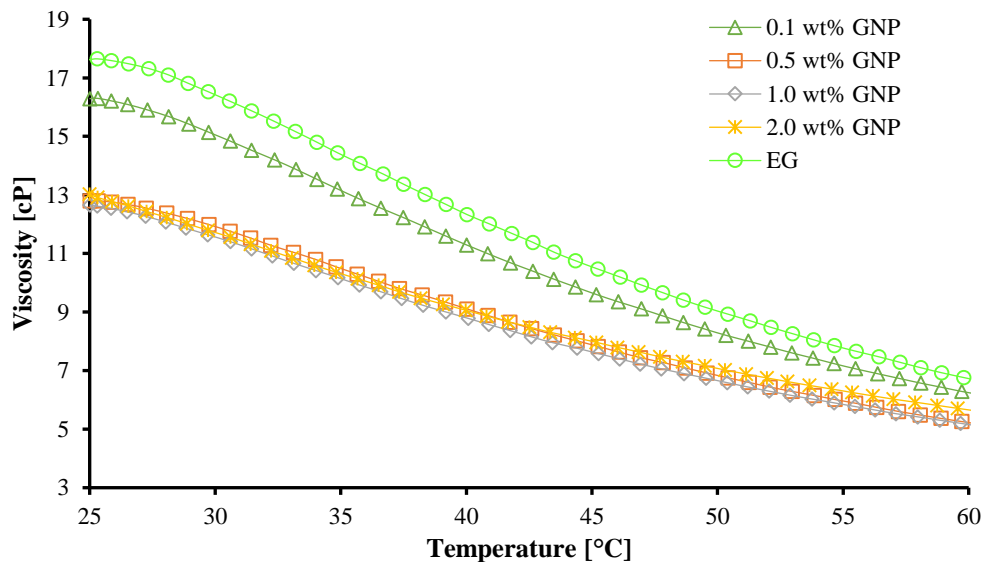


Figure 4.40 : Viscosity as a function of temperature for EG-based GNP ($800 \text{ m}^2/\text{g}$) nanofluids with 0.2 wt% PEG-POSS.

The viscosity versus shear rate of EG based 800 m²/g GNP nanofluids with 0.3 wt% PEG-POSS is given in Figure 4.41. Compared to other PEG-POSS concentrations, there was no change in the viscosities of 0.1 and 0.5 wt% GNP nanofluids. The viscosities of 1.0 and 2.0 wt% GNP nanofluids measured as 15 cP by Newtonian behavior and between 41 cP and 15 cP by shear thinning behavior. Considering all PEG-POSS concentrations, the increase in PEG-POSS was effective on decreasing the viscosity of samples having high nanoparticle concentration. This can be attributed to the fact that use of PEG-POSS increases nanofluid stability, as shown in Figure 4.4. The decrease in viscosity was observed due to the stability of the nanofluids.

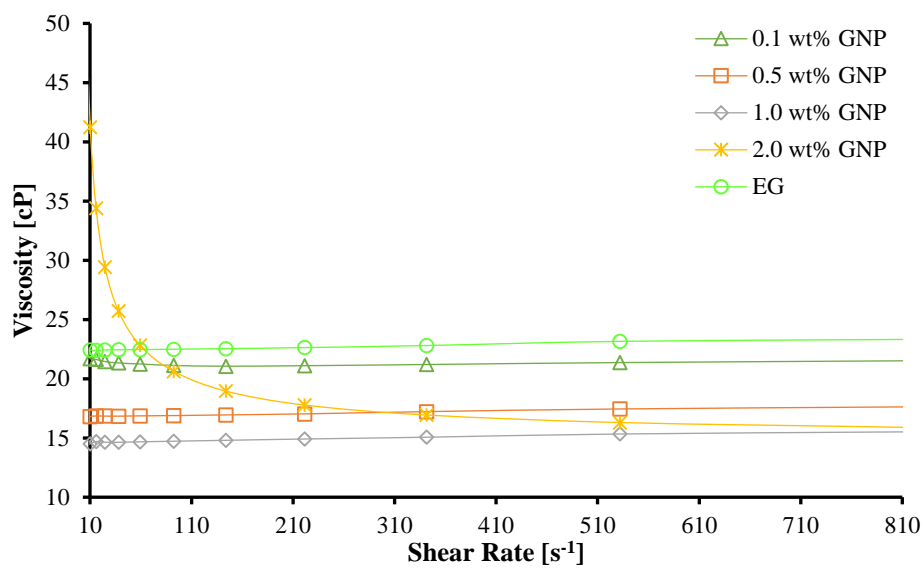


Figure 4.41 : Viscosity as a function of shear rate for EG-based GNP (800 m²/g) nanofluids with 0.3 wt% PEG-POSS.

Figure 4.42 shows that the increase in PEG-POSS concentration decreases the viscosity values of nanofluids when compared with other PEG-POSS concentrations. The lowest viscosity values are 9.9 cP and 4.3 cP at 25°C and 60°C for the 1.0 wt% GNP nanofluid, respectively.

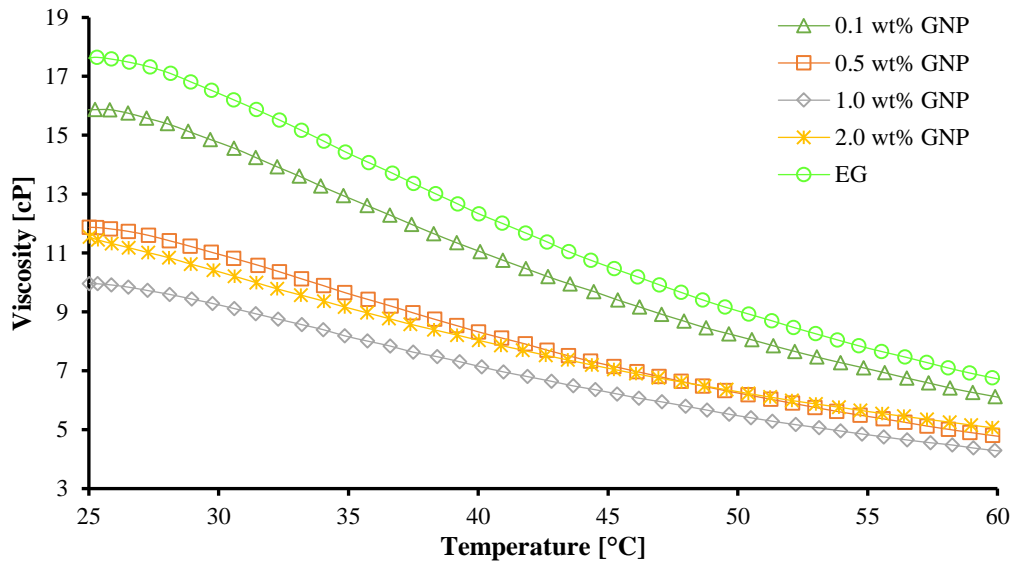


Figure 4.42 : Viscosity as a function of temperature for EG-based GNP ($800 \text{ m}^2/\text{g}$) nanofluids with 0.3 wt% PEG-POSS.

Viscosity as a function of shear rate for EG-based $530 \text{ m}^2/\text{g}$ GNP nanofluids with no PEG-POSS is given in Figure 4.43. Nanofluids containing 0.1, 0.5, and 1.0 wt% nanoparticles had a viscosity of about 22 cP and these nanofluids exhibited Newtonian behavior. When the nanoparticle concentration increased to 2.0 wt%, the viscosity value was measured as 48 cP at 10 s^{-1} shear rate and decreased to 23 cP at 810 s^{-1} shear rate due to separation of nanoparticle aggregation. Shear thickening behavior was not observed in the studied shear rate range due to the formation of agglomeration [91].

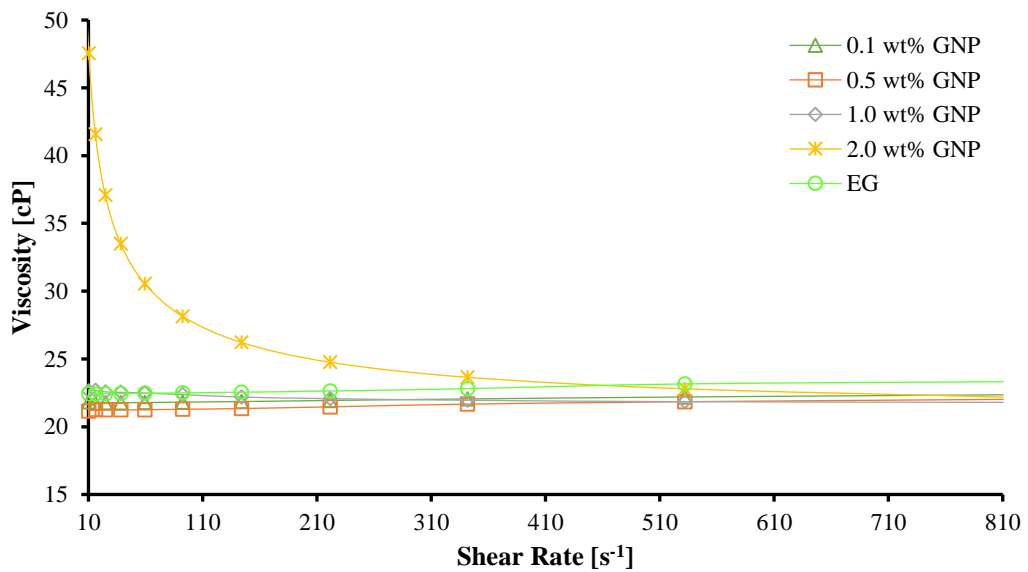


Figure 4.43 : Viscosity as a function of shear rate for EG-based GNP ($530 \text{ m}^2/\text{g}$) nanofluids with no PEG-POSS.

In Figure 4.44, viscosity as a function of temperature is given, viscosity decrease of 11 cP was observed between 25°C and 60°C for all nanofluids. The highest viscosity values were belonged 2.0 wt% GNP nanofluid and measured as 19 and 8.6 cP at 25°C and 60°C, respectively.

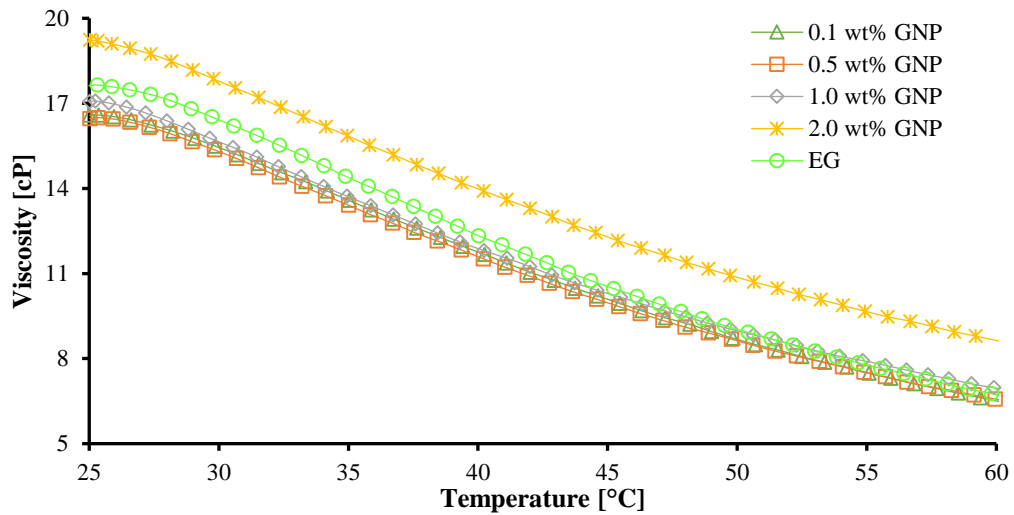


Figure 4.44 : Viscosity as a function of temperature for EG-based GNP (530 m²/g) nanofluids with no PEG-POSS.

Figure 4.45 shows viscosity as a function shear rate for EG-based 320 m²/g GNP nanofluids with no PEG-POSS. The nanofluid having 0.1 wt% GNP showed Newtonian behavior with the viscosity value about 22 cP. Due to the decrease in surface area and increase Van der Waals attractive forces between molecules, the formation of agglomeration in nanoparticles was supported by the shear thinning behavior of nanofluids having 0.5, 1.0, and 2.0 wt% GNP. The viscosity values of these samples were measured as 25 cP, 30 cP, and 50 cP at the shear rate of 10 s⁻¹, respectively, and these values decreased to 22 cP with reached shear rate 810 s⁻¹.

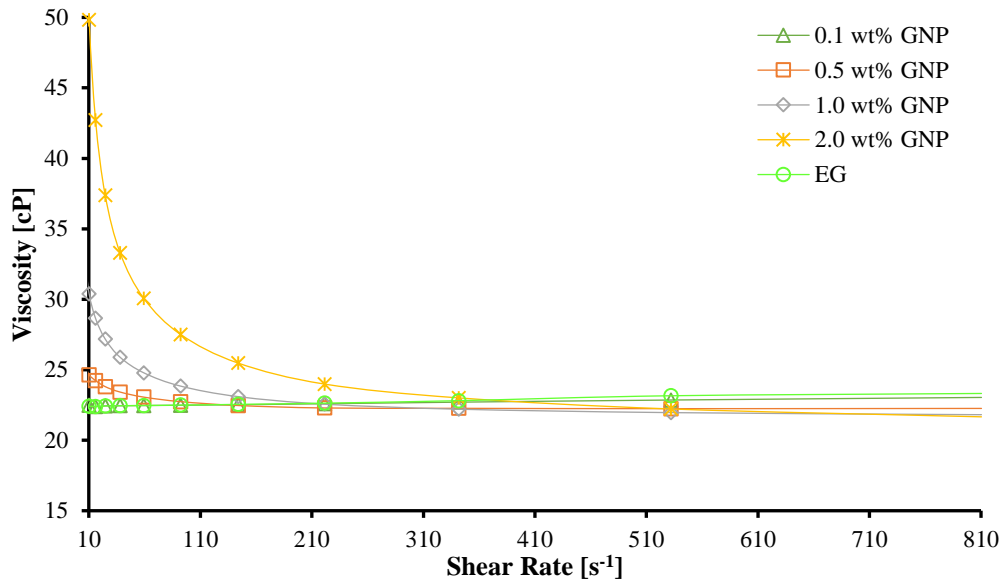


Figure 4.45 : Viscosity as a function of shear rate for EG-based GNP ($320 \text{ m}^2/\text{g}$) nanofluids with no PEG-POSS.

Viscosity as a function of temperature for EG-based $320 \text{ m}^2/\text{g}$ GNP nanofluids with no PEG-POSS is given in Figure 4.46. For 0.1, 0.5, and 1.0 wt% GNP nanofluids, viscosity reduction of about 10 cP was observed between 25°C and 60°C , while the viscosity reduction of 2.0 wt% GNP nanofluid recorded around 9 cP.

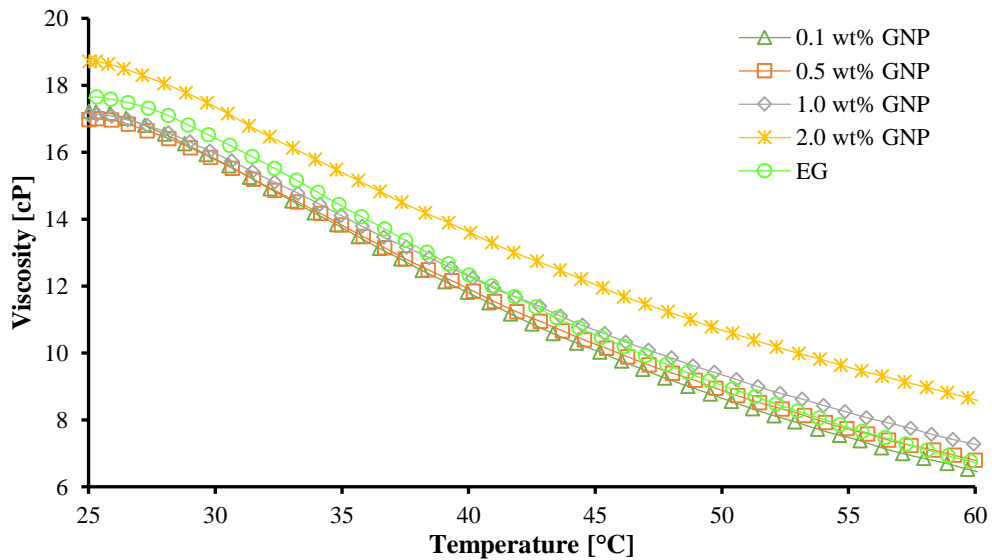


Figure 4.46 : Viscosity as a function of temperature for EG-based GNP ($320 \text{ m}^2/\text{g}$) nanofluids with no PEG-POSS.

Figure 4.47 shows viscosity as a function of shear rate for EG-based 0.1 wt% GNP nanofluids with different surface areas and without PEG-POSS. The lowest viscosity

belongs to the 530 m²/g GNP nanofluid with an average value of 22 cP. The viscosities of GNP nanofluids with surface area of 800 and 320 m²/g were measured about 22.5. For these nanofluids with the lowest nanoparticle concentration, the viscosity values were very close to each other.

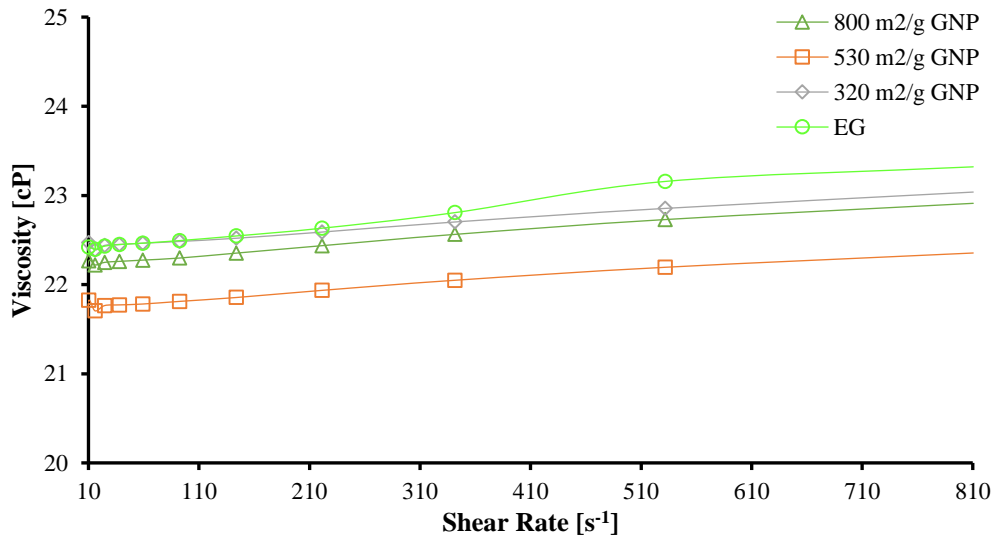


Figure 4.47 : Viscosity as a function of shear rate for EG-based 0.1 wt% GNP nanofluids with different surface areas and without PEG-POSS.

Viscosity as a function of temperature for EG-based nanofluids having GNP with different surface areas given in Figure 4.48, the viscosity values for all nanofluids were measured as approximately 17 cP and 6.8 cP at 25°C and 60°C, respectively.

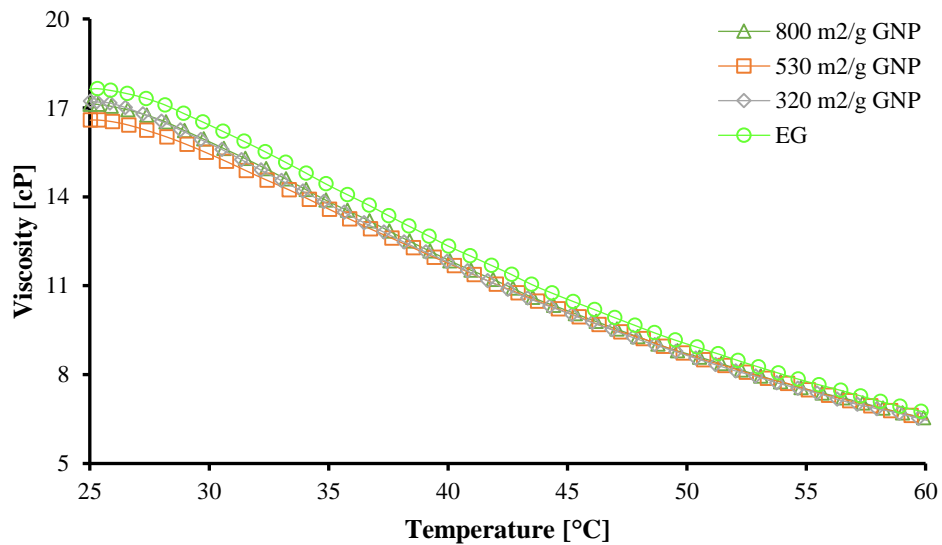


Figure 4.48 : Viscosity as a function of temperature for EG-based 0.1 wt% GNP nanofluids with different surface areas and without PEG-POSS.

The lowest viscosity value in the viscosity versus shear rate graph of EG-based 0.5 wt% GNP nanofluids with different surface areas given in Figure 4.49, was 20.7 cP for 800 m²/g GNP nanofluid. The 530 m²/g GNP nanofluid had an average viscosity of 21.5 cP, while the 320 m²/g GNP nanofluid had 24.7 and 22.25 cP at shear rate of 10 and 810 s⁻¹, respectively. As the shear rate increases, shear thinning behavior was observed. So it was seen that the 320 m²/g GNP nanofluid was more unstable than other samples of this concentration.

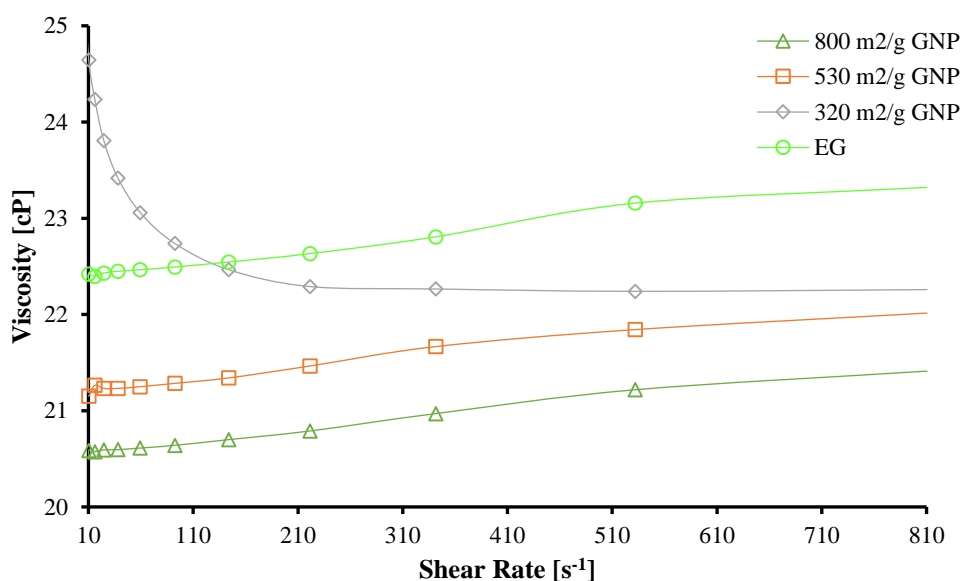


Figure 4.49 : Viscosity as a function of shear rate for EG-based 0.5 wt% GNP nanofluids with different surface areas and without PEG-POSS.

Graph showing the effect of temperature on viscosity of EG based 0.5 wt% GNP nanofluids with different surface areas, is given in Figure 4.50. The viscosities of 800 m²/g, 530 m²/g, and 320 m²/g GNP nanofluids were 15.7 cP and 6.2 cP, 16.5 cP and 6.6 cP, 16.9 cP and 6.7 cP at 25°C and 60°C, respectively.

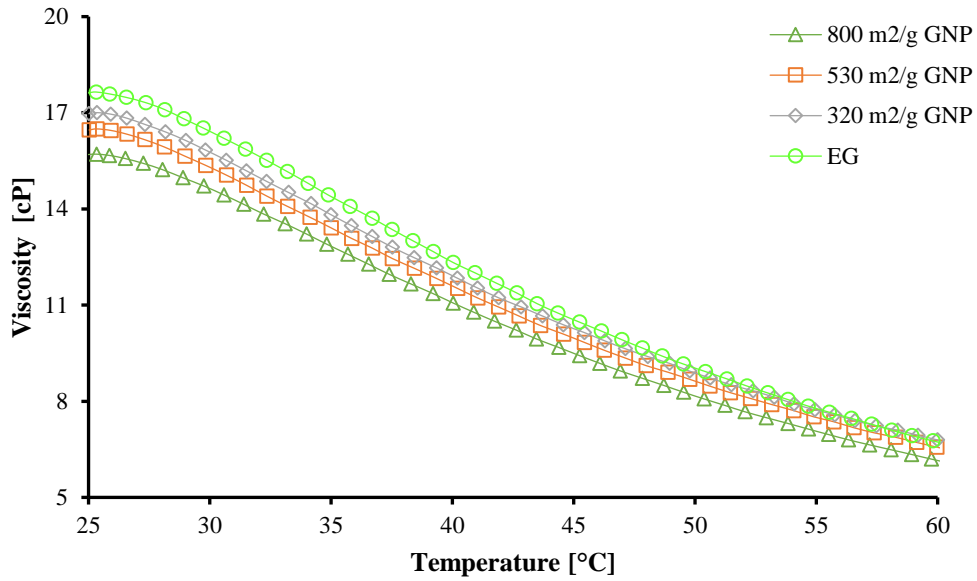


Figure 4.50 : Viscosity as a function of temperature for EG-based 0.5 wt% GNP nanofluids with different surface areas and without PEG-POSS.

Figure 4.51 illustrates viscosity as a function of shear rate for EG-based 1.0 wt% GNP nanofluids with different surface areas, without PEG-POSS. The lowest viscosity value was 20.5 cP and belonged to 800 m²/g GNP nanofluid. The viscosity of 530 m²/g GNP nanofluid 22.2 cP, while viscosities of GNP nanofluid with surface area of 320 m²/g were 30 cP and 21.8 cP at a shear rate of 10 and 810 s⁻¹, respectively.

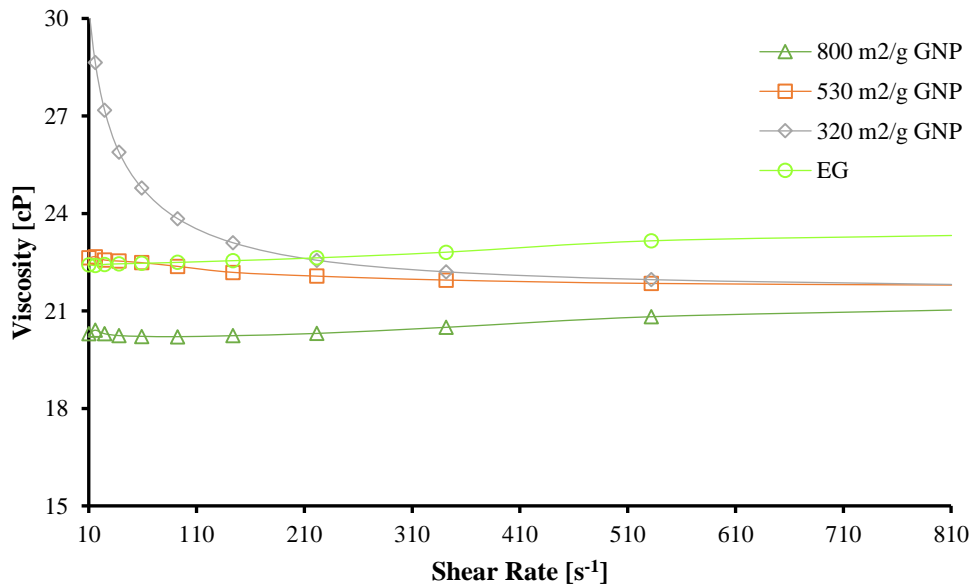


Figure 4.51 : Viscosity as a function of shear rate for EG-based 1.0 wt% GNP nanofluids with different surface areas and without PEG-POSS.

The effect of temperature change on viscosity is seen in Figure 4.52 and 1.0 wt% GNP nanofluids With different surface areas showed the viscosity increases with decreasing surface area. At 25°C and 60°C, the viscosities were 15.7 cP and 6.7 cP for 800 m²/g GNP nanofluids; 17 cP and 6.7 cP for 530 m²/g GNP nanofluids; 17 cP and 7.3 cP for 320 m²/g GNP nanofluids.

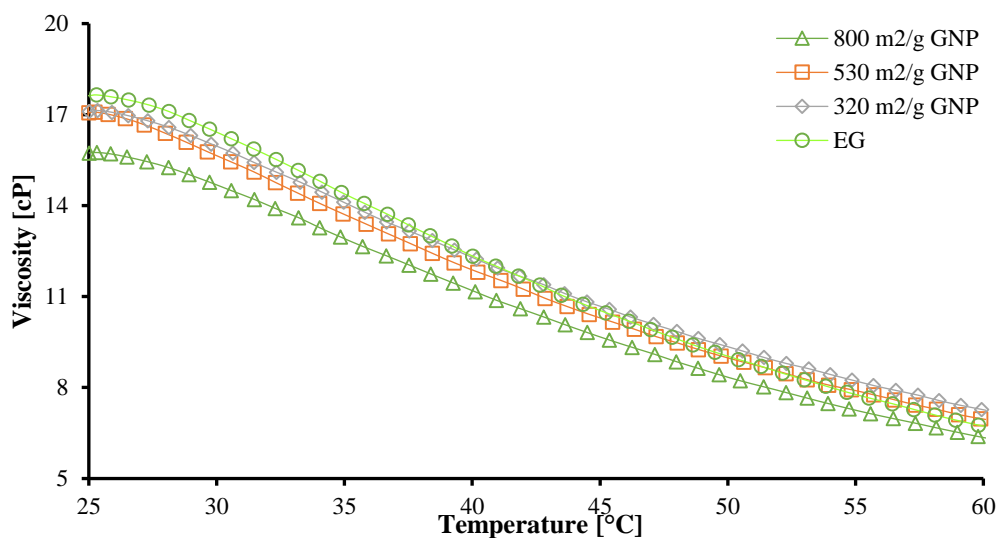


Figure 4.52 : Viscosity as a function of temperature for EG-based 1.0 wt% GNP nanofluids with different surface areas and without PEG-POSS.

The viscosity versus shear rate graph of EG-based nanofluids containing the highest concentration of nanoparticle with 2.0 wt% GNP with different surface areas is shown in Figure 4.53. All samples showed shear thinning behavior but no shear thickening was observed after a certain shear rate, such as aqueous samples. This situation shows that the nanofluids still tend to agglomerate under the applied shear stress in the studied shear rate range [91]. The viscosities of the 320 m²/g and 530 m²/g samples were 50 cP and 21.6 cP, 48 cP and 22 cP at shear rate of 10 s⁻¹ and 810 s⁻¹, respectively. These values were 59.4 cP and 24.3 cP for nanofluids containing nanoparticles with surface area of 800 m²/g.

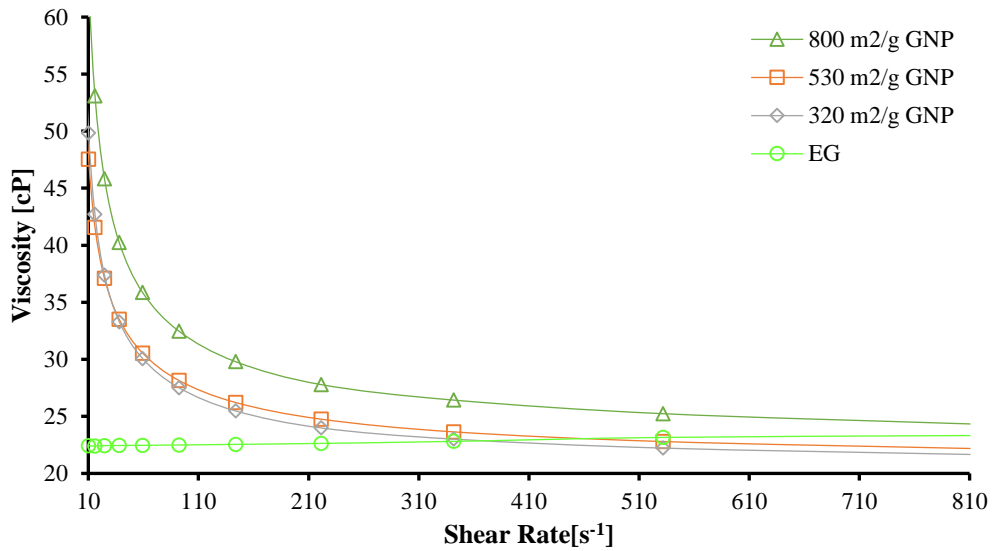


Figure 4.53 : Viscosity as a function of shear rate for EG-based 2.0 wt% GNP nanofluids with different surface areas and without PEG-POSS.

Figure 4.54 illustrates viscosity as a function of temperature for 2.0 wt% GNP nanofluids with different surface areas. At 25°C and 60°C the viscosities were 17 cP and 6.7 cP for 800 m²/g GNP nanofluids, 19.2 cP and 8.6 cP for 530 m²/g nanofluids, 18.7 cP and 8.5 cP for 320 m²/g GNP nanofluids.

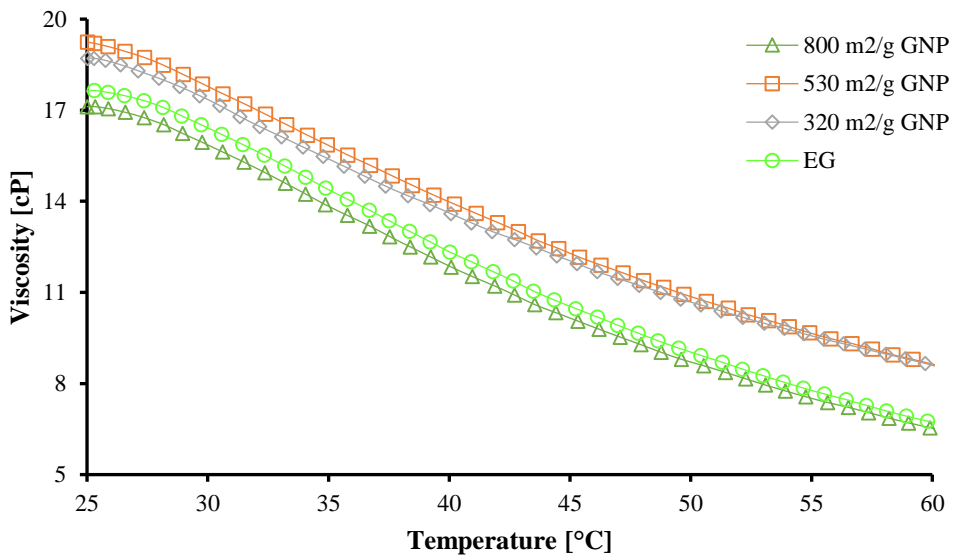


Figure 4.54 : Viscosity as a function of temperature for EG-based 2.0 wt% GNP nanofluids with different surface areas and without PEG-POSS.

Figure 4.55 shows viscosity as a function of shear rate for aqueous SWCNT nanofluids without PEG-POSS. Viscosities increased with increasing nanoparticle concentration. Shear thinning behavior was observed in all samples at low shear rate ranges due to the distribution of the aggregation in nanofluids. For 0.1, 0.5, and 1.0 wt% SWCNT nanofluids, shear thickening was observed after the shear rate of approximately 220 s^{-1} , whereas for 2.0 wt% SWCNT nanofluid, the shear rate which the shear thickening behavior starts was approximately 320 s^{-1} . The higher shear stress required for the shear thickening behavior of the high concentration sample proves that agglomeration increases with rises nanoparticle concentration.

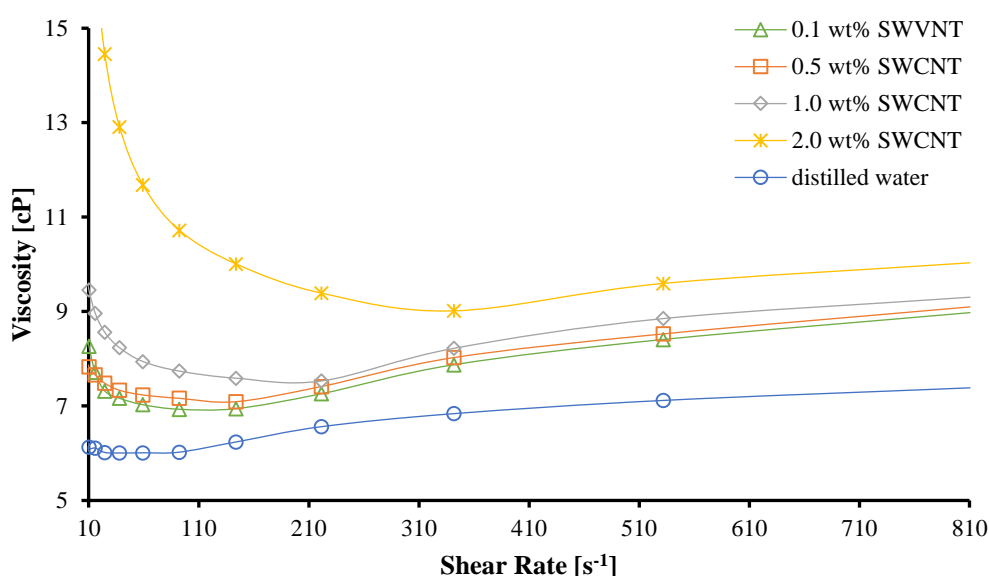


Figure 4.55 : Viscosity as a function of shear rate for aqueous SWCNT nanofluids with no PEG-POSS.

Viscosity as a function of temperature for aqueous SWCNT nanofluids with no PEG-POSS is given in Figure 4.56. Between 25°C and 60°C viscosities of the 0.1, 0.5, and 1.0 wt% SWCNT samples were the same, except small fluctuations. The nanofluid containing the highest nanoparticle concentration with 2.0 wt% SWCNT showed viscosity reduction of approximately 1 cP between 25°C and 60°C .

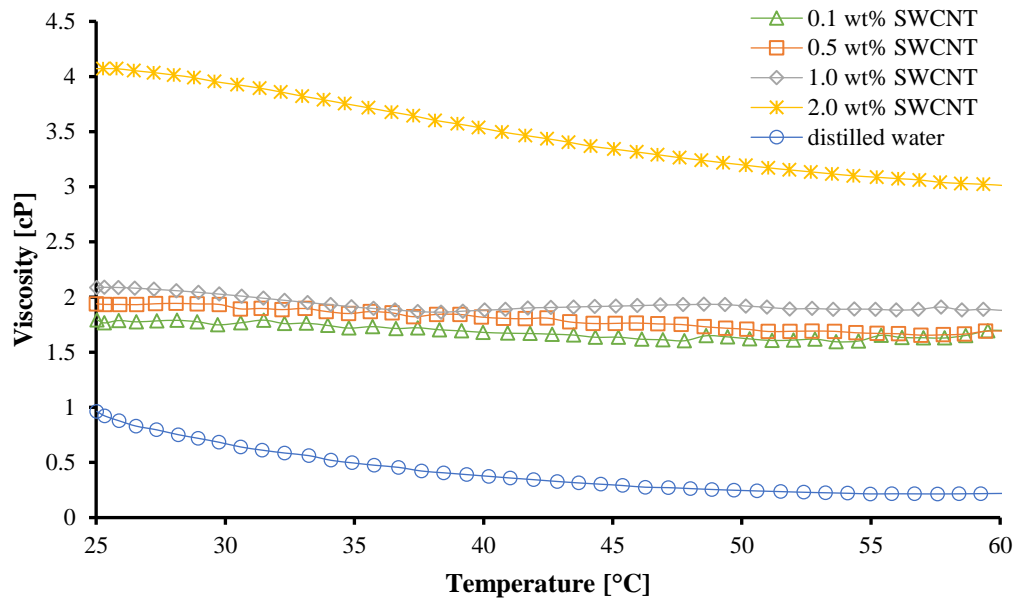


Figure 4.56 : Viscosity as a function of temperature for aqueous SWCNT nanofluids with no PEG-POSS.

Viscosity as a function of shear rate for aqueous SWCNT nanofluids with 0.1 wt% PEG-POSS is given in Figure 4.57. With the use of PEG-POSS, there was an increase in viscosity of the nanofluids and the highest increase was measured for the highest concentration of SWCNT sample having 2.0 wt%. At low shear rates, shear thinning behavior was observed due to the agglomeration of the nanoparticles and with increasing shear rate, the viscosity of the nanoparticles raised.

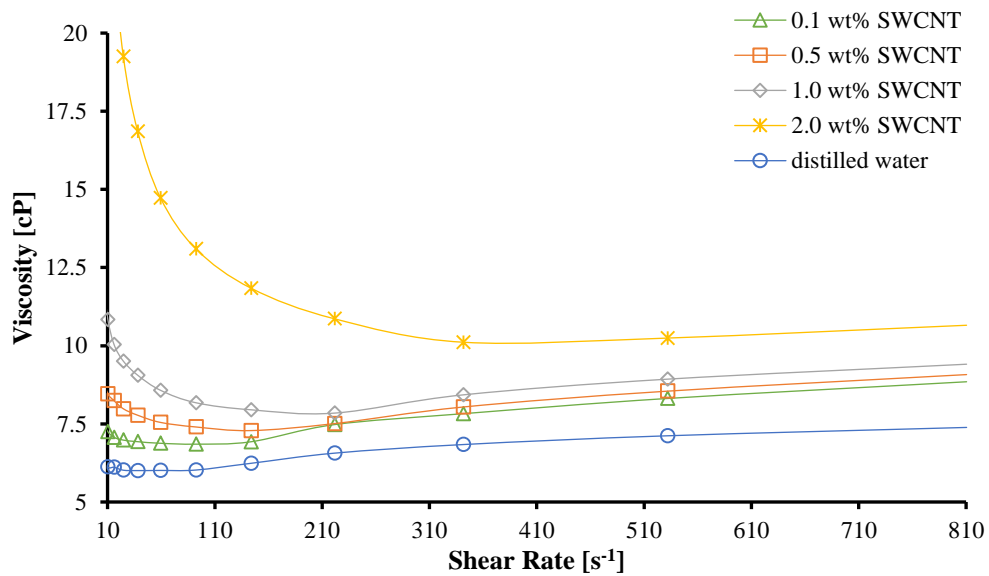


Figure 4.57 : Viscosity as a function of shear rate for aqueous SWCNT nanofluids with 0.1 wt% PEG-POSS.

As in Figure 4.58, viscosity as a function of temperature for aqueous SWCNT nanofluids with 0.1 wt% PEG-POSS. As the nanoparticle concentration increased, viscosity increases were observed and viscosity decreased with increasing temperature. The highest viscosity reduction value was approximately 1.2 cP for 2.0 wt% SWCNT nanofluid.

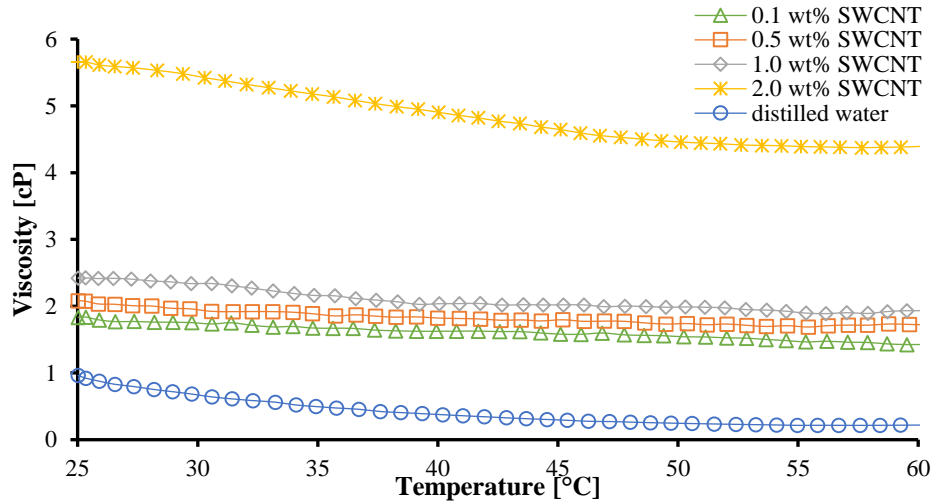


Figure 4.58 : Viscosity as a function of temperature for aqueous SWCNT nanofluids with 0.1 wt% PEG-POSS.

Figure 4.59 illustrates the viscosity versus shear rate for aqueous SWCNT nanofluids with 0.2 wt% PEG-POSS. The increase in the use of PEG-POSS to 0.2 wt% did not cause a significant change in viscosities. Nanofluids showed shear thinning behavior at low shear rates and shear thickening behavior at increasing shear rates.

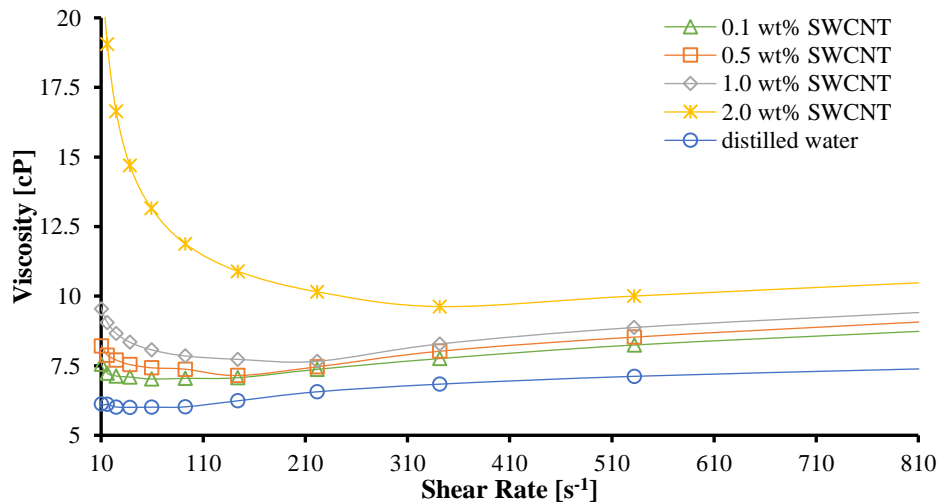


Figure 4.59 : Viscosity as a function of shear rate for aqueous SWCNT nanofluids with 0.2 wt% PEG-POSS.

In Figure 4.60, the viscosity and temperature changes of aqueous SWCNT nanofluids with 2.0 wt% PEG-POSS are given. The viscosity of 2.0 wt% SWCNT sample reduced of approximately 1.2 cP. Although fluctuations occurred in viscosity of samples at low concentrations, changes in viscosity values were small enough to be neglected.

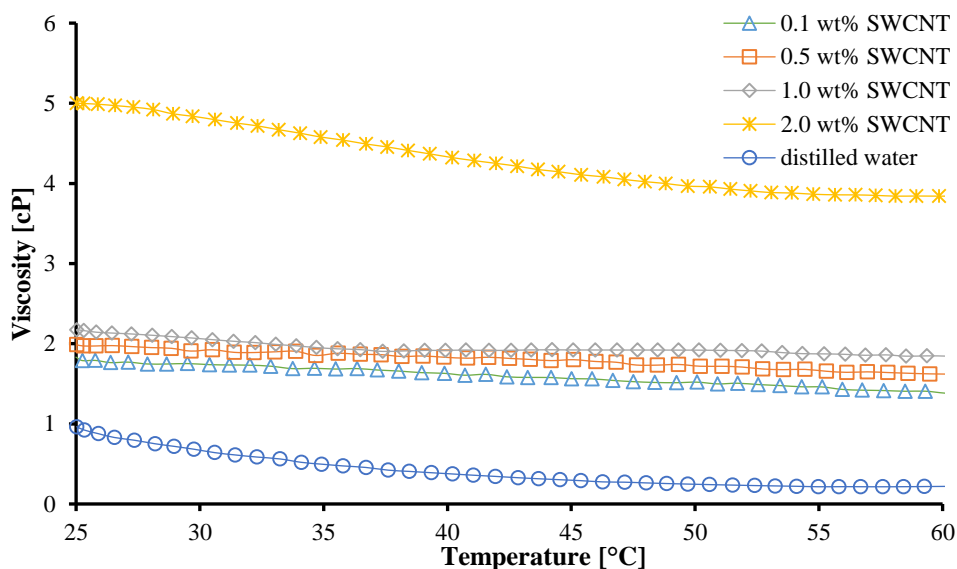


Figure 4.60 : Viscosity as a function of temperature for aqueous SWCNT nanofluids with 0.2 wt% PEG-POSS.

Figures 4.61, 4.62, and 4.63 illustrate relative viscosities for the aqueous GNP, EG-based GNP, and aqueous SWCNT nanofluids, respectively. Figures 4.61 and 4.62 show that, although the base fluid changed, the viscosities decreased with increasing surface area of the nanoparticles. Due to having high surface area nanoparticle, the viscosity of stable samples were increased. The use of PEG-POSS, for aqueous samples containing GNP, did not affect viscosity much. In aqueous nanofluids containing SWCNT with high nanoparticle concentration, the viscosity increased with raised PEG-POSS concentration. Only for aqueous samples, the increase in viscosity was directly proportional to the increase in nanoparticle concentration. Due to the lubricant effect of EG-based nanofluids, their viscosities decreased up to 1.0 wt% and then increased. In addition, the use of PEG-POSS in EG-based nanofluids has an effect that reduces viscosity.

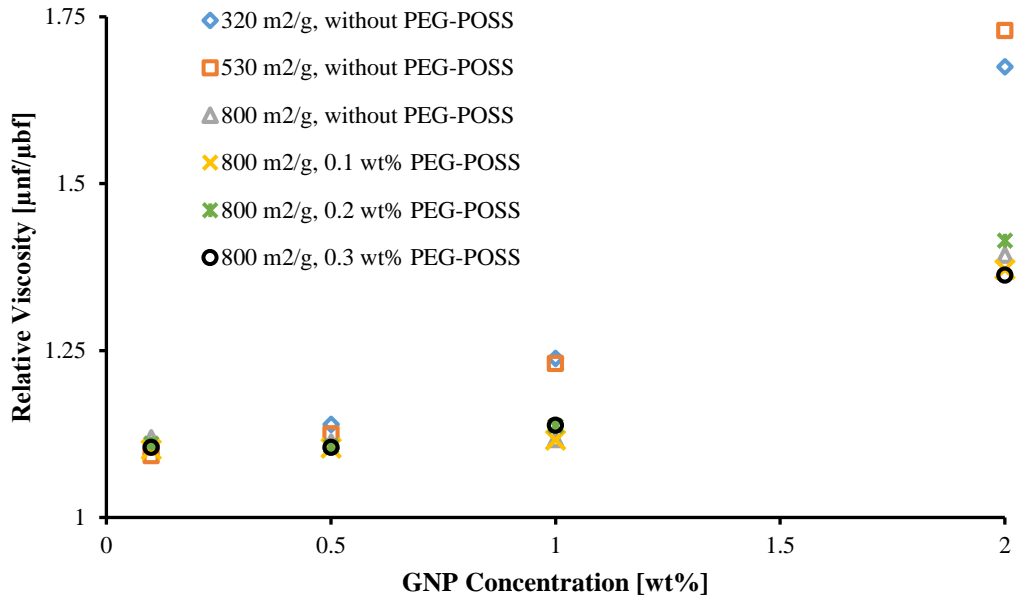


Figure 4.61 : Relative viscosity as a function of GNP concentration for aqueous nanofluids.

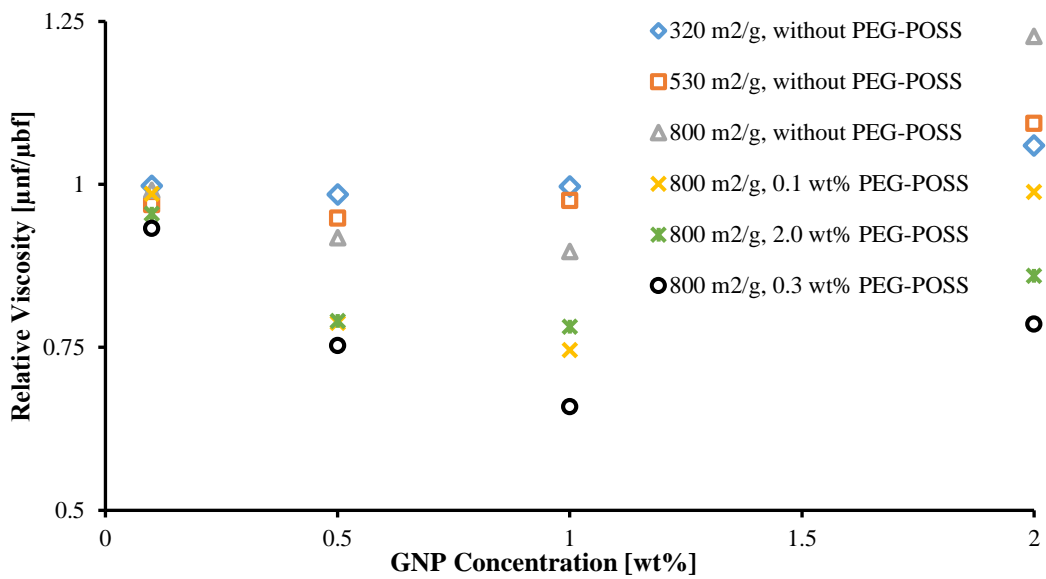


Figure 4.62 : Relative viscosity as a function of GNP concentration for EG-based nanofluids.

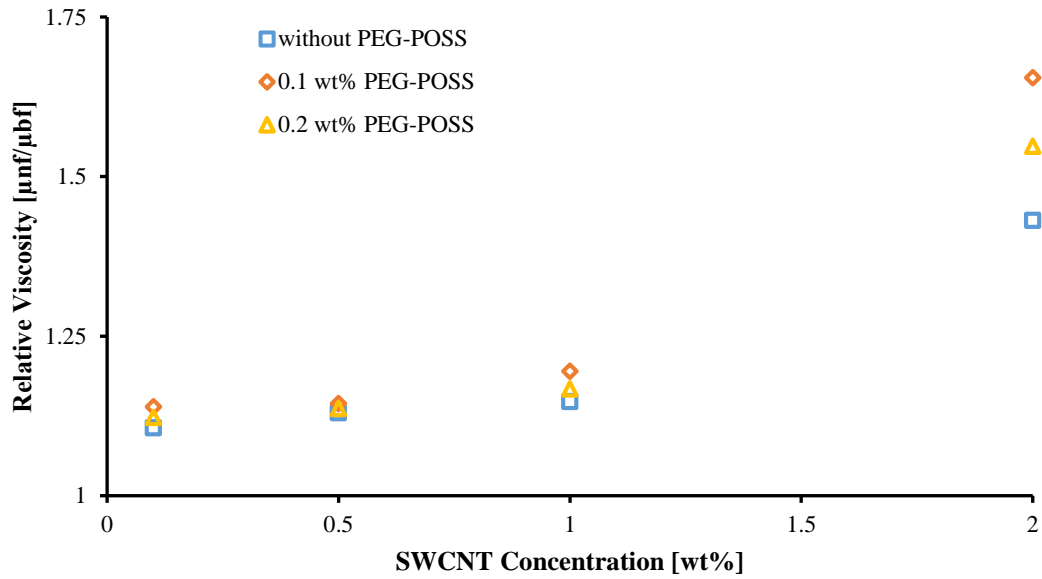


Figure 4.63 : Relative viscosity as a function of SWCNT concentration for aqueous nanofluids.

4.3 3 ω Thermal Conductivity Measurements

The 3 ω method was employed for thermal conductivity measurements. Its easy applicability, repeatability, high sensitivity in base fluids such as water, ethylene glycol, mineral oil, and methanol, as well as its success in different types of nanoparticles such as metal oxides, graphene or carbon nanotubes were the reasons of selecting this method [84;94;95]. The thermal conductivity measurements were only performed for nanofluids containing 1.0 and 2.0 wt% nanoparticles, since 0.1 and 0.5 wt% nanoparticle concentrations did not have a significant effect on thermal conductivity.

The stability of nanofluids is the most important condition for the use of these fluids in heat transfer systems. The sedimentation and phase separation of the nanoparticles is undesirable due to inefficient thermal conduction, corrosion or clogging of the heat conduction systems [3]. On the other hand, nanofluids consist of three phases: base fluid, nanoparticles, and interface, so the equilibrium of aggregation at the interface positively affects the increase in thermal conductivity [96]. Thermal conductivity results of aqueous GNP (800 m²/g) nanofluids with PEG-POSS are given in Figure 4.64. The highest increase in thermal conductivity was observed as 3.6% for the 2.0 wt% GNP nanofluid with no PEG-POSS. Also, this sample had the highest zeta potential value of -35.6 mV among all aqueous GNP nanofluids. The thermal

conductivity enhancements of aqueous 2.0 wt% GNP (800 m²/g) nanofluids with 0.1, 0.2, and 0.3 wt% PEG-POSS were 2.0, 2.3, and 2.2%, respectively. The zeta potential values of these samples were -27.0, -27.3 and -27.2 mV, respectively. Among 1.0 wt% GNP nanofluids, the highest increase in thermal conductivity was 1.8% for the sample with 0.2 wt% PEG-POSS which showed the highest zeta potential value. When these results are taken into consideration, it is clear that the stability of the nanofluid is important to increase the thermal conductivity.

In the literature, Transient Hot Wire (THW) technique is generally used for thermal conductivity measurement of nanofluids. Even at low nanoparticle concentration in the range of 0.005 - 0.02 wt%, thermal conductivity increases vary between 3% and 22.9% [7]. In our work, the lower thermal conductivity enhancement were obtained by 3 ω method, in comparison to previous results measured by THW method claimed to be inconsistent [83].

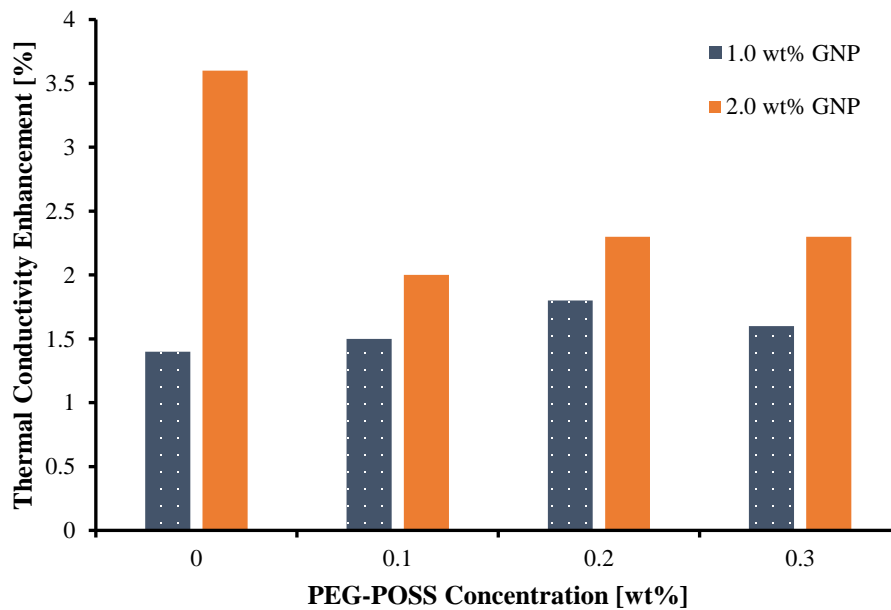


Figure 4.64 : Thermal conductivity enhancement as a function of PEG-POSS concentration for aqueous nanofluids at different GNP (800 m²/g) concentrations.

To the best of our knowledge, the previous studies on aqueous nanofluids having GNP with different surface areas are very inadequate.

Figure 4.65 shows the increase in thermal conductivity of nanofluids containing 1.0 and 2.0 wt% GNP with different surface areas. Thermal conductivity enhancements for 1.0 wt% GNP (320 m²/g, 530 m²/g, and 800 m²/g) nanofluids were measured as

8%, 5.4%, and 1.4%, respectively. As for 2.0 wt% GNP nanofluids, thermal conductivity enhancements were recorded as 12%, 8.4%, and 3.6%, with respect to increase in surface area. Although the zeta potentials of GNP nanofluids with surface areas of 320 and 530 m²/g were lower than those of 800 m²/g GNP, their thermal conductivities were higher due to the re-dispersion ability of those samples [84]. In our study, the thermal conductivity decreased with increasing surface area. On the contrary, Mehrali et al. (2014) recorded the increase in thermal conductivity with higher surface area, measured by THW method, for GNP (350 m²/g, 500 m²/g, and 750 m²/g) nanofluids.

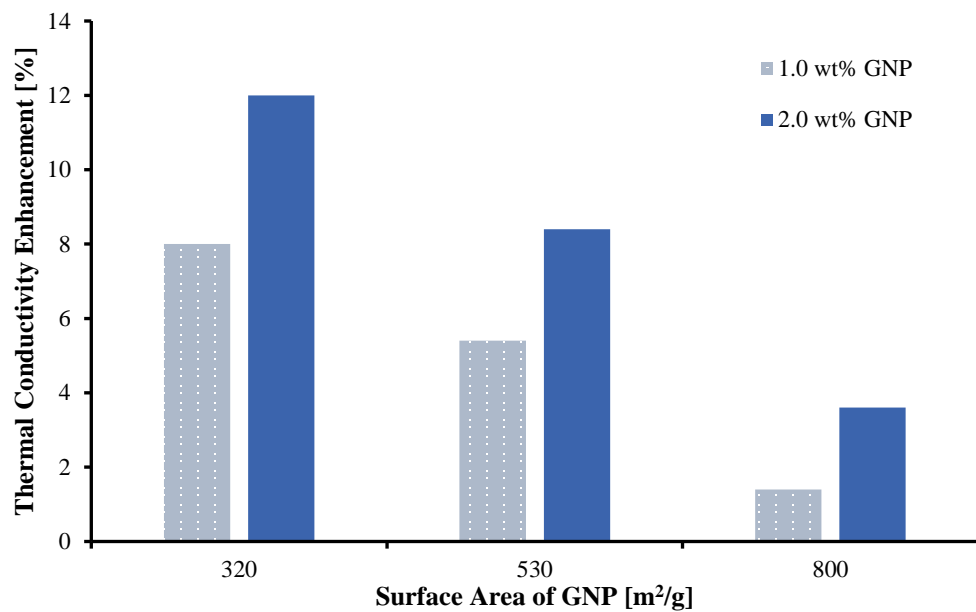


Figure 4.65 : Thermal conductivity enhancement as a function of surface area of GNP for aqueous nanofluids without PEG-POSS at different GNP concentrations.

Figure 4.66 shows the thermal conductivity increase for EG-based GNP (800 m²/g) nanofluids with PEG-POSS. As PEG-POSS concentration increased, thermal conductivity increased. The highest thermal conductivity enhancement was measured as 32% for 2.0 wt% GNP nanofluid with 0.3 wt% PEG-POSS. The increase in thermal conductivity gave the same trend with the zeta potential for those samples. The thermal conductivity increments were the lowest for PEG-POSS-free nanofluids; likewise, those samples had the lowest zeta potential values. Our results were in good agreement with Lee and Rhee's study (2014) in which the thermal conductivity measured by Lambda method increased up to 32%, with increasing nanoparticle concentration up to 4.0 vol% for EG-based GNP nanofluids [97]. In viscous base fluids such as EG,

there is little error in thermal conductivity results measured by different methods and the values are close to each other.

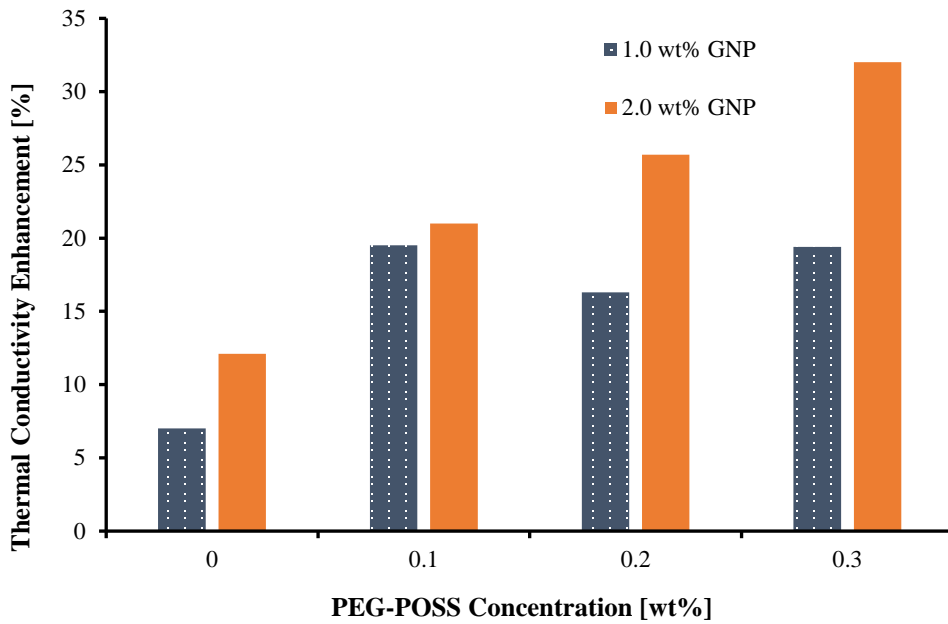


Figure 4.66 : Thermal conductivity enhancement as a function of PEG-POSS concentration for EG-based nanofluids at different GNP ($800 \text{ m}^2/\text{g}$) concentrations.

Figure 4.67 shows the thermal conductivity increases of nanofluids having 1.0 and 2.0 wt% GNP with different surface areas. As in aqueous nanofluids, the thermal conductivity of EG-based nanofluids decreased with increasing surface area. Thermal conductivity increase of nanofluids having 1.0 wt% and 2.0 wt% GNP were 17 and 20% for $320 \text{ m}^2/\text{g}$ GNP nanofluids, 9.6 and 18.5% for $530 \text{ m}^2/\text{g}$ GNP nanofluids, 7 and 12.1% for $800 \text{ m}^2/\text{g}$ GNP nanofluids. The zeta potentials of samples of EG-based GNP with surface areas of 320 and $530 \text{ m}^2/\text{g}$ could not be measured due to dilution problems. As in aqueous nanofluids, EG-based GNP (320 and $530 \text{ m}^2/\text{g}$) nanofluids resulted in phase separation. Since re-dispersibility was observed in these samples, with a reduced surface area the thermal conductivities increased.

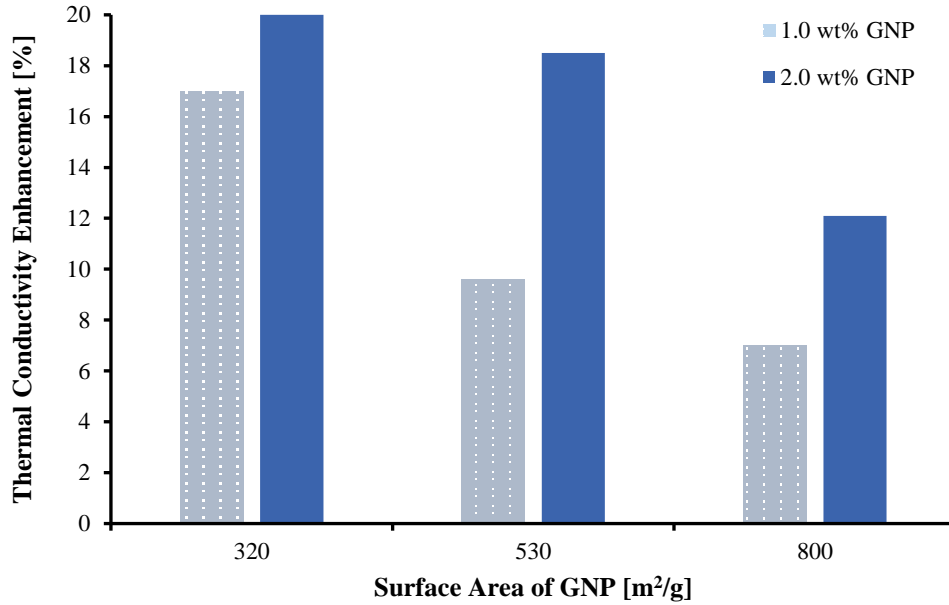


Figure 4.67 : Thermal conductivity enhancement as a function of surface area of GNP for EG-based nanofluids without PEG-POSS at different GNP concentrations.

Thermal conductivity increases of aqueous 1.0 wt% and 2.0 wt% SWCNT nanofluids with PEG-POSS are given in Figure 4.68. Two different ultrasonication times, 50 min and 100 min, were performed for the preparation of these samples. When the thermal conductivity of the samples without PEG-POSS and with 0.1 wt% PEG-POSS are compared, the use of PEG-POSS increased thermal conductivity by approximately 0.6%. Considering the 0.5% margin error of the 3ω method, the use of 0.1 wt% PEG-POSS did not affect the increase of thermal conductivity. When PEG-POSS concentration was increased to 0.2 wt%, thermal conductivity enhancement decreased. The use of stabilizers in aqueous SWCNT nanofluids increased the thermal resistance of the nanofluid [98]. Thermal conductivity increment of 50 min ultrasonicated 1.0 and 2.0 wt% SWCNT samples without PEG-POSS were 2.2% and 4.1%, respectively. For 100 min ultrasonicated 1.0 and 2.0 wt% SWCNT samples, the thermal conductivity increments were 2.1 and 4%, respectively. Thermal conductivity enhancement of 50 min ultrasonicated 1.0 and 2.0 wt% SWCNT samples with 1.0 wt% PEG-POSS were 2.9% and 4.3%, respectively. For those samples with 100 min ultrasonication, these values were 2.4 and 4.3%. Thermal conductivity increases of 50 min ultrasonicated 1.0 and 2.0 wt% SWCNT nanofluids with 0.2 wt% PEG-POSS are 1.6% and 2.9%. For samples with 100 min ultrasonication, these values were 2.0 and 2.6%. While there is evidence that the increase in ultrasonication time reduces the

thermal conductivity due to the reduction of nanotube length, there are studies that only clusters are reduced with an optimum ultrasonication time without damaging the dimensions of the nanotubes [99]. Due to the high precision of the 3ω method, obtained data are highly reliable. Due to this reliability, the same thermal conductivity values of nanofluids proved that the structure of nanoparticles did not deteriorate at studied ultrasonication times (50 min and 100 min), and only aggregations were separated.

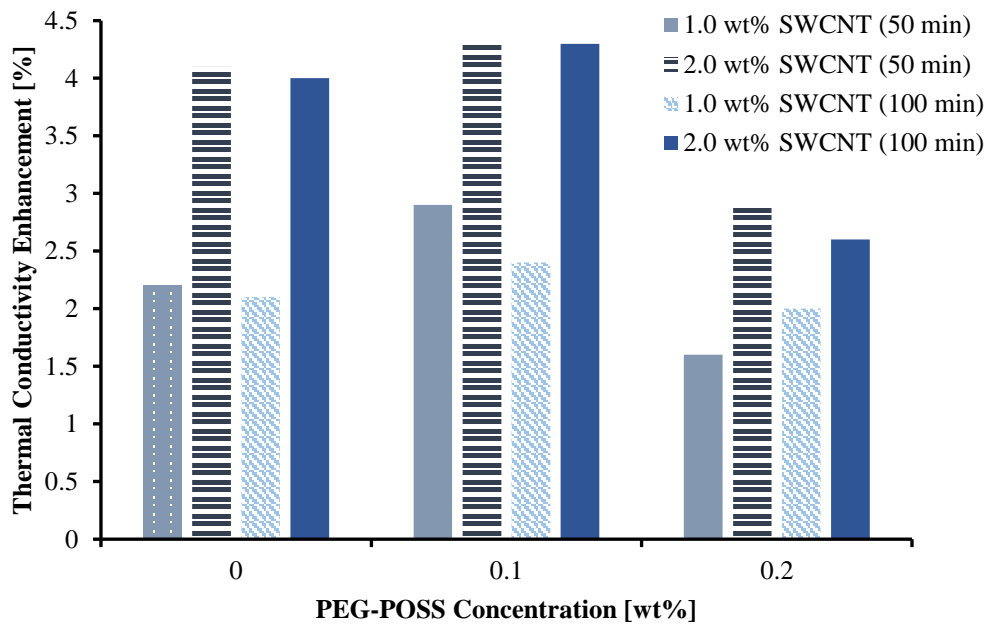


Figure 4.68 : Thermal conductivity enhancement as a function of PEG-POSS concentration for aqueous nanofluids at different SWCNT concentrations and ultrasonication time.

Figure 4.69 shows an increase in thermal conductivity versus PEG-POSS concentration of oil-based nanofluids containing GNP with surface area of $800 \text{ m}^2/\text{g}$. The thermal conductivity increment of nanofluids having 1.0 and 2.0 wt% GNP without PEG-POSS are 3.5 and 6.8%, respectively. While PEG-POSS concentration was 0.1 wt%, thermal conductivity increment values decreased to 3.4% and 5.0% for samples having 1.0 wt% and 2.0 wt% GNP, respectively. Due to the sedimentation of the oil-based samples, zeta potential measurements could not be performed. However, the addition of 0.1 wt% of PEG-POSS to oil-based nanofluids had an undesirable effect in the fluid medium and the reduction in thermal conductivity enhancement was observed. When PEG-POSS concentration increased to 0.2 wt%, intermolecular orientation was achieved and thermal conductivity increased. With the presence of a

large amount of nonionic stabilizers (0.3 wt% PEG-POSS) in the medium, the thermal conductivity decreased [100].

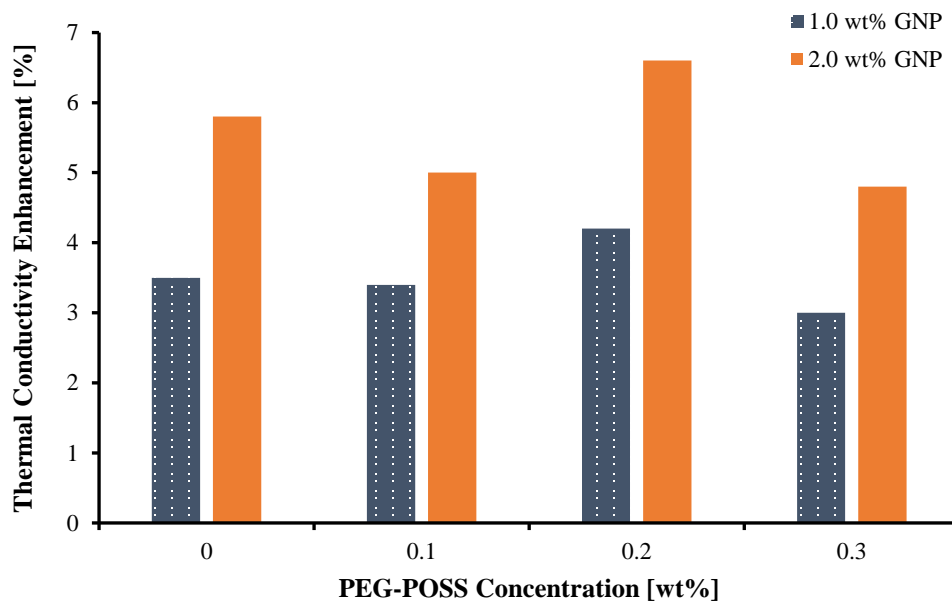


Figure 4.69 : Thermal conductivity enhancement as a function of PEG-POSS concentration for oil-based nanofluids at different GNP ($800 \text{ m}^2/\text{g}$) concentrations.

Figure 4.70 illustrates the increase in thermal conductivity of nanofluids having 1.0 and 2.0 wt% GNP with different surface areas. It is seen that the thermal conductivity of oil-based nanofluids decreased with increasing surface area, as in water and EG-based nanofluids. The thermal conductivity enhancement of nanofluids containing 1.0 wt% and 2.0 wt% GNP with surface area of $320 \text{ m}^2/\text{g}$ were 11% and 9.5%, respectively. The high thermal conductivity value of the nanofluid with low nanoparticle concentration indicates that oil-based nanofluids with surface area of $320 \text{ m}^2/\text{g}$ were unstable. For nanofluids having 1.0 wt% and 2.0 wt% GNP with surface areas of $530 \text{ m}^2/\text{g}$ and $800 \text{ m}^2/\text{g}$, the thermal conductivity enhancements were 7% and 8%, 3.5% and 5.8%, respectively. As with water and EG-based nanofluids, oil-based nanofluids having GNP with surface areas of 320 and $530 \text{ m}^2/\text{g}$ had phase separation. As these samples were re-dispersed, the increase in thermal conductivity enhancement was observed with a decrease in surface area.

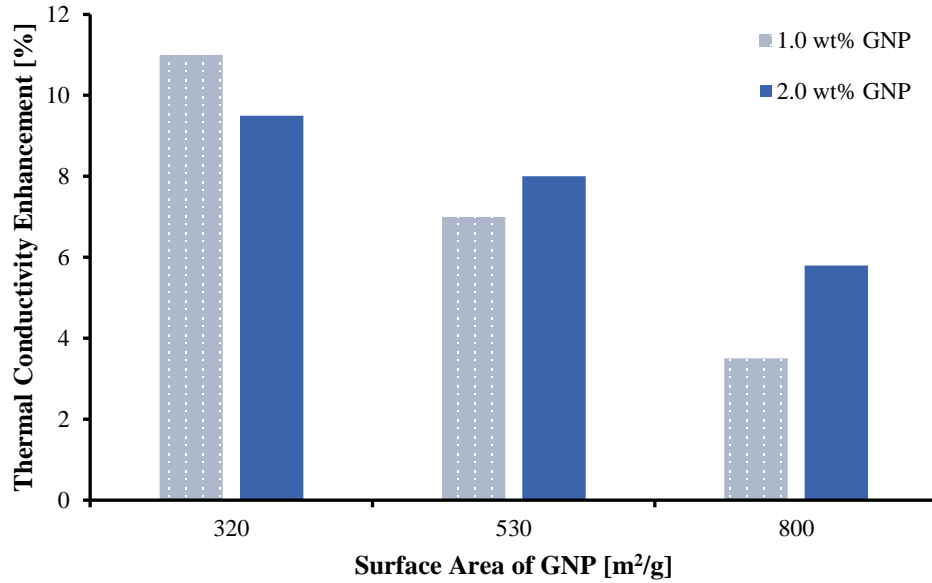


Figure 4.70 : Thermal conductivity enhancement as a function of surface area of GNP for oil-based nanofluids without PEG-POSS at different GNP concentrations.

4.4 Contact Angle and Surface Tension Measurements

The addition of nanoparticles to water and refrigerants is an effective way to increase critical heat flow. Wettability is significant for boiling heat transfer and critical heat flow. The increase in wettability of nanofluids provides an increase in critical heat flow. With the increase in concentration, nanoparticles are deposited on the heat transfer surface, resulting in decreased contact angle between the surface and nanofluid due to increased surface roughness and adhesion forces [101].

Figure 4.71 shows contact angle values of aqueous 800 m²/g GNP nanofluids at different concentrations of PEG-POSS. With the addition of PEG-POSS to aqueous nanofluids, a drop in contact angle was observed, except for aqueous 2.0 wt% GNP nanofluid. Surface tension decreases with the addition of stabilizer. Due to the weakening of the cohesive forces on the drop surface, the nanofluid tends to spread on the glass surface. Similarly, Ferrari et al. observed that when the concentration of surfactant in water increased, contact angle and surface tension decreased [102]. Increase in the nanoparticle concentration increases the surface tension of the nanofluids. The droplet takes the form of a sphere that minimizes the surface area by the effect of surface tension. The contact angle value of the drop that takes the form of the sphere on the surface will be high. In addition, as the amount of hydrophobic GNP nanoparticles in liquid increases, the contact angle value will increase. Similarly,

Radiom et al. in their study, increased the contact angle increased TiO₂ nanoparticle concentration in water [103].

Although it is known that the contact angle will increase with increasing particle concentration in nanofluids. As seen in Figure 4.71, the contact angle value is lower than the others when we look at the 2.0 wt% GNP nanofluid with no PEG-POSS. This situation is made think to be caused by any agglomeration and stability deterioration in the sample. Furthermore, the lowest contact angle was observed at the 0.5 wt% GNP nanofluid with 0.3 wt% PEG-POSS, that is associated with the deterioration of the stability as shown in the zeta potential graph in Figure 4.1.

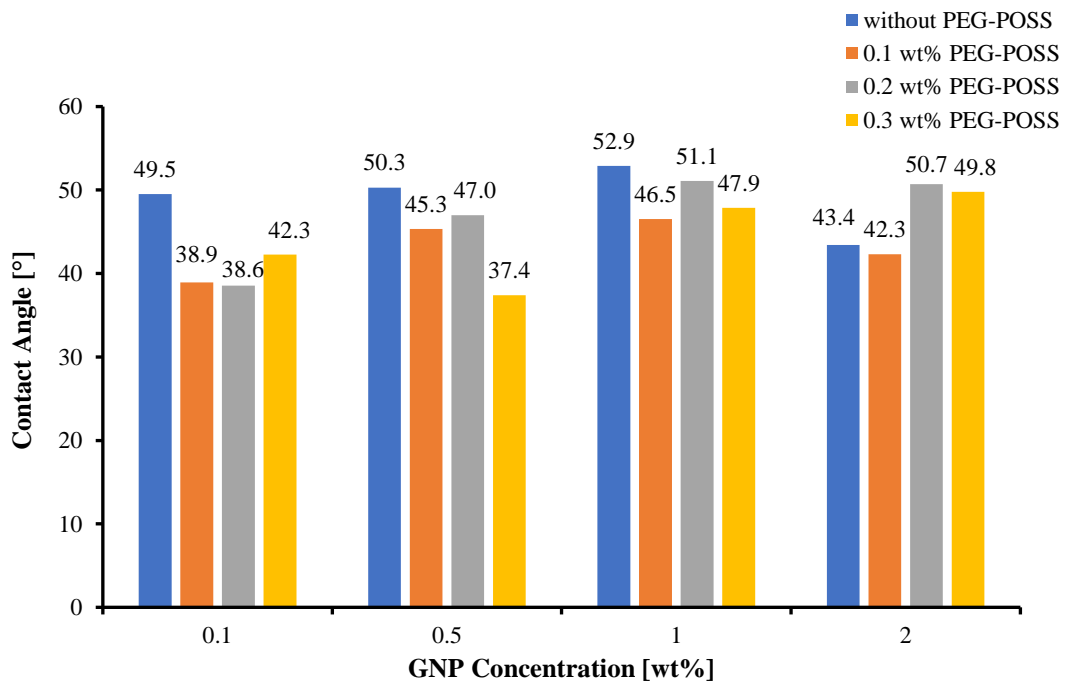


Figure 4.71 : Contact angle as a function of 800 m²/g GNP concentration for aqueous nanofluids with PEG-POSS at different concentrations.

As seen in Figure 4.72, as the nanoparticle surface area increased for aqueous nanofluids having at the same concentration of GNP the contact angle was mostly increased, except for the 2.0 wt% GNP sample. The highest contact angle values belonged to 800 m²/g GNP nanofluids, excluding the 2.0 wt% GNP sample. The reactivity of the nanoparticles increases as the surface area increases. For samples containing the same concentration of GNP, the reduction of surface area caused an increase in contact angle. With their small surface area, reactive nanoparticles provide

more homogeneous distribution in the nanofluid. Therefore, the hydrophobic GNP nanoparticles have a direct effect on the contact angle value [104].

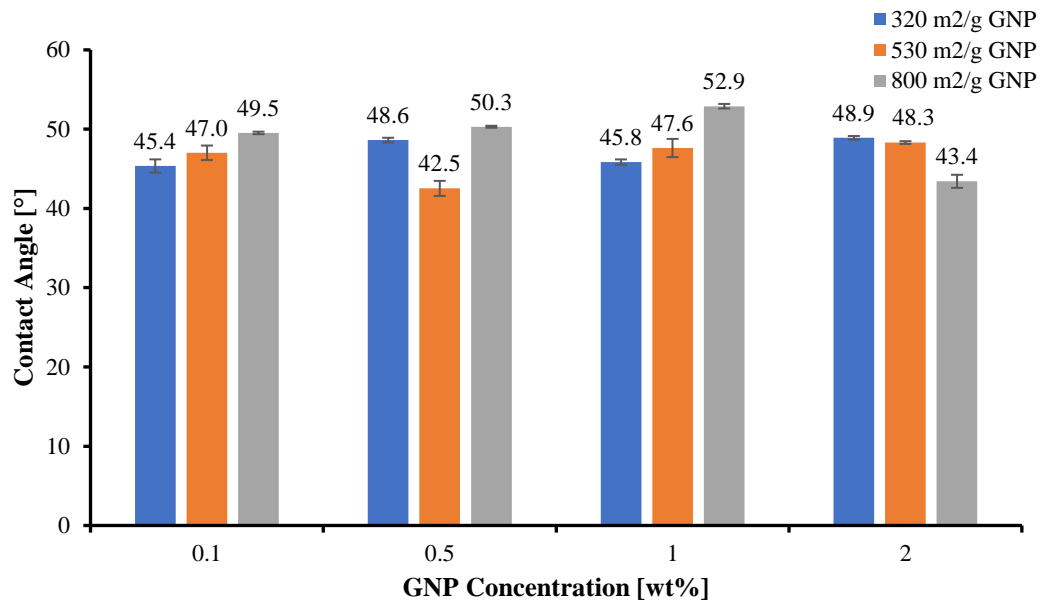


Figure 4.72 : Contact angle as a function of GNP concentration with different surface areas for aqueous nanofluids without PEG-POSS.

Contact angle values of EG-based 800 m²/g GNP nanofluids with different PEG-POSS concentrations are given in Figure 4.73. In samples with low nanoparticle concentration as low as 0.1 wt%, the use of PEG-POSS decreased the contact angle, and as the nanoparticle concentration increased, the use of stabilizer increased the contact angle due to favorable nanoparticle distribution and nanofluid stability.

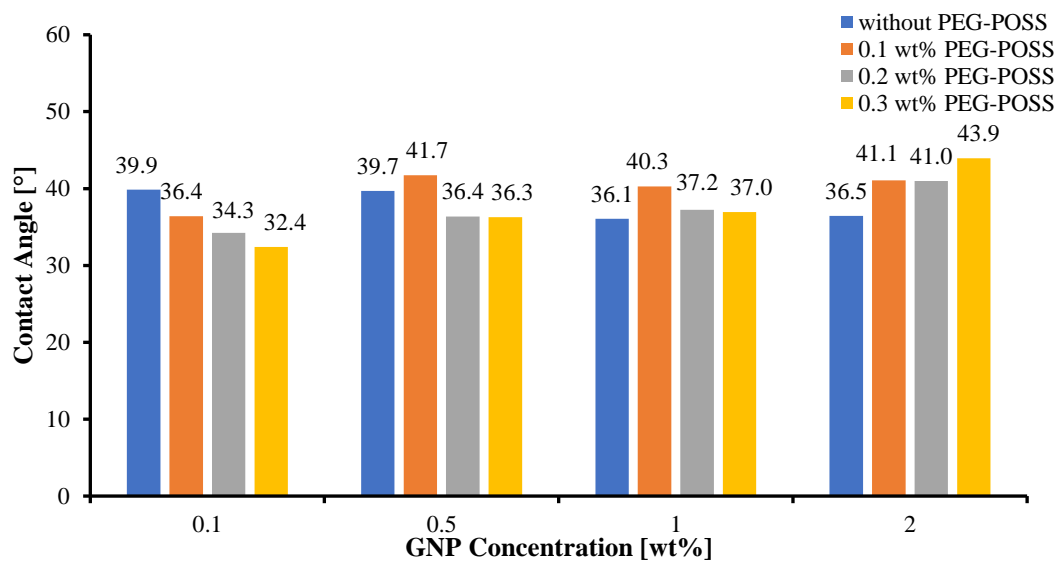


Figure 4.73 : Contact angle as a function of 800 m²/g GNP concentration for EG-based nanofluids with PEG-POSS at different concentrations.

Figure 4.74 shows that the increase in surface area of GNP, the EG-based nanofluids containing GNP with different surface areas reduced the contact angle.

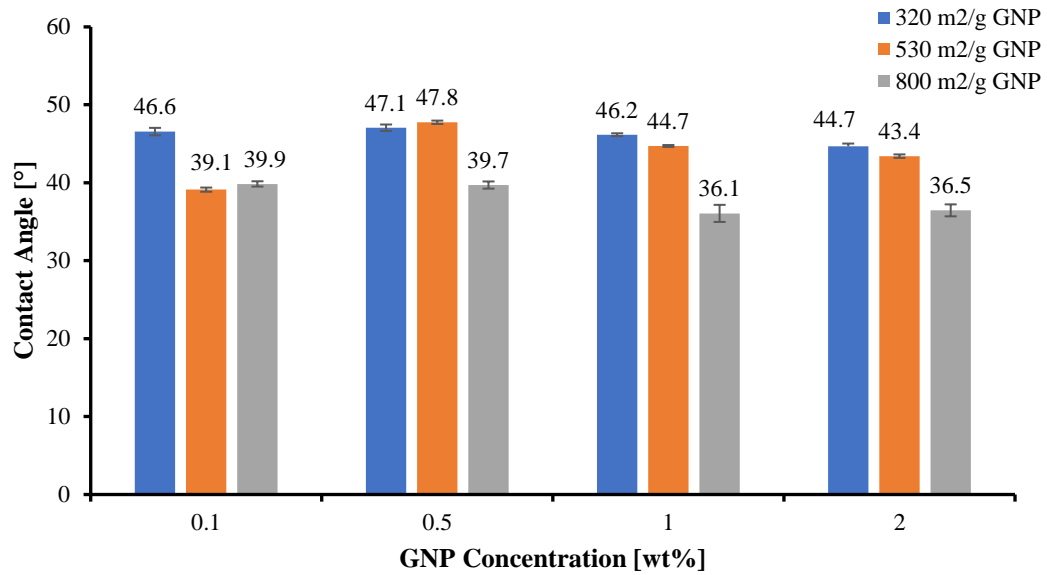


Figure 4.74 : Contact angle as a function of GNP concentration with different surface areas for EG-based nanofluids without PEG-POSS.

In oil-based nanofluids, as in aqueous nanofluids, it was observed that the contact angle mostly increased as the GNP surface area increased for the samples at the same concentration of GNP. In the oil-based results given in Figures 4.75 and 4.76, an increase in contact angle, in other words, an increase in wettability were observed with increasing GNP concentration. The highest contact angle values for all GNP concentrations were measured in nanofluids without PEG-POSS. Similar to water and EG based nanofluids, PEG-POSS increased wettability. The fact that the measured values are approximately three-fold lower than the results in water and EG-based samples indicate that the wettability of the compressor oil is higher than water and EG.

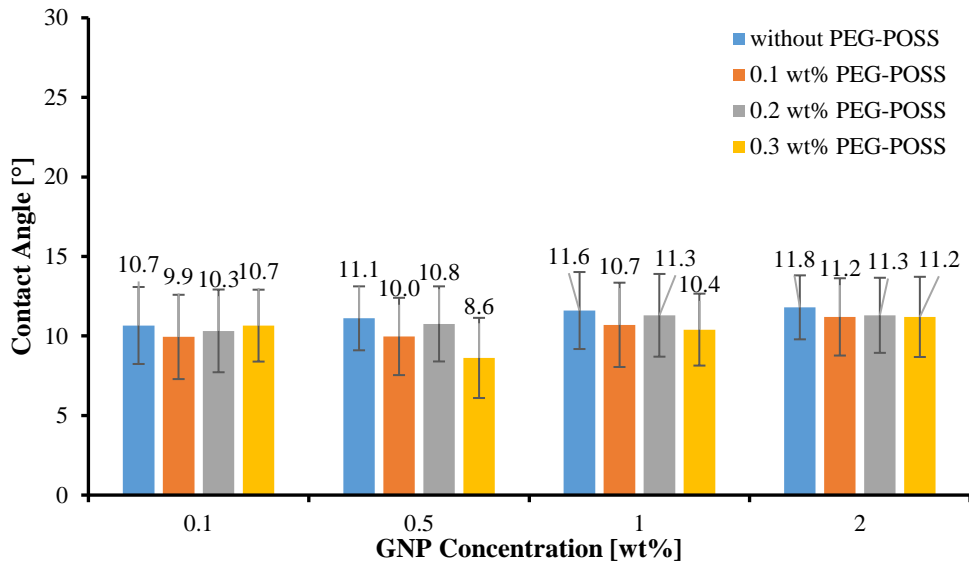


Figure 4.75 : Contact angle as a function of 800 m²/g GNP concentration for oil-based nanofluids with PEG-POSS at different concentrations..

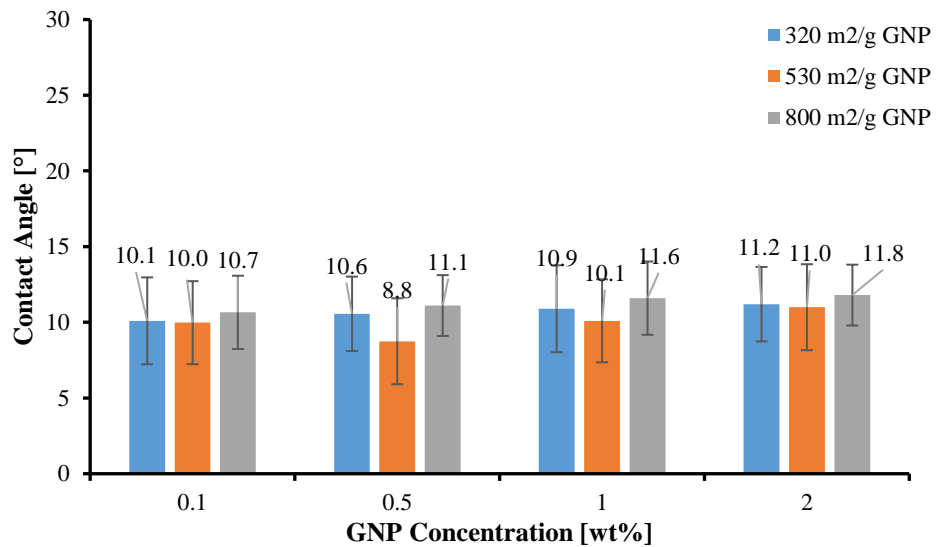


Figure 4.76 : Contact angle as a function of GNP concentration with different surface areas for oil-based nanofluids without PEG-POSS.

The best wettability results were obtained at 2.0 wt% SWCNT sample having highest concentration of PEG-POSS with 0.2 wt%, given in Figure 4.77. As the SWCNT concentration increased, the contact angle decreased. Especially with an increase in stabilizer concentration was caused that situation by the functionalization of SWCNT nanoparticles [105].

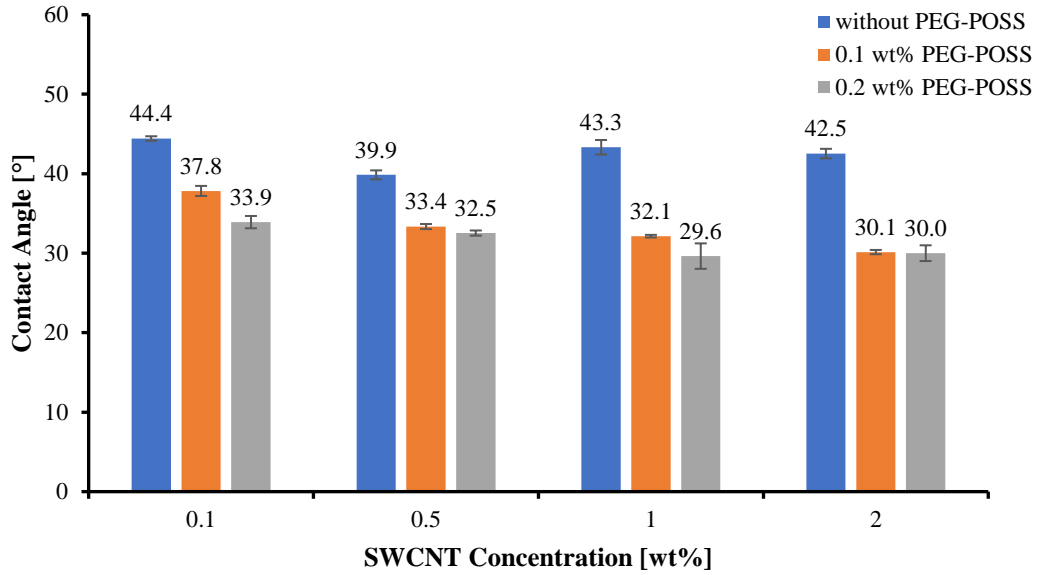


Figure 4.77 : Contact angle as a function of SWCNT concentration for aqueous nanofluids with PEG-POSS at different concentrations.

Surface tension, the amount of surface free energy per unit area of the liquid droplet, is one of the main factors affecting the transfer performance of a thermal system. The heat performance of the boiling heat transfer and heating pipes varies depending on the shape of the drop and bubble which is the result of surface tension. Nanoparticle concentration and diameter, stabilizer content, base fluid, and temperature are some of the important parameters affecting the surface tension of nanofluids. Although there are not enough studies about the surface tension of graphene and carbon nanotube-based nanofluids in the literature, results are conflicting [80;106].

The surface tension values of 800 m²/g GNP nanofluids with different PEG-POSS concentration are given in Figure 4.78. The increased concentration of GNP caused an increase in surface tension. As the concentration of nanoparticles in the liquid increases, the number of molecules trying to approach each other on the liquid surface increases. This increases the cohesion force and surface tension [82]. Also, as the concentration increases, the average gap between molecules and nanoparticles decreases. Thus, the attractive Van der Waals forces on the surface are superior to the repulsive electrostatic forces [107]. This results in increased surface tension. Surface tension decreased with PEG-POSS addition. It is known that the surface tension of the fluids decreases with the addition of surfactant. These substances cover the solid surface of the particles and form a layer between particles and the surrounding liquid

molecules. These layers create repulsive forces between the particles, causing a decrease in surface tension and surface free energy of the fluid [108;109]. As shown in Figure 4.78, the use of PEG-POSS at low nanoparticle concentrations as low as 0.1 and 0.5 wt% caused a decrease in surface tension, but this effect of PEG-POSS was not sufficient at high nanoparticle concentrations.

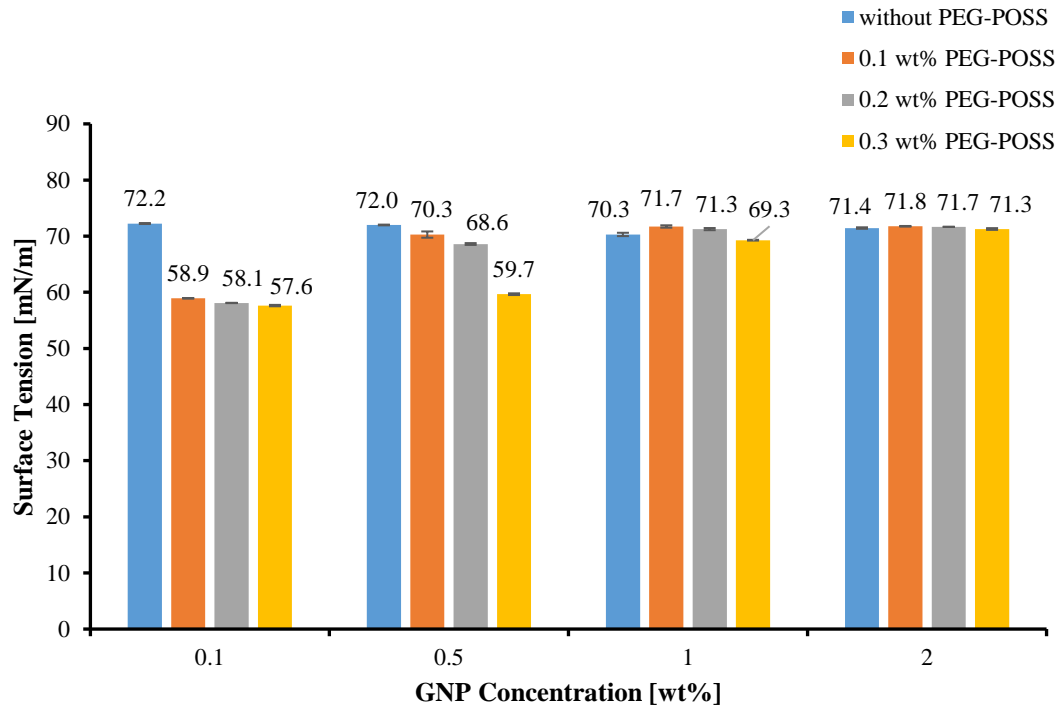


Figure 4.78 : Surface tension as a function of 800 m²/g GNP concentration for aqueous nanofluids with PEG-POSS at different concentrations.

Surface tension changes of water and EG-based nanofluids containing GNP with different surface areas are given in Figure 4.79 and 4.80, respectively. It was observed that the surface tension for the same GNP concentration was mostly decreased as the surface area increased. For why smaller nanoparticles exhibit a higher surface charge density compared to larger nanoparticles [110]. Due to the high surface charge density, electrostatic repulsion forces between nanoparticles and liquid molecules are increased. As the adsorption from the liquid to the surface increases, intermolecular interactions on the surface decrease and surface tension decrease [111]. In addition, as the particle size increases, the surface area, and surface free energy decrease, so that thermodynamically the molecules are less likely to bond. Since it will cause weaken the interaction of the molecules and nanoparticles in the liquid; the forces acting on the bonds on the surface and the surface tension of the nanofluid are reduced [107]. In

the literature, it was stated that the surface tension increased with increasing particle size [82]. Similarly, as the particle size decreases and as the surface area increases, it is usual to observe a decrease in surface tension.

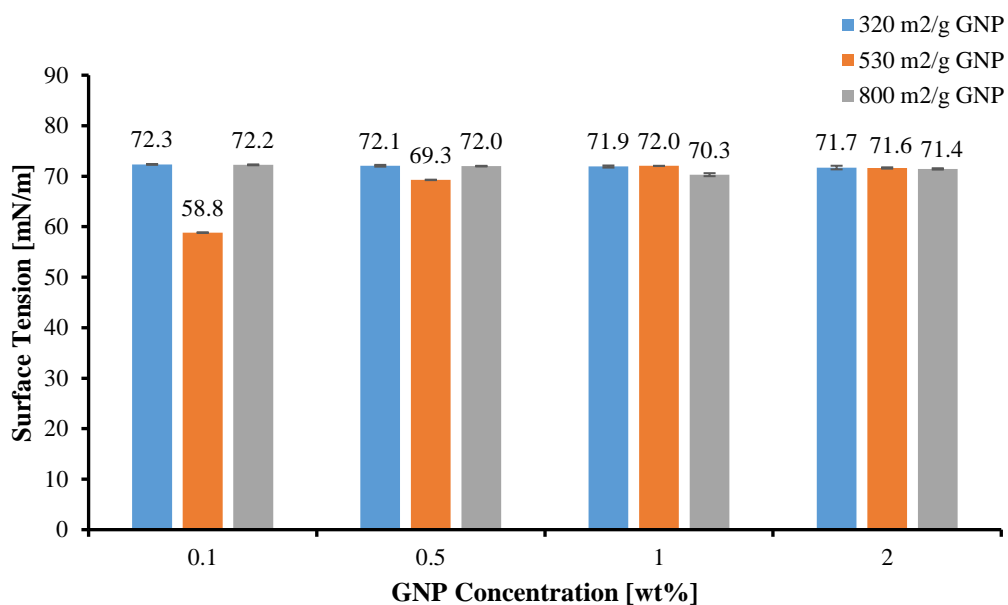


Figure 4.79 : Surface tension as a function of GNP concentration with different surface areas for aqueous nanofluids with no PEG-POSS.

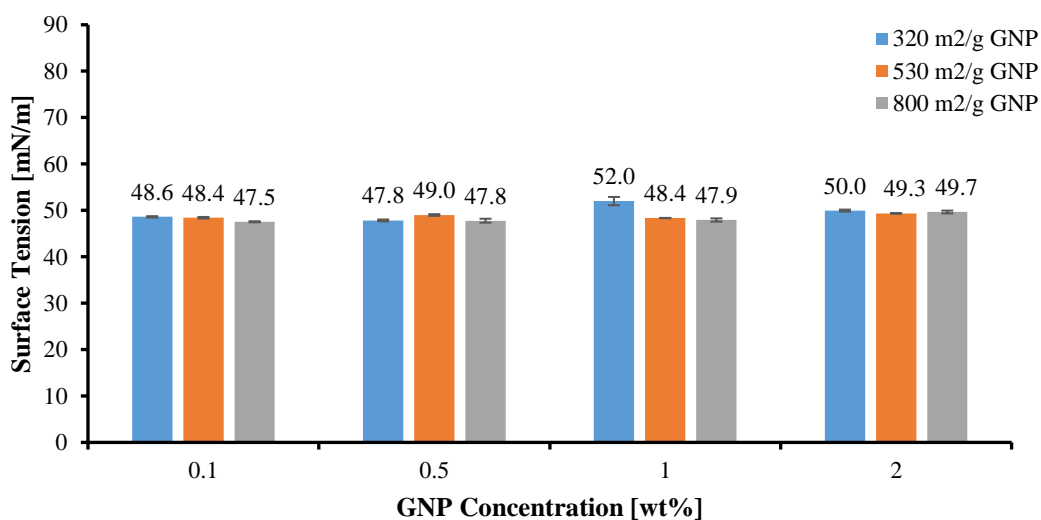


Figure 4.80 : Surface tension as a function of GNP concentration with different surface areas for EG-based nanofluids with no PEG-POSS.

As seen in Figure 4.81, due to the similar structure of ethylene glycol and polyethylene glycol-POSS, the use of PEG-POSS with a different concentration in the EG-based 800 m²/g GNP nanofluids did not affect the surface tension. As in aqueous

nanofluids, increase in nanoparticle concentration and an increase in surface tension were observed in EG based fluids.

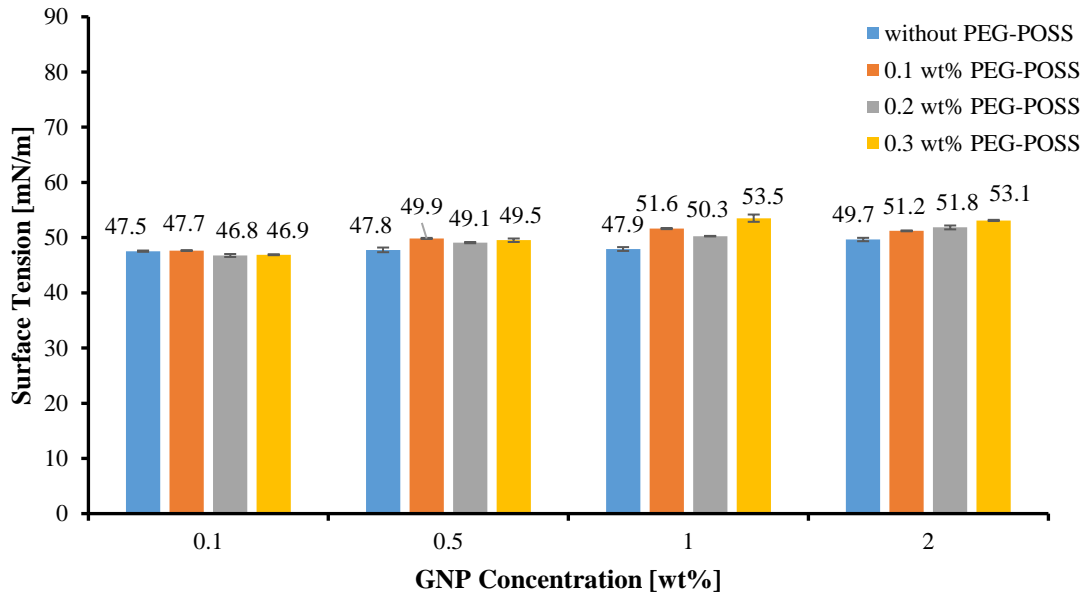


Figure 4.81 : Surface tension as a function of 800 m²/g GNP concentration for EG-based nanofluids with PEG-POSS different concentrations.

In Figure 4.82, surface tension values of aqueous SWCNT samples with different PEG-POSS concentrations are given. Increasing the SWCNT concentration resulted in both decrease and increase in surface tension. The increase in surface tension is caused by the greater agglomeration of the high concentration of dispersed nanoparticles [82]. Molecular interactions between the stabilizer and the nanoparticles complicate the analysis. It is not clear whether the concentration of the nanoparticle or the effect of the stabilizer is predominant, and how efficiently the stabilizers surrounded to the nanoparticles. Similar to these results, there are conflicting results in the literature regarding the effect of concentrations of nanofluids on surface tension [109;112]. Jeong et al. prepared water Al₂O₃ nanofluids, the surface tension of the nanofluids increased until up to 1.0 wt% Al₂O₃ and then decreased slightly. Additionally, the surface tension value for a concentration of 4.0% nanoparticle by volume decreased by almost 20% [113]. Similarly, Pantzali et al. prepared aqueous CuO nanofluids, surface tension decreased with 2.0 wt% CuO concentration and remained constant between 3.0 wt% and 4.0 wt% CuO concentration [114]. Tanvir and Qiao in their study, the surface tension of ethanol and n-decane-based MWCNT, aluminum, aluminum oxide, and boron nanoparticles nanofluids with surfactants

measured. They observed that the surface tension of all nanofluids, except nanofluids containing MWCNT, increased with nanoparticle size and concentration. In samples containing MWCNT, surface tension decreased first and then increased as nanoparticle concentration increased [82]. These results coincide with the results in Figure 4.82.

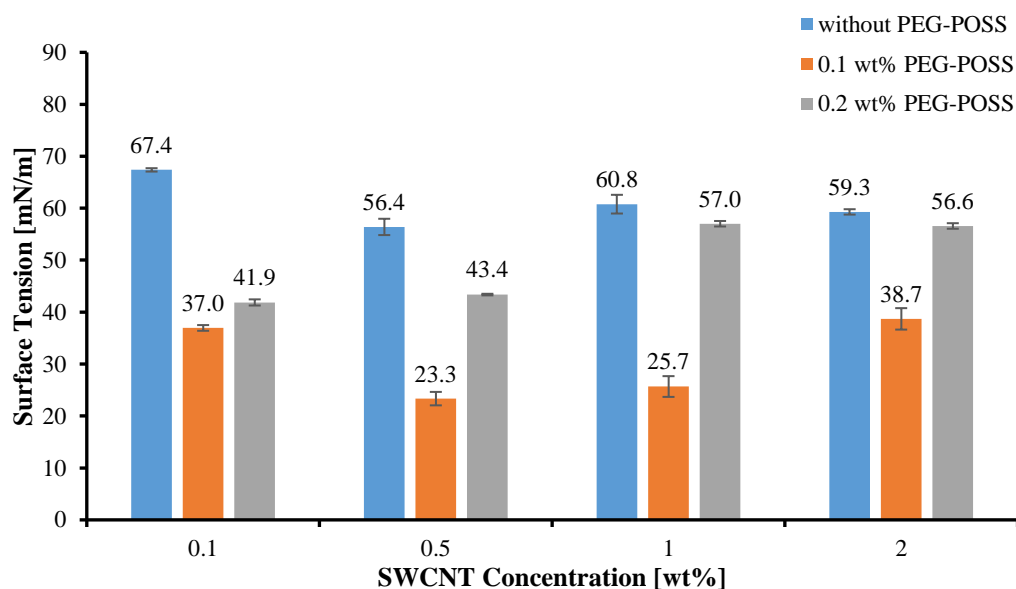


Figure 4.82 : Surface tension as a function of SWCNT concentration for aqueous nanofluids with PEG-POSS at different concentrations.

The surface tension values of oil-based 800 m²/g GNP nanofluids with PEG-POSS at different concentrations; and the surface tension values of oil-based GNP nanofluids with different surface areas without PEG-POSS are given in Figures 4.83 and 4.84, respectively. When the graphs are examined, it is seen that properties such as stabilizer and nanoparticle concentration and nanoparticle surface area did not affect surface tension in oil-based nanofluids. When the different base fluids were examined, the highest surface tension values were observed in water, EG and oil-based samples, respectively. The molecules beneath the surface of the liquid that is attracted evenly by the molecules around them. As the molecules on the surface do not have any other molecules on them, they want to interact more with their neighbors on the surface to reach thermodynamic equilibrium. The stronger attractive forces cause the greater the surface tension. Since polar liquids have some charged areas in the molecule, the molecules on their surface will affect more. Non-polar liquids do not have that attractiveness and they are held together by the side wall of the container. In other words, they stick to each other less than polar molecules. Apolar molecules, therefore,

have lower surface tension than polar molecules [115]. Water and EG are polar molecules with hydrogen bonds. Compressor oil is a nonpolar molecule with London (Van der Waals) interactions. Therefore, the interactions between the water molecules on the surface are stronger and the surface tension of the aqueous samples is higher [116].

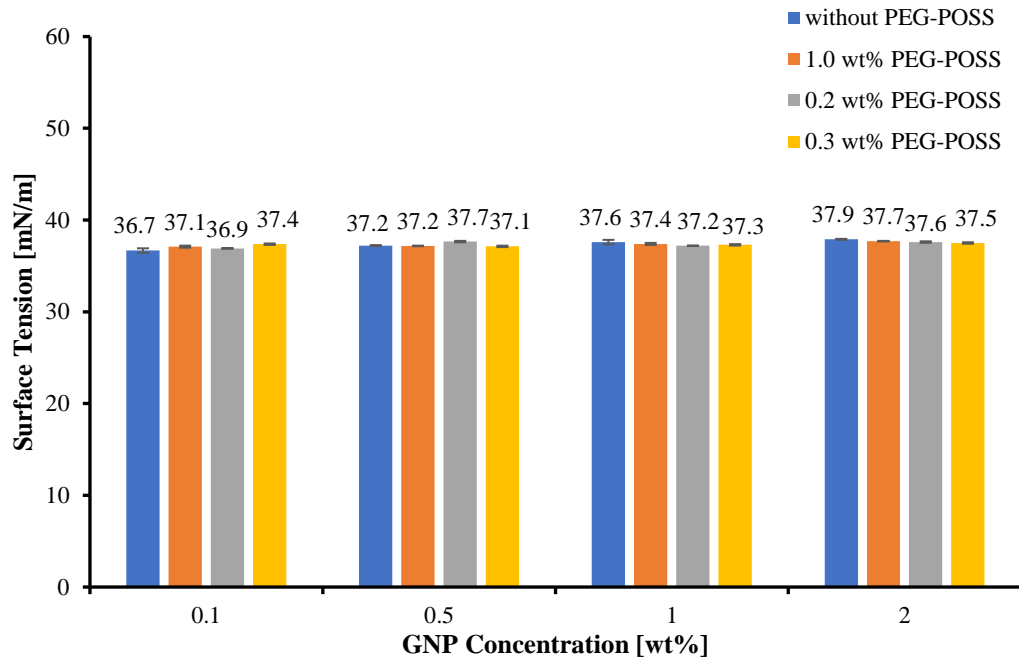


Figure 4.83 : Surface tension as a function of 800 m²/g GNP concentration for oil-based nanofluids with PEG-POSS different concentrations.

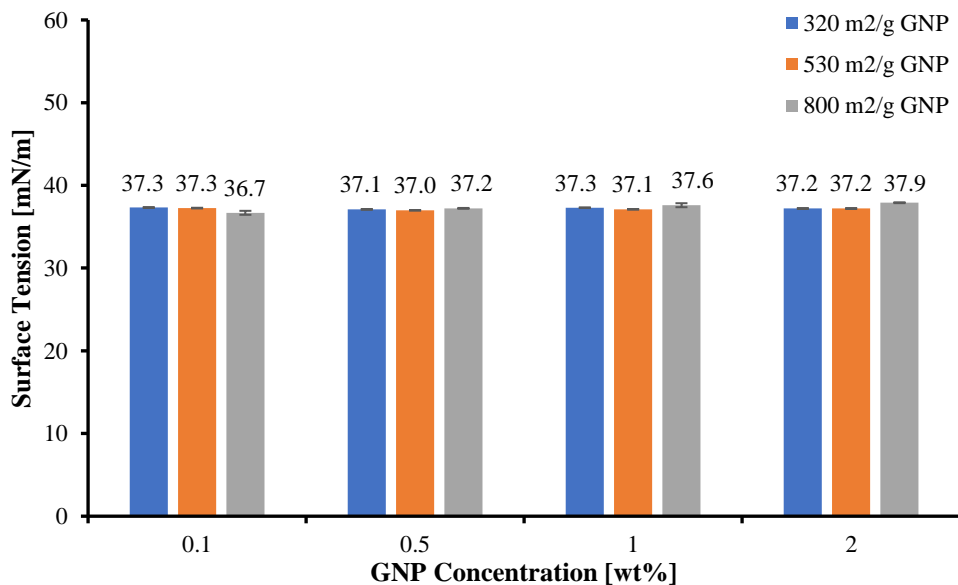


Figure 4.84 : Surface tension as a function of GNP concentration with different surface areas for oil-based nanofluids with no PEG-POSS.

5. CONCLUSIONS

Carbon-based nanofluids were successfully prepared with ultrasound technology, using distilled water, ethylene glycol, and compressor oil as base fluids. Two different nanoparticle types; GNP and SWCNT were used. The nanoparticle concentrations were chosen as 0.1, 0.5, 1.0, and 2.0 wt%. In addition, GNPs with three different surface areas of 320 m²/g, 530 m²/g and, 800 m²/g were used.

With this study, the potential of PEG-POSS as a stabilizer in nanofluid production has been demonstrated for the first time in literature.

In order to evaluate the stability of nanofluids, zeta potential and UV-Vis spectrophotometry analyses were carried out. The effect of nanoparticle concentration on the zeta potential was observed systematically. The highest zeta potential value of -68.2 mV was measured for the aqueous dispersion containing 0.1 wt% PEG-POSS and 1.0 wt% SWCNT. The relatively high values of the zeta potentials ensured the good colloidal stability of the disperse systems studied. Increasing surface area of the GNP raised the Van Der Waals forces and the zeta potential values. The UV-Vis spectra proved that the GNP and SWCNT nanoparticles were successfully dispersed in distilled water. Relative concentrations of the samples were calculated after 60 days and the samples were found to have different sedimentation rates independent from the nanoparticle concentration.

Detailed rheology studies were performed to investigate the changes in the viscosity of aqueous GNP and SWCNT containing and EG-based GNP nanofluids as a function of stabilizer concentration, surface area, shear rate, and temperature change. The increase in nanoparticle concentration caused an increment on viscosity as the applied stress increased to reach a certain shear rate. For EG-based nanofluids, lower viscosity values were recorded than that of the base fluid due to the lubricant effect of GNP nanoparticles. In addition, as the surface area of GNP decreased, the viscosity increased due to the agglomeration of the particles. For aqueous nanofluids, shear thinning was observed in the low shear rate region; whereas, shear thickening behavior was followed up at high shear rates. The use of PEG-POSS at different concentrations

had no effect on the viscosity. As for EG-based nanofluids, Newtonian behavior was first recorded at low nanoparticle concentrations; later, with increasing the concentration, shear thinning behavior was observed at low shear rates. The trend of thermal conductivity enhancement measured by 3ω method was in good agreement with the zeta potential values of nanofluids. The maximum thermal conductivity increment for aqueous samples without PEG-POSS and having 2.0 wt% GNP with a surface area of $800 \text{ m}^2/\text{g}$ was measured as 3.6%. It was also observed that for the same weight percentage, the lower surface area of GNP nanofluids presents higher thermal conductivity values than those of the other nanofluids with GNPs that had higher specific surface area. The thermal conductivity enhancement of nanofluid containing 2.0 wt% GNP with a surface area of $320 \text{ m}^2/\text{g}$ was measured as 12%. In EG-based samples containing $800 \text{ m}^2/\text{g}$ GNP, raising PEG-POSS concentration increased thermal conductivity. The maximum thermal conductivity enhancement of 32% belongs to the nanofluid with 2.0 wt% GNP and 0.3 wt% PEG-POSS. The highest thermal conductivity enhancement in GNP nanofluids was measured as 20% for the GNP nanofluid (surface area $320 \text{ m}^2/\text{g}$) prepared without PEG-POSS. Additionally, thermal conductivity increase in oil-based samples containing 0.2 wt% PEG-POSS and having 2.0 wt% GNP with the surface area of $800 \text{ m}^2/\text{g}$ was 6.6%. The rise in ultrasonication time in samples containing aqueous SWCNT did not cause a change in thermal conductivity. This is indicative of no deterioration in the structure of the nanotubes during the 50 min and 100 min ultrasonication times studied in the samples. The highest thermal conductivity value for these samples having 2.0 wt% SWCNT and 0.2 wt% PEG-POSS was recorded as 4.3%.

In water and oil-based samples, the contact angle values raised as the concentration and surface area of the hydrophobic GNPs increased. The uniform distribution of nanoparticles with high surface area in the base fluid is one of the major factors that increase the contact angle. In samples containing SWCNT, the contact angle reduced as the nanoparticle concentration increased. This proves that SWCNTs are more hydrophilic than GNPs. The addition of PEG-POSS to aqueous nanofluids showed a decrease in contact angle. Some studies in the literature have obtained similar data to these results. No direct correlation was found between PEG-POSS and contact angle in EG and oil-based samples. The surface tension of GNP nanofluids decreased with

increasing surface area; whereas, high surface tension was observed with increase in GNP concentration.

There is a lot of contradiction in the studies about nanofluids in the literature. Sharing the details of all steps and analyses performed during the production and characterization of nanofluids will shed light on future studies and help overcome the difficulties encountered during the research.

REFERENCES

- [1] John, G. (1997). *Richard Feynman: A life in science*. NY: Dutton.
- [2] Binnig, G., Quate, C. F., & Gerber, C. (1986). Atomic force microscope. *Phys Rev Lett*, 56(9), 930-933.
- [3] Tawfik, M. M. (2017). Experimental studies of nanofluid thermal conductivity enhancement and applications: A review. *Renewable and Sustainable Energy Reviews*, 75, 1239-1253.
- [4] Murshed, S. M. S., & Nieto de Castro, C. A. (2014). Superior thermal features of carbon nanotubes-based nanofluids – A review. *Renewable and Sustainable Energy Reviews*, 37, 155-167.
- [5] Rasheed, A. K., Khalid, M., W, R., Gupta, T., & Chan, A. (2016). Graphene based nanofluids and nanolubricants – Review of recent developments. *Renewable and Sustainable Energy Reviews*, 63, 346-362.
- [6] Mehrali, M., Sadeghinezhad, E., Latibari, S. T., Kazi, S. N., Mehrali, M., Zubir, M. N. B. M., & Metselaar, H. S. C. J. N. R. L. (2014). Investigation of thermal conductivity and rheological properties of nanofluids containing graphene nanoplatelets. 9(1), 15.
- [7] Sadeghinezhad, E., Mehrali, M., Saidur, R., Mehrali, M., Tahan Latibari, S., Akhiani, A. R., & Metselaar, H. S. C. (2016). A comprehensive review on graphene nanofluids: Recent research, development and applications. *Energy Conversion and Management*, 111, 466-487.
- [8] Yu, W., Xie, H., & Chen, L. (2012). Nanofluids. In A. Hashim (Ed.), *Smart Nanoparticles Technology*: IntechOpen.
- [9] Yu, W., & Xie, H. (2012). A Review on Nanofluids: Preparation, Stability Mechanisms, and Applications. *Journal of Nanomaterials*, 2012, 17.
- [10] Arshad, A., Jabbal, M., Yan, Y., & Reay, D. (2019). A Review on Graphene based Nanofluids: Preparation, Characterization and Applications. *Journal of Molecular Liquids*, 279.
- [11] Slonczewski, J. C., & Weiss, P. R. (1958). Band Structure of Graphite. *Physical Review*, 109(2), 272-279.
- [12] Novoselov, K. S., Geim, A. K., Morozov, S. V., Jiang, D., Zhang, Y., Dubonos, S. V., . . . Firsov, A. A. (2004). Electric field effect in atomically thin carbon films. *Science*, 306(5696), 666-669.
- [13] Novoselov, K. S., Geim, A. K., Morozov, S. V., Jiang, D., Katsnelson, M. I., Grigorieva, I. V., . . . Firsov, A. A. (2005). Two-dimensional gas of massless Dirac fermions in graphene. *Nature*, 438(7065), 197-200.
- [14] Lee, C., Wei, X., Kysar, J. W., & Hone, J. (2008). Measurement of the Elastic Properties and Intrinsic Strength of Monolayer Graphene. *Science*, 321(5887), 385.
- [15] Singh, V., Joung, D., Zhai, L., Das, S., Khondaker, S., & Seal, S. (2011). Graphene Based Materials: Past, Present and Future. *Progress in Materials Science*, 56(8), 1178–1271.
- [16] Zhang, T., Xue, Q., Zhang, S., & Dong, M. (2012). Theoretical approaches to graphene and graphene-based materials. *Nano Today*, 7(3), 180-200.

- [17] Papageorgiou, D. G., Kinloch, I. A., & Young, R. J. (2017). Mechanical properties of graphene and graphene-based nanocomposites. *Progress in Materials Science*, 90, 75-127.
- [18] Iijima, S., & Ichihashi, T. (1993). Single-shell carbon nanotubes of 1-nm diameter. *Nature*, 363(6430), 603-605.
- [19] Göktepe, F. (2015). Eğrilebilir Karbon Nanotüpler ve Bu Özel Liflerden Üretilen Teknik İplikler. *Tekstil ve Mühendis*, 22(100), 1-12.
- [20] Ganesh, E. N. (2013). Single Walled and Multi Walled Carbon Nanotube Structure. Synthesis and Applications. *International Journal of Innovative Technology and Exploring Engineering*, 2(4), 2278-3075.
- [21] Ouyang, M., Huang, J.-L., Cheung, C. L., & Lieber, C. M. (2001). Atomically Resolved Single-Walled Carbon Nanotube Intramolecular Junctions. *Science*, 291(5501), 97-100.
- [22] Peigney, A., Laurent, C., Flahaut, E., Bacsa, R. R., & Rousset, A. (2001). Specific surface area of carbon nanotubes and bundles of carbon nanotubes. *Carbon*, 39(4), 507-514.
- [23] Eatemadi, A., Daraee, H., Karimkhanloo, H., Kouhi, M., Zarghami, N., Akbarzadeh, A., . . . Joo, S. (2014). Carbon nanotubes: properties, synthesis, purification, and medical applications. *Nanoscale Res Lett*, 9(1), 393.
- [24] Ebbesen, T. W., Lezec, H. J., Hiura, H., Bennett, J. W., Ghaemi, H. F., & Thio, T. (1996). Electrical conductivity of individual carbon nanotubes. *Nature*, 382(6586), 54-56.
- [25] Treacy, M. M. J., Ebbesen, T. W., & Gibson, J. M. (1996). Exceptionally high Young's modulus observed for individual carbon nanotubes. *Nature*, 381(6584), 678-680.
- [26] Kim, Y. J., Ma, H., & Yu, Q. (2010). Plasma nanocoated carbon nanotubes for heat transfer nanofluids. *Nanotechnology*, 21(29), 295703.
- [27] Yu, C., Shi, L., Yao, Z., Li, D., & Majumdar, A. (2005). Thermal Conductance and Thermopower of an Individual Single-Wall Carbon Nanotube. *Nano Letters*, 5(9), 1842-1846.
- [28] Kasuya, A., Saito, Y., Sasaki, Y., Fukushima, M., Maedaa, T., Horie, C., & Nishina, Y. (1996). Size dependent characteristics of single wall carbon nanotubes. *Materials Science and Engineering: A*, 217-218, 46-47.
- [29] Maeda, T., & Horie, C. (1999). Phonon modes in single-wall nanotubes with a small diameter. *Physica B: Condensed Matter*, 263-264, 479-481.
- [30] Popov, V. N. (2004). Theoretical evidence for T^{1/2} specific heat behavior in carbon nanotube systems. *Carbon*, 42(5), 991-995.
- [31] Georgakilas, V., Kordatos, K., Prato, M., Guldi, D. M., Holzinger, M., & Hirsch, A. (2002). Organic Functionalization of Carbon Nanotubes. *Journal of the American Chemical Society*, 124(5), 760-761.
- [32] Saeed, K., & Khan, I. (2013). *Carbon nanotubes—properties and applications: a review* (Vol. 14).
- [33] Li, G., Wang, L., Ni, H., & Pittman, C. (2001). Polyhedral Oligomeric Silsesquioxane (POSS) Polymers and Copolymers: A Review. *Journal of Inorganic and Organometallic Polymers*, 11(3), 123-154.
- [34] Scott, D. W. (1946). Thermal Rearrangement of Branched-Chain Methylpolysiloxanes. *Journal of the American Chemical Society*, 68(3), 356-358.
- [35] Kuo, S.-W., & Chang, F.-C. (2011). POSS related polymer nanocomposites. *Progress in Polymer Science*, 36(12), 1649-1696.

- [36] Ayandele, E., Sarkar, B., & Alexandridis, P. (2012). Polyhedral Oligomeric Silsesquioxane (POSS)-Containing Polymer Nanocomposites. *Nanomaterials*, 2(4), 445-475.
- [37] Wu, J., & Mather, P. T. (2009). POSS Polymers: Physical Properties and Biomaterials Applications. *Polymer Reviews*, 49(1), 25-63.
- [38] Ullah, A., Ullah, S., Khan, G. S., Shah, S. M., Hussain, Z., Muhammad, S., . . . Hussain, H. (2016). Water soluble polyhedral oligomeric silsesquioxane based amphiphilic hybrid polymers: Synthesis, self-assembly, and applications. *European Polymer Journal*, 75, 67-92.
- [39] Rao, Y. (2010). Nanofluids: Stability, phase diagram, rheology and applications. *Particuology*, 8(6), 549-555.
- [40] Kaszuba, M., Corbett, J., Watson, F. M., & Jones, A. (2010). High-concentration zeta potential measurements using light-scattering techniques. *Philosophical transactions. Series A, Mathematical, physical, and engineering sciences*, 368(1927), 4439-4451.
- [41] Thermo-Spectronic. (2001). Basic UV-Vis Theory, Concepts and Applications. In (pp. 1-28).
- [42] Shah, R. R., Pawar, R. B., & Gayakar, P. P. (2015). UV-Visible Spectroscopy-A Review. *International Journal of Institutional Pharmacy and Life Sciences*, 5, 490-505.
- [43] Jayakumar, S. (2016). Components, Principle and Applications of UV Vis-Spectrophotometer.
- [44] Chirtoc, M., & Henry, J. F. (2008). 3 omega hot wire method for micro-heat transfer measurements: From anemometry to scanning thermal microscopy (SThM). *The European Physical Journal Special Topics*, 153(1), 343-348.
- [45] Chirtoc, M., Filip, X., Henry, J. F., Antoniow, J. S., Chirtoc, I., Dietzel, D., . . . Pelzl, J. (2004). Thermal probe self-calibration in ac scanning thermal microscopy. *Superlattices and Microstructures*, 35(3), 305-314.
- [46] S. Carslaw, H., & C. Jaeger, J. (1959). *Conduction of Heat in Solids*. London: Oxford Univ. Press.
- [47] Cahill, D. (1990). Thermal conductivity measurement from 30 to 750 K: the 3omega method. *Rev. Sci. Instrum.*, 61, 802-808.
- [48] Whitepaper - A Basic Introduction to Rheology. (2016). In M. I. Limited (Ed.), (pp. 9-19).
- [49] Ding, Y., Alias, H., Wen, D., & Williams, R. A. (2006). Heat transfer of aqueous suspensions of carbon nanotubes (CNT nanofluids). *International Journal of Heat and Mass Transfer*, 49(1), 240-250.
- [50] Barnes, H. A. (1999). The yield stress—a review or ‘παντα ρει’—everything flows? *Journal of Non-Newtonian Fluid Mechanics*, 81(1), 133-178.
- [51] Bonn, D., & Denn, M. M. (2009). Yield Stress Fluids Slowly Yield to Analysis. *Science*, 324(5933), 1401.
- [52] Elçioğlu, E. B., Güvenç Yazıcıoğlu, A., & Kakaç, S. (2014). Nanoakışkan Viskozitesinin Karşılaştırmalı Değerlendirmesi. *Isı Bilimi ve Tekniği Dergisi*, 34(1), 137-151.
- [53] Hackley, V. A., & Ferraris, C. F. (2001). *Guide to Rheological Nomenclature*: National Institute of Standards and Technology.
- [54] Xu, X., & Wang, X. (2010). Derivation of the Wenzel and Cassie Equations from a Phase Field Model for Two Phase Flow on Rough Surface. *SIAM Journal of Applied Mathematics*, 70, 2929-2941.

- [55] Vafaei, S., Borca-Tasciuc, T., Podowski, M. Z., Purkayastha, A., Ramanath, G., & Ajayan, P. M. (2006). Effect of nanoparticles on sessile droplet contact angle. *Nanotechnology*, 17(10), 2523-2527.
- [56] Morita, A., Carastan, D., & Demarquette, N. (2002). Influence of drop volume on surface tension evaluated using the pendant drop method. *Colloid and Polymer Science*, 280, 857-864.
- [57] Berry, J. D., Neeson, M. J., Dagastine, R. R., Chan, D. Y. C., & Tabor, R. F. (2015). Measurement of surface and interfacial tension using pendant drop tensiometry. *Journal of Colloid and Interface Science*, 454, 226-237.
- [58] Eastman, J. A., Choi, S. U. S., Li, S., Yu, W., & Thompson, L. J. (2001). Anomalous increased effective thermal conductivities of ethylene glycol-based nanofluids containing copper nanoparticles. *Applied Physics Letters*, 79(6), 718-720.
- [59] Xie, H., Lee, H., Youn, W., & Choi, M. (2003). Nanofluids containing multiwalled carbon nanotubes and their enhanced thermal conductivities. *Journal of Applied Physics*, 94(8), 4967-4971.
- [60] Assael, M. J., Chen, C.-F., Metaxa, I., & Wakeham, W. A. (2004). Thermal Conductivity of Suspensions of Carbon Nanotubes in Water. *International Journal of Thermophysics*, 25(4), 971-985.
- [61] Liu, M.-S., Ching-Cheng Lin, M., Huang, I. T., & Wang, C.-C. (2005). Enhancement of thermal conductivity with carbon nanotube for nanofluids. *International Communications in Heat and Mass Transfer*, 32(9), 1202-1210.
- [62] Assael, M. J., Metaxa, I. N., Arvanitidis, J., Christofilos, D., & Lioutas, C. (2005). Thermal Conductivity Enhancement in Aqueous Suspensions of Carbon Multi-Walled and Double-Walled Nanotubes in the Presence of Two Different Dispersants. *International Journal of Thermophysics*, 26(3), 647-664.
- [63] Assael, M. J., Metaxa, I. N., Kakosimos, K., & Constantinou, D. (2006). Thermal Conductivity of Nanofluids – Experimental and Theoretical. *International Journal of Thermophysics*, 27(4), 999-1017.
- [64] Hwang, Ahn, Y. C., Shin, H. S., Lee, C. G., Kim, G. T., Park, H. S., & Lee, J. K. (2006). Investigation on characteristics of thermal conductivity enhancement of nanofluids. *Current Applied Physics*, 6(6), 1068-1071.
- [65] Hwang, Park, H. S., Lee, J. K., & Jung, W. H. (2006). Thermal conductivity and lubrication characteristics of nanofluids. *Current Applied Physics*, 6, e67-e71.
- [66] Chen, L., Xie, H., Li, Y., & Yu, W. (2008). Nanofluids containing carbon nanotubes treated by mechanochemical reaction. *Thermochimica Acta*, 477(1), 21-24.
- [67] Amrollahi, A., Hamidi, A. A., & Rashidi, A. M. (2008). The effects of temperature, volume fraction and vibration time on the thermo-physical properties of a carbon nanotube suspension (carbon nanofluid). *Nanotechnology*, 19(31), 315701.
- [68] Nanda, J., Maranville, C., Bollin, S. C., Sawall, D., Ohtani, H., Remillard, J. T., & Ginder, J. M. (2008). Thermal Conductivity of Single-Wall Carbon Nanotube Dispersions: Role of Interfacial Effects. *The Journal of Physical Chemistry C*, 112(3), 654-658.
- [69] Glory, J., Bonetti, M., Helezen, M., Mayne-L'Hermitte, M., & Reynaud, C. (2008). Thermal and electrical conductivities of water-based nanofluids prepared with long multiwalled carbon nanotubes. *Journal of Applied Physics*, 103(9), 094309.

- [70] Chen, L., & Xie, H. (2009). Silicon oil based multiwalled carbon nanotubes nanofluid with optimized thermal conductivity enhancement. *Colloids and Surfaces A: Physicochemical and Engineering Aspects*, 352(1), 136-140.
- [71] Jha, N., & Ramaprabhu, S. (2009). Thermal conductivity studies of metal dispersed multiwalled carbon nanotubes in water and ethylene glycol based nanofluids. *Journal of Applied Physics*, 106(8), 084317.
- [72] Liu, M., Lin, M. C., & Wang, C. (2011). Enhancements of thermal conductivities with Cu, CuO, and carbon nanotube nanofluids and application of MWNT/water nanofluid on a water chiller system. *Nanoscale Res Lett*, 6(1), 297.
- [73] Aravind, S. S. J., Baskar, P., Baby, T. T., Sabareesh, R. K., Das, S., & Ramaprabhu, S. (2011). Investigation of Structural Stability, Dispersion, Viscosity, and Conductive Heat Transfer Properties of Functionalized Carbon Nanotube Based Nanofluids. *The Journal of Physical Chemistry C*, 115(34), 16737-16744.
- [74] Harish, S., Ishikawa, K., Einarsson, E., Aikawa, S., Chiashi, S., Shiomi, J., & Maruyama, S. (2012). Enhanced thermal conductivity of ethylene glycol with single-walled carbon nanotube inclusions. *International Journal of Heat and Mass Transfer*, 55(13), 3885-3890.
- [75] Ma, W., Yang, F., Shi, J., Wang, F., Zhang, Z., & Wang, S. (2013). Silicone based nanofluids containing functionalized graphene nanosheets. *Colloids and Surfaces A: Physicochemical and Engineering Aspects*, 431, 120-126.
- [76] Hadadian, M., Goharshadi, E. K., & Youssefi, A. (2014). Electrical conductivity, thermal conductivity, and rheological properties of graphene oxide-based nanofluids. *Journal of Nanoparticle Research*, 16(12), 2788.
- [77] Hemmat Esfe, M., Afrand, M., Karimipour, A., Yan, W.-M., & Sina, N. (2015). An experimental study on thermal conductivity of MgO nanoparticles suspended in a binary mixture of water and ethylene glycol. *International Communications in Heat and Mass Transfer*, 67, 173-175.
- [78] Zheng, Z. Z. (2015). Experimental Investigation on Surface Tension of Water-Based Graphene Oxide Nanofluids. *Advanced Materials Research*, 1082, 297-301.
- [79] Kamatchi, R., Venkatachalapathy, S., & Srinivas, B. (2015). Synthesis, stability, transport properties, and surface wettability of reduced graphene oxide/water nanofluids. *International Journal of Thermal Sciences*, 97, 17-25.
- [80] Ahammed, N., Asirvatham, L. G., & Wongwises, S. (2016). Effect of volume concentration and temperature on viscosity and surface tension of graphene–water nanofluid for heat transfer applications. *Journal of Thermal Analysis and Calorimetry*, 123(2), 1399-1409.
- [81] Kumar, R., & Milanova, D. (2009). Effect of surface tension on nanotube nanofluids. *Applied Physics Letters*, 94, 073107-073107.
- [82] Tanvir, S., & Qiao, L. J. N. R. L. (2012). Surface tension of Nanofluid-type fuels containing suspended nanomaterials. 7(1), 226.
- [83] Antoniadis, K. D., Tertsinidou, G. J., Assael, M. J., & Wakeham, W. A. J. I. J. o. T. (2016). Necessary Conditions for Accurate, Transient Hot-Wire Measurements of the Apparent Thermal Conductivity of Nanofluids are Seldom Satisfied. 37(8), 78.
- [84] Alasli, A., Evgin, T., & Turgut, A. (2018). Re-dispersion ability of multi wall carbon nanotubes within low viscous mineral oil. *Colloids and Surfaces A: Physicochemical and Engineering Aspects*, 538, 219-228.

- [85] Mukherjee, S., Mishra, P. C., & Chaudhuri, P. (2018). Stability of Heat Transfer Nanofluids – A Review. *ChemBioEng Reviews*, 5(5), 312-333.
- [86] Devre, R. D., Budhlall, B. M., & Barry, C. F. (2016). Enhancing the Colloidal Stability and Electrical Conductivity of Single-Walled Carbon Nanotubes Dispersed in Water. *217*(5), 683-700.
- [87] Sarsam, W. S., Amiri, A., Kazi, S. N., & Badarudin, A. (2016). Stability and thermophysical properties of non-covalently functionalized graphene nanoplatelets nanofluids. *Energy Conversion and Management*, 116, 101-111.
- [88] Nasiri, A., Shariaty-Niasar, M., Rashidi, A. M., & Khodafarin, R. (2012). Effect of CNT structures on thermal conductivity and stability of nanofluid. *International Journal of Heat and Mass Transfer*, 55(5), 1529-1535.
- [89] Murshed, & Estellé, P. (2017). A state of the art review on viscosity of nanofluids. *Renewable and Sustainable Energy Reviews*, 76, 1134-1152.
- [90] Bashirnezhad, K., Bazri, S., Safaei, M. R., Goodarzi, M., Dahari, M., Mahian, O., . . . Wongwises, S. (2016). Viscosity of nanofluids: A review of recent experimental studies. *International Communications in Heat and Mass Transfer*, 73, 114-123.
- [91] Tseng, & Wu. (2002). Aggregation, rheology and electrophoretic packing structure of aqueous Al₂O₃ nanoparticle suspensions. *Acta Materialia*, 50(15), 3757-3766.
- [92] Murshed, Tan, S.-H., & Nguyen, N.-T. (2008). Temperature dependence of interfacial properties and viscosity of nanofluids for droplet-based microfluidics. *Journal of Physics D: Applied Physics*, 41(8), 085502.
- [93] Nabeel Rashin, M., & Hemalatha, J. (2013). Synthesis and viscosity studies of novel ecofriendly ZnO–coconut oil nanofluid. *Experimental Thermal and Fluid Science*, 51, 312-318.
- [94] Turgut, A., Sauter, C., Chirtoc, M., Henry, J. F., Tavman, S., Tavman, I., & Pelzl, J. J. T. E. P. J. S. T. (2008). AC hot wire measurement of thermophysical properties of nanofluids with 3 ω method. *153*(1), 349-352.
- [95] Turgut, A., Tavman, I., Chirtoc, M., Schuchmann, H. P., Sauter, C., & Tavman, S. (2009). Thermal Conductivity and Viscosity Measurements of Water-Based TiO₂ Nanofluids. *International Journal of Thermophysics*, 30(4), 1213-1226.
- [96] Timofeeva, E. V., Yu, W., France, D. M., Singh, D., & Routbort, J. L. (2011). Nanofluids for heat transfer: an engineering approach. *Nanoscale Res Lett*, 6(1), 182.
- [97] Lee., & Rhee. (2014). Enhanced thermal conductivity of nanofluids containing graphene nanoplatelets prepared by ultrasound irradiation. *Journal of Materials Science*, 49(4), 1506-1511.
- [98] Fuskele, V., & Sarviya, R. M. (2017). Recent developments in Nanoparticles Synthesis, Preparation and Stability of Nanofluids. *Materials Today: Proceedings*, 4(2, Part A), 4049-4060.
- [99] Taherian, H., Alvarado, J. L., & Languri, E. M. (2018). Enhanced thermophysical properties of multiwalled carbon nanotubes based nanofluids. Part 1: Critical review. *Renewable and Sustainable Energy Reviews*, 82, 4326-4336.
- [100] Mingzheng, Z., Guodong, X., Jian, L., Lei, C., & Lijun, Z. (2012). Analysis of factors influencing thermal conductivity and viscosity in different kinds of surfactant solutions. *Experimental Thermal and Fluid Science*, 36, 22-29.
- [101] Kim, S. J., Bang, I. C., Buongiorno, J., & Hu, L. W. (2007). Surface wettability change during pool boiling of nanofluids and its effect on critical heat flux. *International Journal of Heat and Mass Transfer*, 50(19), 4105-4116.

- [102] Ferrari, & Ravera. (2010). Surfactants and wetting at superhydrophobic surfaces: Water solutions and non aqueous liquids. *Advances in colloid and interface science*, 161, 22-28.
- [103] Radiom, M., Yang, C., & Chan, W. (2009). Characterization of Surface Tension and Contact Angle of Nanofluids. *Proceedings of SPIE - The International Society for Optical Engineering*, 7522.
- [104] Yarmand, H., Gharekhani, S., Ahmadi, G., Shirazi, S. F. S., Baradaran, S., Montazer, E., . . . Dahari, M. (2015). Graphene nanoplatelets–silver hybrid nanofluids for enhanced heat transfer. *Energy Conversion and Management*, 100, 419-428.
- [105] Pavese, M., Musso, S., Bianco, S., Giorcelli, M., & Pugno, N. (2008). An analysis of carbon nanotube structure wettability before and after oxidation treatment. *Journal of Physics: Condensed Matter*, 20, 474206.
- [106] Estellé, P., Cabaleiro, D., Żyła, G., Lugo, L., & Murshed, S. M. S. (2018). Current trends in surface tension and wetting behavior of nanofluids. *Renewable and Sustainable Energy Reviews*, 94, 931-944.
- [107] Bhuiyan, M. H. U., Saidur, R., Amalina, M. A., Mostafizur, R. M., & Islam, A. (2015). Effect of Nanoparticles Concentration and Their Sizes on Surface Tension of Nanofluids. *Procedia Engineering*, 105, 431-437.
- [108] Moffat, J. R., Sefiane, K., & Shanahan, M. E. R. (2009). Effect of TiO₂ Nanoparticles on Contact Line Stick–Slip Behavior of Volatile Drops. *The Journal of Physical Chemistry B*, 113(26), 8860-8866.
- [109] Chen, R.-H., Phuoc, T. X., & Martello, D. (2011). Surface tension of evaporating nanofluid droplets. *International Journal of Heat and Mass Transfer*, 54(11), 2459-2466.
- [110] Abbas, Z., Labbez, C., Nordholm, S., & Ahlberg, E. (2008). Size-Dependent Surface Charging of Nanoparticles. *The Journal of Physical Chemistry C*, 112(15), 5715-5723.
- [111] Brown, M. A., Duyckaerts, N., Redondo, A. B., Jordan, I., Nolting, F., Kleibert, A., . . . Abbas, Z. (2013). Effect of Surface Charge Density on the Affinity of Oxide Nanoparticles for the Vapor–Water Interface. *Langmuir*, 29(16), 5023-5029.
- [112] Okubo, T. (1995). Surface Tension of Structured Colloidal Suspensions of Polystyrene and Silica Spheres at the Air-Water Interface. *Journal of Colloid and Interface Science*, 171(1), 55-62.
- [113] Jeong, y., Joon Chang, W., & Chang, S. (2008). Wettability of heated surfaces under pool boiling using surfactant solutions and nano-fluids. *International Journal of Heat and Mass Transfer*, 51, 3025-3031.
- [114] Pantzali, M. N., Kanaris, A., Antoniadis, K., Mouza, A., & Paras, S. (2009). Effect of nanofluids on the performance of a miniature plate heat exchanger with modulated surface. *International Journal of Heat and Fluid Flow*, 30, 691-699.
- [115] Wu, S. (1973). Polar and Nonpolar Interactions in Adhesion. *The Journal of Adhesion*, 5(1), 39-55.
- [116] Albaiti, Liliyasi, Sumarna, O., & Martoprawiro, M. A. (2017). A Study of Oil Viscosity Mental Model. *Journal of Physics: Conference Series*, 812, 012030.

CURRICULUM VITAE



PERSONAL INFORMATION

Name : Tuğçe FİDAN ASLAN
Date of Birth : 16.01.1993
Driving Licence : Class B (2012)
Languages : English (advanced), Turkish (native)
Smoking : Non-smoking
GSM : +90 (539) 250 3096
E-mail : tugcefid@gmail.com

EDUCATION

2016-2019 **MS**, Department of Materials Science and Engineering, Katip Çelebi University, İzmir, Turkey.
2012-2016 **BS**, Department of Chemical Engineering (100% English), Ege University, İzmir, Turkey
2011-2012 **Preparation School**, Ege University School of Foreign Language, İzmir, Turkey.
2007-2011 **High School**, İzmir Atatürk High School, İzmir, Turkey.

WORK EXPERIENCES

2015 **Enercon Gmbh**, Intern, İzmir, Turkey
Composite materials and production of wind turbines
2014 **Gema Electro Plastic**, Intern, İzmir, Turkey
Production of filled polymer composites
Production, Q&C, and R&D departments

TECHNICAL COMPETENCE

Instruments:

Zeta Potential Analyzer

UV-Vis Spectroscopy

Surface Tensiometer

Contact Angle Goniometer

Rheometer

Programs:

Very Good Knowledge of MS Word, MS Excel, MS PowerPoint

Medium Knowledge of AutoCAD, MATLAB

PROJECTS

TÜBİTAK 3001 – Preparation of Stable Nanofluids with Surface Functionalized Nanoparticles and Determination of the Change in Thermal Conductivity of Nanofluids

Graduation Project – Microencapsulation (MC) Performance of Healing Agents Used in Self-Healing Coatings

CERTIFICATES & SEMINARS & WORKSHOPS

2018 **International Conference on Engineering Technologies, Oral Presentation**, Evaluating the Stability and Heat Transfer Performance of Carbon-based Aqueous Nanofluids

2018 **16th International Conference on Clean Energy, Oral Presentation**, Preparation of Stable Nanofluids with Surface Functionalized Nanoparticles and Determination of the Change in Thermal Conductivity of Nanofluids

2018 **2nd Carbon Conference, Poster Presentation**, Preparation and Characterization of Carbon Nanofluids

2017 **5th International Polymeric Composites Symposium and Workshops**, Organizing Committee

2017 **Polymer Rheology and Processing Workshop**, Participant

- 2015 **KOMPEGE-III, Poster Presentation**, Flame Retardant Fillers Used
in Cable Sheaths Composite Materials
- 2012 **Diction Certificate**, Elginkan Foundation, Manisa, Turkey

SCHOLARSHIPS

TÜBİTAK 3001 Scholarship (2017-2019)

EXAMS

Entrance Examination for Academic Personnel and Postgraduate Education
(ALES) (2017) – Score: 80

Council of Higher Education Foreign Language Exam (YOKDIL) (2017) –
Score: 75

MEMBERSHIPS

Ege Engineering Society (President of the board, 2014-2015).